39

THE TRIPLE-HELICAL DNA FOUR-WAY JUNCTION

NEO MAKUBE

Thesis presented for the Degree of

DOCTOR OF PHILOSOPHY

in the Department of Biochemistry

UNIVERSITY OF CAPE TOWN

JUNE 1999

...dedicated to my grandmother.

ABSTRACT

This Thesis will show that third strands can be incorporated into the four-way junctions combining the properties of the triple helices and those of branched structures within one system without compromising either of the two. It is now known that folding into secondary and tertiary structures by nucleic acids is crucial for their biological functions. However, what remain to be clarified are the mechanisms involved in the folding of nucleic acids into noncanonical structures. It requires a thorough understanding of the chemical and physical properties of the structure in question. This in turn will improve the design of new secondary and tertiary structures that may add to the DNA nanotechnology.

With this aim, thermodynamic and structural properties of two triple-helical DNA four-way junctions (J_{T1T3} and J_{T2T4}) are reported and discussed. J_{T1T3} and J_{T2T4} differ only in the polarity of the third strands (and/or position of the loops). Both junctions contain the same Watson-Crick double-helical four-way junction, named Js, as a core structure. Js was constructed from four 20-mer oligomers, two of which consists of purines and the other two strands pyrimidines. Extending each of the pyrimidine strands of Js at the 3' end by four cytosines followed by twenty pyrimidine bases results in J_{T1T3}. Similarly, J_{T2T4} is formed by extending the same pyrimidine strands at the 5' end. The junctions are named according to the position of the C4-loops. J_{T1T3} and J_{T2T4} are further simplified into J_{T1}, J_{T2}, J_{T3} and J_{T4}. Lowering the pH from 12 to 2 allows the oligomers to fold sequentially from random coil into the double-helical four-way junction, Js, and finally into the triple-helical four-way junction.

The analysis of the structures discussed is based on the biochemical methods such as native polyacrylamide gel electrophoresis and chemical footprinting using osmium tertroxide as a probe. The analysis is also based on the physical methods, UV spectroscopy and DSC. The native polyacrylamide gel electrophoresis has been used to verify the formation of the complete four-way junctions. Chemical footprinting has been used to detect the formation of the junctions as well as to indicate the conformations these junctions assume under different pH and/or salt conditions. The phase diagrams enthalpies and entropies of the structures are determined mainly by DSC.

The results indicate that all the junctions are highly sensitive to salt concentrations and/or pH. The Tm vs. $[Na^+]$ results show that above 0.4M Na^+, the structures adopt a conformation that suggests that the junctions are folded into stacked helix structures. The differences in thermal stabilities of the junctions J_{T1}, J_{T2}, J_{T3} and J_{T4} are due to the sequence composition of the arms and not the loops. J_{T1}, J_{T2}, J_{T3} and J_{T4} are thermally more stable than the underlying double-helical junction, Js. Similarly; the complete triple-helical four-way junctions J_{T1T3} and J_{T2T4} are thermally more stable than their substructures J_{T1}, J_{T2}, J_{T3} and J_{T4}. The compiled transition enthalpies obtained for the individual arms of Js, J_{T1}, J_{T2}, J_{T3} and J_{T4} are less than the transition enthalpies associated with the melting of the complete junctions. The higher calorimetric enthalpies of the structures are due in part to the contribution from the single strands resulting from the partly unfolded arms. The overall results show that third strands have a stabilizing effect on the structure of the four-way junction.

ACKNOWLEDGEMENTS

I wish to express my sincere gratitude to the following people:

My supervisor, Professor Horst Klump, for ensuring the completion of this thesis. His invaluable contribution and eagerness in my work is really appreciated. I wish to thank him sincerely for always believing in me and accepting me in his team. His patience and willingness to see to it that I become a better scientist is really appreciated.

Dr Paul Hüsler, who introduced me to Biophysics.

Madhu Chauhan for being such a wonderful teacher and for always being there for me both in and outside the laboratory. Her technical expertise has helped me tremendously.

My colleagues, Dr Martin Mills and Renata Petry for providing stimulating discussions.

Pei-Yin Ma for the synthesis and purification of the oligonucleotides over the past few years.

Theresa Anderson for assistance with the gel photography and HPLC.

My family who has stood by me throughout my studies.

Finally, I acknowledge the support from the National Research Foundation (NRF) and the UCT/Mellon Foundation Scholarship.

TABLE OF CONTENTS

FIGURES AND TABLES

FIGURES

TABLES

ABBREVIATIONS

A	adenine
C	cytosine
CD	circular dichroism
DNA	deoxyribonucleic acid
DSC	differential scanning calorimeter
ε^{-1}	extinction coefficient
EDTA	ethylenediaminetetra-acetic acid
G	guanine
HPLC	high performance liquid chromatography
IR	infrared
$[Na^+]$	sodium ion concentration
Na_3PO_4	trisodium phosphate
NMR	nuclear magnetic resonance
OsO_4	osmium tetroxide
PAGE	polyacrylamide gel electrophoresis
RNA	ribonucleic acid
TRNA	transfer RNA
T	thymine
UV	ultraviolet

CHAPTER 1

INTRODUCTION

Nucleic acids are polymer molecules that play an essential role in the processing and storage of genetic information. To understand these functions, the structural features of the nucleic acids must be known in detail. The basic building blocks of nucleic acids are the nucleotides which are linked by 5'-3' phosphodiester bonds. Nucleotides are composed of a furanoside-type sugar, a phosphate group and one of the four heterocyclic bases (adenine, guanine, cytosine and thymine or uracil). There are two types of nucleic acids, deoxyribonucleic acid (DNA) and ribonucleic acids (RNA). RNA differs from DNA in that the latter contains a 2'-deoxyribose instead of ribose and it contains 5 methyl-uracil (thymine) residue in places of the canonical uracil residue. DNA in general assumes a double-stranded helical structure (Watson and Crick, 1953b) with the backbones running anti-parallel to each other and the heterocyclic bases of one strand base pairing with the complementary bases on the opposite strand. Under selected physical conditions, the DNA double helix is able to adopt different conformations, the right-handed A and B forms and the left-handed Z-form. The B-form is the common conformation in dilute aqueous solutions and in the cell. On the other hand, RNA commonly exists as a single stranded linear molecule. The few naturally occurring RNA molecules that form double stranded helices are confined to the right handed A-type conformation. DNA–RNA hybrids often occur in the cells and they always adopt the A-DNA or A-RNA conformation. The Watson-Crick base-pairing is conserved throughout these conformations.

The main stabilizing interactions within the double helix are Hydrogen bonds between complementary base pairs and stacking of consecutive base pairs. The repulsion of the negatively charged phosphate groups located in the backbone of nucleic acids is often the source of

instability of the double helix. The structural properties of nucleic acids have been elucidated by chemical and physical methods including UV, CD, IR, NMR and ESR spectroscopy, Calorimetry, X-ray diffraction, PAGE and footprinting using various chemical probes etc.

DNA and RNA conformational flexibility

One of the most important features of nucleic acids is their intrinsic conformational flexibility that allows them to assume a variety of structures (secondary or tertiary), depending on the sequence and the environment conditions (pH, ionic strength). The development and improvement of techniques used in studying the structures of nucleic acids has produced (in)direct evidence of the participation of these structure in biological functions. That is, the conformation of any nucleic acid is associated with a specific function in a living cell. It follows from here that determining the structures of nucleic acids is of fundamental importance in understanding the biological functions in which nucleic acids take part. These structures may be helical or non-helical and they may include hairpin structures, loops and bulges, pseudoknots, ribozymes, quadruplexes, triple helices and helical junctions. The following paragraphs contain brief descriptions and discussions of the above secondary and tertiary structures. The general properties of DNA junctions and/or triplexes will be especially emphasized since this thesis is about triple-helical DNA four-way junctions.

Secondary structure elements in DNA and RNA

1.1 Hairpins, loops, bulges and internal loops

Single stranded RNA sequences and to a lesser degree DNA, sequences are able to form hairpins. They have been detected at sites that are known to be involved in processes such as

replication, transcription and genetic recombination. Although DNA occurs regularly as a double helix during these processes (replication, transcription etc.) some parts of it will unwind into single strands and thus allow the formation of hairpins, loops or bulges. The formation of DNA hairpins is easier than that of RNAs'. The occurrence of RNA hairpins tends to outnumber DNA hairpins in nature. In any case, the formation of hairpins will only take place under certain specific condition.

The composition, polarity of the loop sequence, size of the loop together with the base composition of the stem, have a major effect on the optimum stability of stem-loop structures (Blommers et al., 1989; Senior et al., 1988; Antao et al., 1991). There is a difference between the optimal stability between RNA hairpins and DNA hairpins depending on loop size. Uhlenbeck et al. studied the stability of RNA hairpin loops using RNA sequences of the form A_6-C_m-U_6 (m = 4, 5, 6 or 8) (Uhlenbeck et al., 1973). These authors could show that the hairpins that contain a six member-loop were the most stable. Gralla and Crothers confirmed these results in showing that hairpins with six or seven bases in the loop were the most stable (Gralla and Crothers, 1973). On the other hand, hairpins formed from single–stranded DNA sequences are stabilized by smaller loops of two to five unpaired bases (Hilbers et al., 1991; 1994; Blommers et al., 1989; Germann et al., 1990; Ippel et al., 1994; Antao et al., 1991). The differences in stability were attributed to the differences in base stacking patterns in the single strands and double helical stems of the hairpin. That is, the geometry (left- or right-handedness) of the stem determined the optimal number of bases in the loop which give the maximum stability to the hairpin. The structure and thermodynamics of the mini hairpin-loops (size 2) depend on the closing base pair and also on the base sequence of the loop residue (Hilbers et al., 1994; Ippel et al., 1994; Antao et al., 1991).

A bulge is formed by the interruption of two double helical segments, which stack upon each other, with a single-stranded region in one strand that loops out. An internal loop arises when short regions of unpaired bases opposite each other interrupt the double helix.

1.2 Pseudoknots

A pseudoknot is known as the RNA secondary structure that forms when single-stranded regions of a hairpin loop base pair with their complementary sequence outside of the double-helix on the other end of the stem. The most studied pseudoknots are classified as H-type [Pleij et al., 1985]. The H-type pseudoknot consists of two helical stems with minimum length of two to three base pairs and two connecting loops. The two helical stems seem to stack coaxially to form a quasi-continuous double helix.

One of the first pseudoknot to be studied was found in the turnip yellow mosaic virus (TYMV) RNA (Rietvield et. al 1982). Others were found in non-coding regions of tobacco mosaic virus (TMV) RNA (van Belkum et al., 1985). They were eventually also found in eukaryotic messenger RNAs (mRNAs) where they are involved in ribosomal frameshifting, in prokaryotic mRNA where they are involved in translational regulation and in the ribozymes where they appear to play a role in the folding of the catalytic center (Pleij et al., 1990; Kang et al., 1997; Shen & Tinoco, 1995; van Belkum et al., 1985; Rietveld et al., 1982;).

Tertiary structures in DNA and RNA.

1.1 Ribozymes

Ribozymes are RNA molecules that catalyze biochemical reactions. The catalytic property of RNA was first observed for the self-splicing of the introns of *Tetrahymena* rRNAs (Cech et al.,

1986; Cech 1987). Other catalytic RNA molecules have been described. These include the hammerhead, hairpin, and the Hepatitis delta virus (HDV) ribozymes as well as the RNA subunit of Ribonuclease P (RNAse-P). To date only the tertiary structures of the Group I intron splicing complex (Michel and Westhof, 1990; Cate et al., 1996; 1997), HDV ribozyme (Kolk et al., 1997) and the hammerhead ribozymes (Simorre et al., 1997) have been established.

1.2 Quadruplexes

The ends of eukaryotic chromosomes consist of short repetitive sequences containing clusters of guanines (telomeres). The guanine-rich single-strand runs in the 5'-3' direction toward the end of the chromosome resulting in a 3' overhang of several repeats. These sequences can fold up to form intramolecular four-stranded structures that are linked together by guanine quartets (G-quartets) (Guschlbauer et al., 1990; Sen and Gilbert, 1988; 1990; Williamson et al., 1989; Sundquist and Klug, 1989). An intermolecular G-quartet structure can be formed from four parallel strands with each strand contributing a guanine residue to each quartet formed [Sen and Gilbert, 1988; 1990; Jin et al., 1992). Alternatively, two hairpins can dimerize to form an antiparallel complex (Sundquist and Klug, 1989; Henderson et al., 1990; Williamson et al., 1989). Intramolecular quadruple helix structures have also been studied (Panyutin et al., 1990; Harding et al. 1991; Williamson et al., 1989).

The formation of the guanine quartets is highly and specifically cation dependent with sodium and particularly potassium ions being notably the most effective in determining the conformation and stability of these structures (Sen and Gilbert, 1990; Harding et al., 1991; 1992; Lu and Kallenbach, 1992). Oligomer sequences containing tracts of cytidine residues are known to form "i-motif" tetraplexes from two parallel-stranded duplexes that are stabilized by two sets of

intercalating hemi-protonated C•C^+ base pairs (Chen et al., 1994; Mergny et al., 1995; Gehring et al., 1993).

1.3 Triple-helical structures

Triple helix formation involves the interaction of the Watson-Crick pyrimidine-purine duplex with a third strand, resulting in an inter- or intramolecular structure. The third strand lies in the major groove and binds to the purine strand of the Watson-Crick duplex through Hoogsteen or reversed Hoogsteen hydrogen bonds to result in one of two different motifs: the pyrimidine or the purine motif [Beal and Dervan, 1991; Moser and Dervan, 1987].

In the pyrimidine motif, the third strand binds parallel to the purine strand of the duplex by Hoogsteen hydrogen bonding resulting in CG•C^+, TA•T or UA•U base triads (pyrimidine.purine•pyrimidine or py.pu•py), **Figure1.1.** (• Represents the non-Watson–Crick interaction). In the purine motif, the third strand binds antiparallel to the purine strand of the duplex by reverse Hoogsteen hydrogen bonding, forming the pyrimidine.purine•purine (py.pu•pu) triads. Common base triads formed in the purine motif include CG•G and TA•A, **Figure1.1**.

Triple helix formation and stability is greatly influenced by base sequence, base modifications, chain length, the nature of the backbone, ligands and solution conditions (pH, ionic strength) (Plum et al., 1995). For instance, the requirement for the formation of the CG•C^+ triads is that the cytosines of the third strand are protonated at N3 to be able to form the second hydrogen bond with the N7 of guanine of the Watson-Crick duplex. However, the pH dependence can be removed by using modified cytosines e.g., 5-methylcytosine (m^5C), (Xodo et al., 1991; Lee et al., 1984). Methylation of the cytosine on C5 has been shown to enhance triplex formation at

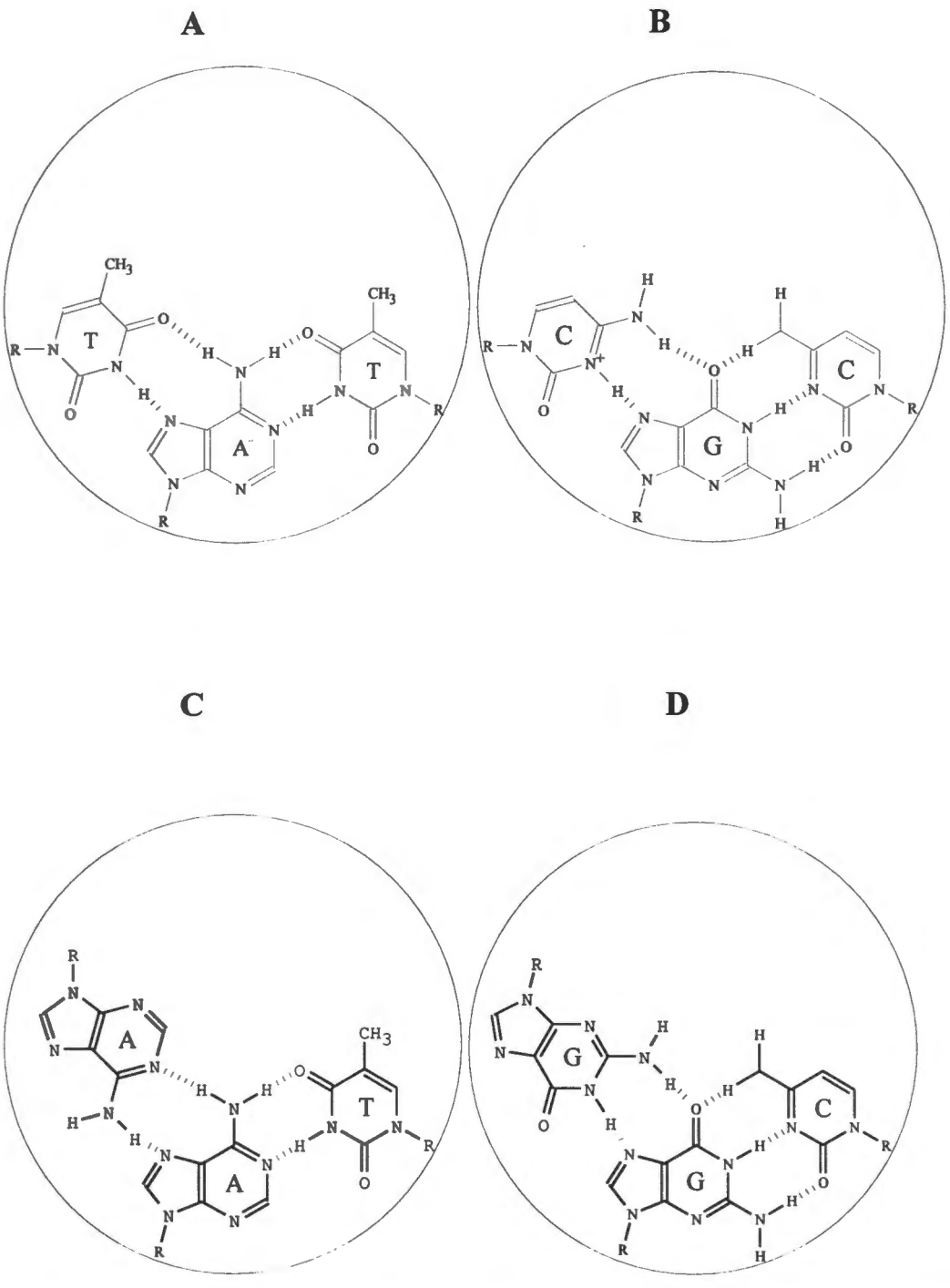

Figure 1.1: The common base triads formed in the pyrimidine motif, (A) TAT and (B) CGC^+, and in the purine motif, (C) AAT and (D) GGC. The third strand bases binds into the major groove of the target duplex DNA *via* Hoogsteen or reverse Hoogsteen hydrogen bonding.

neutral pH and to have raised the melting temperature (Tm) of the triple helix by 10°C. The stabilizing effect of the 5-methyl group may result from favorable changes in vertical base stacking interactions.

Other bases such as 2'-O-methylpseudoisocytidine (Ono et al., 1991b) and N6-methyl-8-oxo-2-deoxyadenine (Jetter and Hobbs, 1993) have been used as they do not require protonation for Hoogsteen hydrogen bond formation. Whereas the CG•C^+ formation is pH dependent, the triplets containing the G/T bases in the third strand do not require protonation of cytosines to form but require high concentrations of divalent cations. It has been shown that these triplexes are destabilized by potassium (Cheng and Van Dyke, 1993; Olivas and Maher, 1995a). Similarly, triplex formation involving the G/T bases can be enhanced by the use of modified guanine and thymine residues such as 7-deazaxanthine (replacing thymine) and 7-deazaguanine for guanine (Milligan et al., 1993). The guanine-rich oligonucleotides have a tendency to form guanine quartets in the presence of K^+ and Na^+. This can lead to competition between triplex and tetraplex formation. The hydrogen bonding pattern leading to tetraplex formation is disrupted by the introduction of 7-deazaguanine. This replacement also decreased triplex stabilization.

Other factors that decrease the binding affinity of the third strand to the Watson-Crick double helix are abasic sites, extra bases and mismatches as part of the binding sequence. A single mismatch destabilizes the triplex by 2.5 – 6.0 kcal/mol (Roberts and Crothers, 1991). In addition to the position of mutations, length and sequence variations have an influence on the extent at which the triplex is destabilized.

Since the discovery of triple helices and the possibility that they may form in living cells, focus has been directed to the possible biological roles triple helices may play in processes such as replication, transcription, recombination, chromosome folding and mutational processes (Sinden

1994; Murray and Morgan, 1973; Manor et al, 1988; Hampel et al., 1993; Sinden and Wells, 1992; Ruskin and Green, 1985.

1.4 DNA junctions

1.4.1 Four-way junctions

1.4.1.1. Design of four-way junctions

Homologous genetic recombination involves breaking, exchanging and rejoining of strands within two homologous DNA duplexes. The process proceeds via an unstable intermediate called the four-way junction (Holliday junction) (Holliday, 1964; Broker and Lehman 1971). The four-way junction then undergoes branch migration that leads to rapid resolving of the junction to two double helices. Branch migration occurs as a result of the two-fold sequence symmetry at the branch point.

Potential cruciform formation in negatively supercoiled DNA also gives rise to mobile four-way junctions. For the cruciform to form the DNA molecule from which it is formed has to be negatively supercoiled and the sequence should have a two-fold symmetry (palindrome) (Gellert et al., 1979; Panayotatos and Wells, 1981). Relaxation or cleaving of the supercoiled structure leads to the instability of the cruciform. It is very difficult to study naturally occurring branched molecules because of their inherent instability due to their sequence symmetry. However, studies done on cruciform structures showed that stable immobile four-way junctions could be constructed. Chemical probing experiments showed that base pairing was not perturbed when the junctions were reacted with bisulphite (Gough et al., 1986) and/or diethyl pyrocarbonate (Furlong and Lilley 1986) which should react with unpaired bases. Similarly, NMR results

showed that canonical base pairing occurs throughout the structure including the base pairs in the vicinity of the branch point (Wemmer et al., 1985).

The construction of the stable four-way junctions is achieved by minimizing or complete removal of the sequence symmetry at the branch point depending on whether semi-mobile or immobile junctions are desired (Seeman, 1982; Seeman and Kallenbach, 1983). Semi-mobile junctions include monomobile junctions (Chen et al., 1988) and bimobile junctions (Lu et al., 1990a). The tetramer sequences that span the branch point should not be complementary to each other. To avoid formation of alternate structures that may compete with the junction, complementary linear sequences must also be removed. Other features can be incorporated into one or several arms of the junction without compromising the sequence at the branch point. These features include restriction enzyme recognition sites (Chen et al., 1989; Duckett et al., 1988); loops (Kimball et al., 1990; Mueller et al., 1991; Pikkemaat et al., 1994; 1996); nicks (Pöhler et al., 1994) and mismatches (Duckett & Lilley, 1991).

1.4.1.2. Solution structure of the DNA four-way junction

The structure of the four-way junction has been studied using a number of chemical and physical methods. The junction formation and molecular geometry has first been investigated by gel electrophoresis of junction J1 (Kallenbach et al, 1983; Chen et al., 1988; Seeman et al., 1989). Earlier studies on the structure of the Holliday junction by Sigal and Alberts (Sigal and Alberts, 1972) suggested that the structure adopted a particular geometry where the helical arms stack pairwise onto each other, forming two stacked helical domains. The same pattern was observed for synthetic junctions. Cleavage of J1 by hydroxyl radicals showed that the structure has a two-fold symmetry, consistent with a conformation in which the helical domains stack pairwise as

proposed by Sigal and Alberts (Churchill et al., 1988). This was further confirmed by transient electric birefringence studies (Cooper and Hagerman, 1989), flourescence energy transfer studies (Murchie et al., 1989) and gel electrophoresis (Cooper and Hagerman, 1988).

1.4.1.3. Divalent metal ions are required to fold the DNA four-way junction into a 'stacked X-structure'.

Divalent metal ions play an important role in the structure and stability of the four-way junction. In the absence of magnesium ions, the four-way junction adopts the extended (open) conformation with a pseudo-four-fold symmetry, (cf. **Figure 1.2,** p12). In the open conformation, the bases at the branch point are not stacked and therefore are susceptible to cleavage by chemical probes such as Osmium tetroxide, OsO_4, (Duckett et al, 1988). Smaller junctions, that is, junctions with arms containing less than 25 nucleotides, do not form at room temperature in the absence of divalent cations. In the presence of sufficient metal ions, the four-way junction folds by pairwise stacking of helical arms to yield two quasicontinuous double helices. The two-fold symmetry further generates two types of strands, the continuous and the "crossover" strands. The continuous strands can run either parallel or antiparallel to one another. However, it is shown that the preferred conformation (see **section 1.6.4.**) of the four-way junction has the two continuous strands antiparallel instead of the previously suggested parallel conformation of the Sigal-Alberts junction (Cooper and Hagerman, 1989; Sigal and Alberts, 1972; Murchie et al., 1989). The restriction enzyme *Mbo*II was used to investigate the presence of coaxial stacking of helical arms (Murchie et al., 1991). *Mbo*II is the restriction enzyme with a recognition site a few nucleotides away from the cleavage site within the same duplex. By designing junctions with the *Mbo*II recognition site positioned on one arm and the restriction site

on its coaxial stacking partner, it was observed that the cleavage pattern corresponded to the coaxial alignment of the two arms. The two quasicontinuous helices are rotated in a right-handed conformation resulting in the X-shaped molecule called 'the stacked X-structure'. Coaxial helix-helix stacking is a mutual structural feature of junctions and provides additional stability.

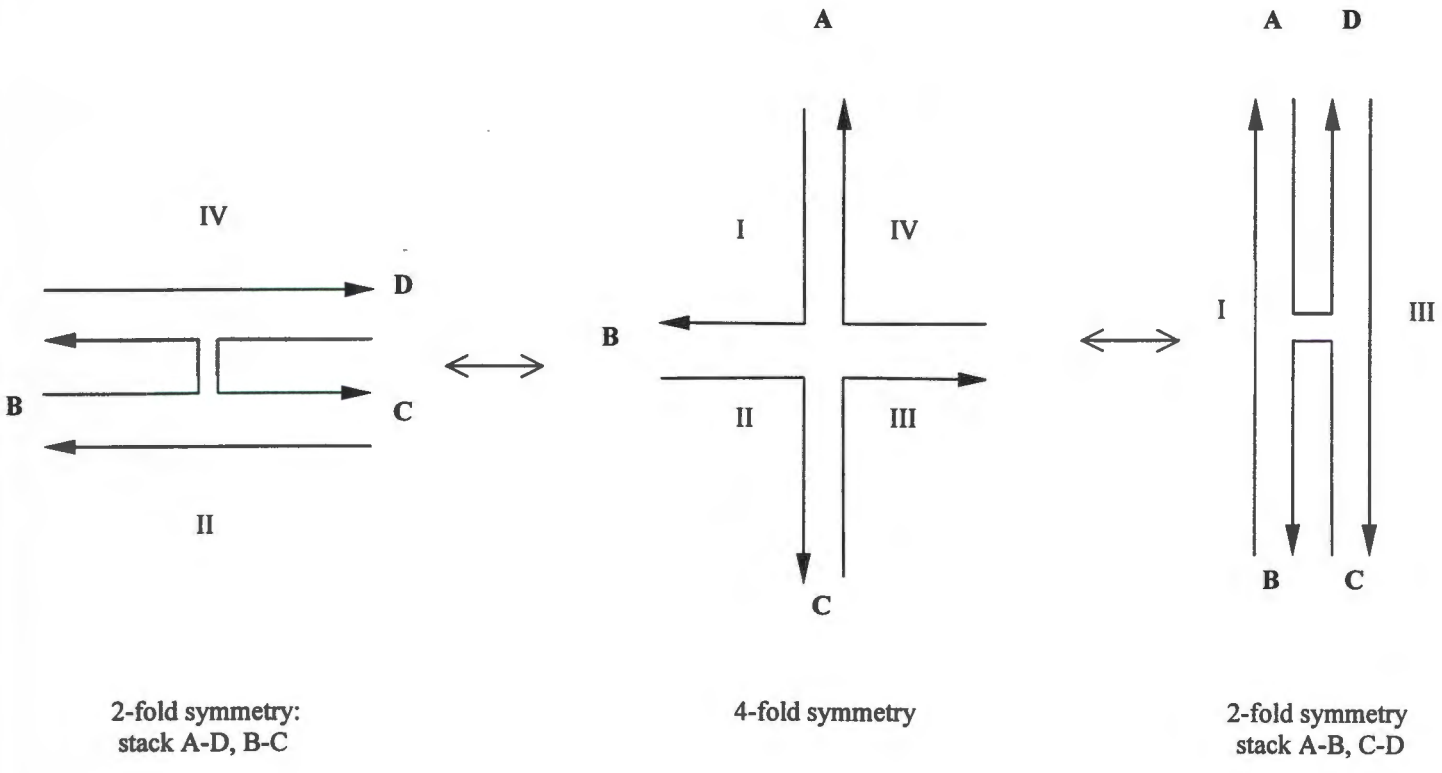

Figure 1.2: Schematic illustration of the unstacked 4-fold symmetric four-way junction (middle structure) and its two different fully stacked conformers

Monovalent metal cations do not support the folding of the four-way junction with the same efficiency as divalent cations. Group I metal cations are capable of folding the four-way junction into the stacked X-structure but high concentrations are required to induce such folding (~500mM) (Duckett et al., 1988). Group II cations fold the structure at concentrations of ~100μM. Multivalent (spermine and hexamminecobalt (III)) cations) are the most efficient in supporting folding the four-way junction at low concentrations (<2μM).

1.4.1.4. Stacking conformers in a four-way junction

The folding of the four-way junction into the stacked X-structure generates two stereochemically equivalent conformers (isomers) that differ in the choice of the stacking partners, (cf. **Figure 1.2**). Several studies on four-way junction show that one conformer is usually preferred over the other. The choice of the stacking partner is considered to be dependent on the nucleotide sequence at the branch point (Carlström et al., 1996). However, the possibility of both conformers existing simultaneously could not be ruled out. Using the enzyme *Mbo*II, it was shown that both conformers coexisted and appeared to be equally stable under specified conditions (Murchie et al., 1991; Grainger et al., 1998). Specified conditions refer to the bases at the branch point and the type of counterions used.

Overmars and Altona measured the rate of exchange between two stacked conformers and their life times using NMR. In the presence of 15mM $MgCl_2$, the NMR resonance's corresponded to the presence of the two stacked conformers in slow dynamic equilibrium. The unfolded (open) structure was not observed at 15mM Mg^{2+} concentration (Overmars and Altona, 1997). On the other hand, Miick et al. (Miick et al, 1997) showed that both conformers co-existed at equilibrium by using deconvolution of time-resolved fluorescence spectra.

1.4.1.5. Intramolecular four-way junctions

Previously, studies on conformational states of DNA four-way junctions were executed on intermolecular junctions. Based on the data obtained from such studies further improvement of the stability and the structure of the four-way junctions could be achieved. Recently, studies done on four-way junctions folded up from linear DNA sequences to form stable intramolecular junctions have been reported (Pikkemaat et al., 1994; 1996; Overmars and Altona, 1997; Overmars et al., 1997; Makube et al., 1999). A selected feature of these intramolecular junctions is that the length of the arms has been greatly reduced (three base pairs in each arm) as compared to the intermolecular junctions where the smallest junction contains eight base pairs per arm (Kallenbach et al., 1983; Carlström and Chazin, 1996). Further advantages of the intramolecular structure are that its thermal stability is independent of the oligomer concentration and that the conformational entropy is grossly reduced, which again improves the thermal stability.

The junction was designed to facilitate NMR studies in the first place, (cf. **Figure 1.3)** (Pikkemaat et al., 1994). NMR studies of this junction, named J4, demonstrate that in the presence of 5 to 15mM magnesium ions maximal base pairing is observed throughout the arms and at the branch point. The absence of cleavage of the thymines abutting the branch point by OsO_4 under the same salt conditions further confirmed this. The helices are fully stacked and the major part of the structures adopts the B-DNA conformation (Makube et al, 1999). These results were confirmed for all other studied four-way junction. What remained a mystery though was the preference of one conformer over the other (cf. **section 1.6.1.4**), in this case the AD/BC stack was preferred over the AB/CD conformer, **Figure 1.4.**

To investigate this further, an analogue of J4, J4M was designed. J4 and J4M contain the same base sequence with the only difference that the latter contains an uncharged methylene-acetal

linkage, O3'-CH_2-O5' instead of a normal phosphodiester linkage –O3'-PO_2-O5'- between residues T18 and C19 at the branch point, **Figure 1.3**. NMR results showed no differences between the two structures and that even when the negative charge is removed (less crowding of charges at the branch point), the AD/BC remains the preferred conformer. That is, there are other factors besides the electrostatic interactions that play an important role in determining the folding pattern of the junction. The thermodynamic properties of both junctions are discussed below.

1.4.2.1. Three-way junctions

Three-way junctions are commonly found in RNA tertiary structures. The first synthetic three-way junctions to be studied were termed tight or perfect junctions where all the three arms of the junction are fully base-paired. In the absence of magnesium ions, the three-way junction adopts an extended Y- shaped conformation in which the arms point toward the corners of an equilateral triangle. Unlike the DNA four-way junction which, in the presence of sufficient metal ions, folds into a stacked structure with a two-fold symmetry, the three-way junction adopts an asymmetric conformation where two of the three arms can be stacked coaxially but remain extended. This is shown by the reactivity of thymine residues at the branch point with OsO_4 in the presence or absence of $MgCl_2$ (Lu et al., 1991) and the reactivity of purine residues located at the branch point with diethyl pyrocarbonate. The helix-helix stacking, as commonly observed with four-way junctions, will require the disruption of at least two base pairs at the branch point. Leontis et al (1995) showed that including unpaired nucleotides at the branch point results in two of the arms stacked to form a quasicontinuous helix. The third arm is pointing away from the branch point. The folding of the three-way junction into a structure with stacked helices generates two non-identical conformers.

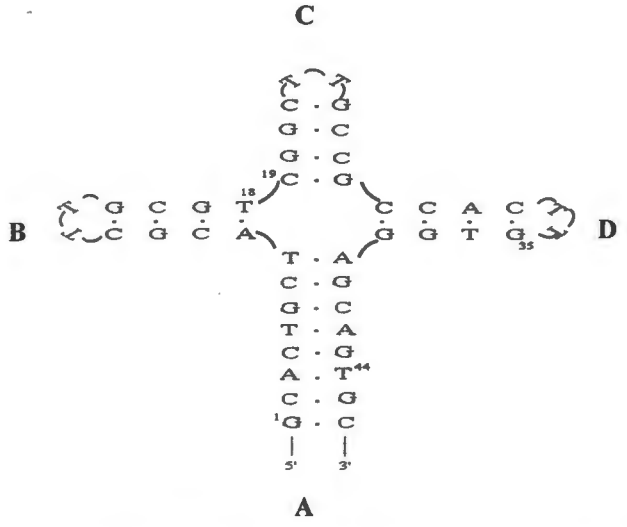

Figure 1.3: Structure of the four-way junction, J4, in the absence of Mg^{2+} ions.

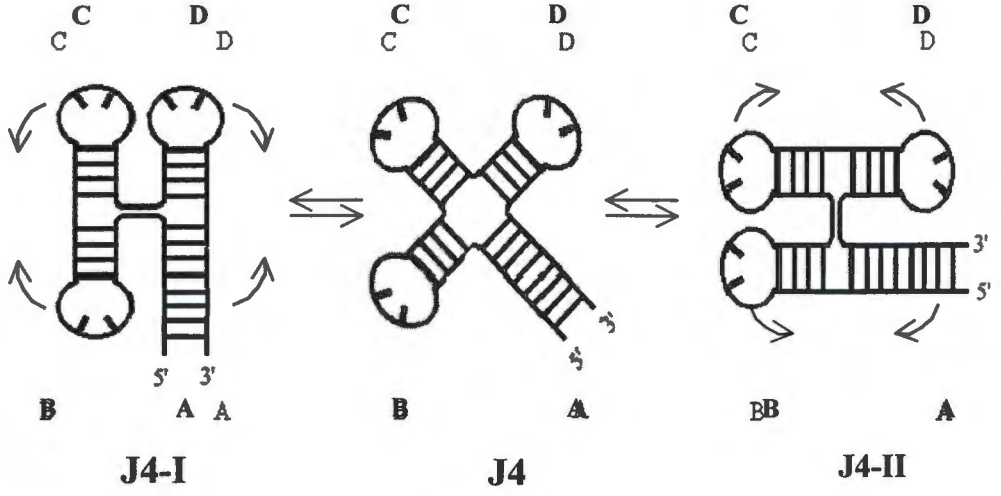

Figure 1.4: Equilibrium between the unfolded (J4) and two possible folded conformers, (J4-I and J4-II) on addition of $MgCl_2$ at ambient temperatures.

However, it was found that one conformer is preferred over the other, similar to the result observed with the four-way junctions. The prevalence of one conformer over the other suggest that the sequence at the branch point together with the type of metal ion present are not the only factors that determine the specific geometry of the three-way or four-way junctions. It is, however, not quite clear what role Mg^{2+} plays in the three-way junction structure as there are conflicting results. Folding of some three-way junction is dependent on Mg^{2+} (Leontis et al., 1995; Welch et al., 1995) whereas other junctions fold in the absence of Mg^{2+} (Overmars et al., 1996; Rosen and Patel, 1993a).

Lately third strands have been successfully incorporated into the double-helical three-way junction to form triple helices (Hüsler and Klump, 1994; 1995). This entailed careful design of stable triple-helical junctions where the requirements for junction formation as well as for the triplex formation are met. Two triple-helical three-way junctions, Watson-Crick and Hoogsteen junctions which differ in the arrangement of the branch point and the position of the loop at the ends of the arms, were constructed from three 33-mer oligonucleotides. The sequential folding of single strands to form the triplex structure was clearly shown by pH titration. This was confirmed by polyacrylamide gel electrophoresis (native and temperature gradient) where the formation of the complete triple-helical three-way junction was shown by the presence of single band corresponding to the equal molar ratios of the strands forming the junction. The presence of the triple helix conformation was further confirmed by CD spectroscopy, which is sensitive to the conformational changes of nucleic acids.

CHAPTER 2

Thermodynamics of DNA triple helices, three- and four-way junction formation

The DNA helix formation and structural stability is governed by base-base stacking interactions and the specific Hydrogen bonding between the bases. The helix stability and its resistance to coil formation is greatly influenced by a number of variables such as selection and concentration of counterions, pH, mismatches between bases, strand concentration and backbone or base modifications. The analysis of the Hydrogen bonding and stacking interactions in terms of the helix stability allows the theoretical prediction of thermodynamic properties of any DNA sequence. The comparisons of the predicted thermodynamic data using the nearest-neighbor parameters with the experimental data often are in good agreement. However, the results from different groups differ substantially (Klump 1990; Delourt and Blake, 1991; Breslauer et al., 1986; Gotoh, 1983). Blake and Delcourt (1998) have recently improved the nearest-neighbor parameters. They have accurately measured the melting temperatures and calculated enthalpies of unfolding of synthetic sequences using high resolution UV melting curves.

The thermodynamic properties of double and triple helices and the factors affecting their stability have been reported (Cheng and Pettitt, 1992; Soyfer and Poteman, 1986; Plum et al, 1990). The prediction of the thermodynamic properties using a nearest-neighbor stacking model works well for the normal Watson-Crick duplex. The model fails to explain the stability of triple helices and any other structural deviation from the canonical Watson-Crick duplex because of the complex nearest-neighbor interaction pattern observed. E.g. in case of the four-way junctions, the NMR chemical shifts displayed by the bases at the branch point showed significant changes compared

to the same base-base interactions in the canonical B-DNA. This suggest that the vertical base-base stacking at the branch point differs from that in linear B-DNA (Overmars et al., 1997).

2.1. Thermodynamic principles

The change in UV absorbance during melting

The thermal unfolding of highly ordered nucleic acid structures can be monitored by following the change in UV absorbance with increasing temperature. The thermal transition obtained can be used to determine the thermodynamic parameters ($\Delta H°$, $\Delta S°$ and $\Delta G°$) relevant to the formation (or unfolding) of the structure given. The melting temperature, Tm, is defined as the temperature at which 50% of the helix is denatured. The van't Hoff transition enthalpy ($\Delta H°_{VH}$) for a process of any molecularity can be derived from the following equation:

$$\Delta H°_{VH} = 2(n+1)RTm^2(\partial\alpha/\partial T)_{Tm}$$

where R is the gas constant, Tm is melting temperature in °K (where $\alpha = 0.5$), n is the molecularity (number of strands involved) and α is the degree of transition. For the validity to calculate $\Delta H°_{VH}$ this way, it is generally assumed that the transition is cooperative and proceeds in a two-state (all-or-none) manner.

Another way of determining the $\Delta H°_{VH}$ is provided by measuring the concentration dependency of the melting temperature. This is given by the equation

$$\frac{1}{Tm} = \frac{(n-1)R}{\Delta H°_{VH}} \ln C_T + \frac{[\Delta S°_{VH} - (n-1)R\ln 2 + R \ln n)}{\Delta H°_{VH}}$$

where C_T is the total strand concentration. The plot of 1/Tm vs $\ln C_T$ yields a straight line with the slope $(n-1)R/\Delta H°_{VH}$. The $\Delta H°_{VH}$ can be calculated from the slope. $\Delta S°_{VH}$ represents the van't Hoff transition entropy. The $\Delta S°_{VH}$ is given by the equation

$$\Delta S°_{VH} = \Delta H°_{VH}/Tm$$

Both the thermodynamic parameters can be calculated for T = Tm.

The free energy of the system can be calculated from either of the following equations:

$$\Delta G°_{VH} = \Delta H°_{VH} - T(\Delta S°_{VH})$$

or

$$\Delta G°_{VH} = \Delta H°_{VH}(1-T/Tm)$$

This equation allows calculating the $\Delta G°$ at any temperature. This is valid under the assumption that $\Delta H°_{VH}$ is temperature independent.

Calorimetry

The assumption that the unfolding follows an all-or-none process does not usually hold for longer oligonucleotides when the cooperative unit is not identical with the molecule. Thus, the calculated ΔH_{VH} might not reflect the actual value. The model-independent transition enthalpy (ΔH_{cal}) e.g. per mole base pairs can be measured directly using differential scanning calorimetry (DSC). In DSC measurements, the difference in electric power supplied to the sample to match the temperatures of the sample and the reference solution, which is proportional to the difference

in heat capacity [excess heat capacity (ΔCp)] of the sample and the reference solution is recorded as a function of temperature over the transition interval. The reference cell contains the appropriate solution to cancel out changes in heat capacity due to the aqueous buffer media in sample and reference. The remaining differences refer only to the unfolding of the biopolymer. ΔH_{cal} is given by the following equation:

$$\Delta H_{cal} = \int \Delta Cp(excess) \, . \, dT$$

Integrating the area under the graph of the excess heat capacity versus temperature curve gives the $\Delta H°_{cal}$. To calculate the molar value the polymer concentration has to be taken into account. The entropy and the free energy of the system are given by the following equations respectively:

$$\Delta S_{cal} = \int Cp(excess).dT / T$$

and

$$\Delta G_{cal} = \Delta H_{cal} (1 - T / Tm)$$

The ratio of ΔH_{cal} over Tm provides the direct entropy change due to the transition.

By comparing the model-dependent ΔH_{VH} and the model-independent ΔH_{cal}, it is possible to determine if the thermal transition proceeds in a two-state manner. If the ratio of ΔH_{cal} and ΔH_{VH} equals one then the transition proceeds in a two-state manner. If $\Delta H_{VH} < \Delta H_{cal}$ then the transition involves intermediate states (Marky and Breslauer, 1987).

2.2. Thermodynamics of the formation triple-helical DNA structures.

The availability of thermodynamic data referring to triplex structure formation is increasing with time yet the data is insufficient to draw general conclusions pertaining to the general structure and energetics of specific triplexes. The data are obtained under different conditions (pH, strand concentration, ionic strength, sequence composition) and as such cannot be directly compared. The thermodynamic data obtained for various studied triplexes are discussed in the literature (cf. Cheng and Pettitt, 1992; Soyfer and Potaman, 1996). The data include the inter- and intramolecular py.pu•py and py.pu•pu triplexes. Important findings arises from these studies and they are as follows:

- Within the triple helices, the third strands are generally less stable than their corresponding Watson-Crick duplex structures (Plum et al., 1990; Pilch et al. 1990a; Manzini et al., 1990).
- Under the same solvent conditions, intermolecular triplexes are less stable than the corresponding intramolecular triplexes. For intramolecular triplexes, the hairpin duplex and its single-stranded overhang are covalently linked and therefore in close proximity to each other. The orientation of the Watson-Crick and Hoogsteen strands are pre-determined by the position of the loop and the hairpin as compared to the intermolecular triplex structure where the three strands are free to align in different orientations. Further advantages of working with an intramolecular structure are that firstly its stability is independent of the oligomer concentration and secondly the conformational entropy is grossly reduced, which contributes to an improved thermal stability.
- CG•C^+ triads are stabilized at acidic pH (Pilch et al., 1990; Xodo et al., 1990; Plum and Breslauer, 1995a; Manzini et al., 1990; Völker et al, 1993; Hüsler and Klump, 1995; Rougée

et al., 1992; Shindo et al., 1993). This appears to hold under conditions were the pH of the solution is above the pKa of cytosine (pKa ~ 4.5). Decreasing the pH of the solution below the pKa of cytosine has a destabilizing effect on both the triplex and the underlying duplex (Völker and Klump, 1994; Hüsler and Klump, 1995).

- The adjacent protonated cytosines appear to have less destabilizing effects on the triplex stability at acidic pH than at neutral pH (crowding) (Völker and Klump, 1994).
- py.pu•py triplexes have larger ΔH_{VH} values than ΔH_{cal} values (Plum and Breslauer, 1995a; Plum et al., 1995b).
- Triplexes are stabilized by mono- and divalent cations (Krakauer and Sturtevant, 1968; Felsenfeld et al., 1957). Divalent ions are more effective in stabilizing the triplex structures. However, the relative stability of the TA•T and the CG•C^+ triads differ at different salt concentrations. Under acidic pH and high salt conditions, some CG•C^+ triads are destabilized whereas the TA•T triads are always stabilized at high salt concentration. Mg^{2+} and other divalent metal ions are effective in stabilizing the pyr.pur•pur (Lyamichev et al., 1990, 1991; Durand et al. 1992a; Frank-Kamenetskii et al., 1991).
- Mismatches (mutations) and abasic sites destabilize the triplex structure (Roberts and Crothers, 1991; Xodo et al, 1993; Mergny et al, 1991b). The thermodynamic studies of the unfolding of triplexes containing a single mismatch showed a decrease in the free energy of about 2.5 to 6 kcal/mol. Furthermore, the replacement of cytosine and/or thymine in the third strand with inosine destabilizes the triplex relatively to the unmutated structure (Mills et al, 1996). The inclusion of inosine tends to distort the backbone and reduce the stacking interactions. The effect is more pronounced when the cytosine is replaced because of the loss of the ion pair between the protonated cytosine and the backbone. Horne and Dervan showed

that a single abasic site eliminated two stacking interactions, which resulted in the decrease of binding affinity and energy of the third strand (Horne and Dervan, 1991).

2.3. Thermodynamics of the three and four-way junction formation.

The free energy associated with the branched DNA formation is the sum of the free energy contributions of several components of the structure. As with all other DNA structures, the structure of the branched molecules is held together and stabilized by the Hydrogen bonds as well as the base-base interactions (stacking). Different groups have studied the thermodynamics of branch formation and here is a summary of some of the results obtained.

2.3.1. The antiparallel four-way junction is more stable than the parallel four-way junction.

The preferred conformation of the fully stacked four-way junction is right-handed and antiparallel (Lu et al., 1991). Lu et al. constructed two junctions, JA and JP, to determine the differences in free energies between the two junctions. The junctions were constrained to adopt either the parallel (JP) or antiparallel (JA) conformation by means of single stranded $d(T)_9$ tethers. The stability of the JP and JA four-way junction was compared using a competition assay and UV thermal melting experiments. It was found that the difference in the free energy between the two conformations is only 2kcal.mol^{-1}, which is sufficient to render the concentration of the parallel conformer negligible. However, this was not conclusive because JA and JP were not equivalent. That is, the size of the hairpin in JA might have had a destabilizing effect on the junction.

2.3.2. Stacking conformers of the four-way junction

Differences in pairwise coaxial stacking of two arms each of the four-way junction has, in most of the experiments performed, resulted in the presence of only one conformer while the stacking alternative was absent. Some experiments suggest that the two types of conformers exist simultaneously at equilibrium. This observation seems to be supported by the small free energy differences (~2 kcal/mol) found between the two conformers. It is expected in any case that the helix-helix stacking should stabilize both conformers in a comparable way.

2.3.3. Thermodynamic parameters of the formation of a four-way DNA junction.

The unfolding of the intermolecular four-way DNA junction J1 was investigated using UV absorbance change as a function of temperature (melting) and DSC at 0.2M Na^+ and 10mM Mg^{2+}(Marky et al., 1987). The thermodynamic properties of the isolated arms were also studied. The results show that ΔH_{cal} (190 kcal/mol) for J1 more or less equals the sum (194 kcal/mol) obtained for individual arms, suggesting that there is no enthalpic barrier with regards to junction formation. Furthermore, $\Delta H_{cal} = \Delta H_{VH}$ which means that the melting behavior of J1 follows a two-state behavior.

Thermodynamic properties of two homologous four-way junctions, J4 and J4M based on 46-mer linear DNA molecules, were also determined ***(cf. Section 1.4.1.5)***(Makube et al., 1999). The comparison of the thermal unfolding of the J4 junction and J4M junction serves to elucidate the effect of an uncharged methylene-acetal linkage in the backbone on the stability of the junction. The analysis was based on UV absorbance spectroscopy and DSC. Almost identical melting temperatures and unfolding enthalpies were obtained for J4 and J4M both by UV (Tm; $H°_{VH}$) and DSC (Tm; H_{cal}). The vant't Hoff enthalpy derived from UV melting equals the enthalpy change

obtained by calorimetric, which means that the melting process of both structures proceeded in a two-state manner. All the results taken together support the conclusion that there are no conformational and energetic differences between J4 and J4M. That is, the inclusion of the uncharged methylene-acetal linkage at the branch point to reduce crowding of negative charges has no effect on the general stability.

The thermodynamic parameters of forming a four-way junction from duplex DNA were determined by Lu et al. (1992) using competition assay on polyacrylamide gels and titration microcalorimetry. The thermodynamic parameters ($\Delta H°$, $\Delta S°$ and $\Delta G°$) of DNA branching were determined for two junctions J1 and J1c and four duplexes D1, D2, D3 and D4 formed by the association of four 16-mer single strands. The free energy change associated with forming a four-way junction at 18°C from duplexes is relatively small, -1.1 kcal/mol, with the enthalpy changes equal to +27 kcal/mol and the entropy change equals +89 cal/mol.K. These values indicate that the free energy difference between the junction formation and the formation of the corresponding duplexes is small at low temperature (18°C).

2.4. The triple-helical three-way junction

The thermodynamic properties of a triple-helical three-way DNA junction were determined by following UV absorbance as a function of temperature and by DSC (Hüsler and Klump, 1994; 1996). Two types of triple helical junctions, the Watson-Crick and the Hoogsteen triplex, were constructed. Their thermal melting was then compared to the thermal melting of the isolated arms. The melting of the junctions into the contributing single strands was described by means of models using statistical thermodynamics. The mathematical models were used to calculate the transition enthalpies and entropies by means of non-linear regression. The thermodynamic

parameters of the two junctions are listed in **Table 2.1**. It is clear from the ΔH_{cal} values observed that the Watson-Crick triple-helical three-way junction is not completely folded at the branch point. This conclusion can be drawn from the obvious discrepancies between the sum of the enthalpies of separate arms as compared to the enthalpy changes for the complete junction. This is different for the Hoogsteen junction where the ΔH_{cal} of the junction is more or less equal to the sum of the ΔH_{cal} of the individual arms, indicating that the arms of the Hoogsteen three-way junction are completely folded and unperturbed at the branch point. The results show that third strands can be incorporated into branched DNA molecules. The results further highlight the fact that the Watson-Crick three-way junctions can be conformationally strained at the branch point.

Table 2.1: Thermodynamic properties of the WC and HG triple-helical three-way junctions together with their isolated arms. *

Structure	[a]ΔHcal	[b]ΔScal	Structure	[a]ΔHcal	[b]ΔScal
[c]Arm A (p4p5)	97.0	380.0	[d]Hp1hp2	45.0	142.9
[c]Arm B (p6p7)	128.0	697.0	[d]Hp1hp3	60.8	192.6
[c]Arm C (p8p9)	135.9	399.4	[d]Hp2hp3	63.7	205.0
[c]WC junction	259.8	778.0	[d]HG junction	163.2	518.2
Total sum of arms	361.6	1176.4	Total sum of arms	170.6	540.5

[a] ΔH units are kcal.mol^{-1} (1 cal = 4.18J).
[b] ΔS units are cal. mol^{-1}.K^{-1}
[c] Buffer: 20mM Na_3PO_4, 1M NaCl
[d] Buffer: 20mM Na_2HPO_4, 1M NaCl
Error margins are less than 5%.
*Data was extracted from The Ph.D. thesis of P Hüsler, 1995

MATERIALS AND METHODS

CHAPTER 3

3.1. Design and formation of the triple helical DNA four-way junction.

The requirement for the double helix formation or any multistranded DNA structure is the presence of aqueous medium. Depending on the sequence composition, the pH of the solvent, the amount of hydration and the type and extend of salt present, DNA molecule will adopt different conformations. Some of these conformations are not stabilized by the canonical Watson-Crick base-base interactions. To achieve maximum stability all the variables that specifically control the stability of these structures have to be thoroughly defined.

The formation of the stable four-way junction requires that the sequence symmetry at or near the branch point should be removed. The potential for alternative base pairing must be eliminated to avoid formation of structures other than the envisioned junction. In addition to this, the type of cations and their amount present will play a significant role in determining the preferred conformation of all the structures possible in the given system.

The triple helix is formed when a third pyrimidine-rich strand binds to the purines in the homopurine.homopyrimidine Watson-Crick duplex via Hoogsteen hydrogen bonds. The third strand lies parallel to the purine strand of the Watson-Crick duplex forming either the TA•T and/or CG•C^+ triads. This is called the pyrimidine motif. In the alternative motif (the purine motif), the third strand lies anti-parallel to the purine strand and CG•G, TA•A or TA•T triads are formed. The CG•C^+ triad forms under acidic conditions and in some cases at reduced ionic strength. The TA•T triad is stable at neutral pH and at relatively high ionic strengths. Similarly the formation of the CG•G and TA•A triads is pH independent but it appears that divalent cations (Mg^{2+}) instead of monovalent cations are required for its stability.

This thesis is about the design of triple-helical DNA four-way junctions where the properties of triple helices and those of the four-way junction will be combined. Construction of such structures will require careful selection of sequences such that when hybridized they will result in stable junctions where none of the requirements for triplex or junction formation are compromised. A double-helical DNA four-way junction was formed from two 20-mer homopurine strands S1 and S3 and two 20-mer homopyrimidine strands S2 and S4 (single strands S1 – S4). The junction was designed in this manner to facilitate triple helix formation at a later stage. Hybridizing all four strands in a 1:1:1:1 ratio and under appropriate buffer conditions should result in the formation of a four-way junction (designated Js) containing four double-helical arms each containing 10 base pairs. The arms are labelled arm 1 to 4.

To form a triple helical four-way junction, the homopyrimidine strands of Js were extended either at the 3' or at 5' end to allow for a four-member cytosine loop to form and a third strand to bind *via* Hoogsteen hydrogen bonds. The extended pyrimidine strands were labelled T1, T2, T3 and T4 respectively. Two triple-helical four-way DNA junctions, J_{T1T3} and J_{T2T4}, were designed. J_{T1T3} is constructed from S1, S2, T1 and T3. S2 and S4 were each extended from the 3' to form T3 and T1 respectively. Hybridizing the strands in equimolar amounts and under appropriate buffer conditions will result in the formation of a triple-helical four-way junction containing four triple helical arms with two of the arms capped with a four-member cytosine loop. The junction is named according to the positions of the cytosine loops. In the case of J_{T1T3} the loops are capping arm 1 and arm 3. J_{T2T4} is constructed from homopurine strands S1 and S3 and homopyrimidine strands T2 and T4. In the case of J_{T2T4} S2 and S4 are extended from the **5'** end to form T2 and T4 respectively. The resulting triple-helical four-way junction should contain four triple-helical arms with the loops on arm 2 and arm 4, hence the name J_{T2T4} **(Fig 3.1).**

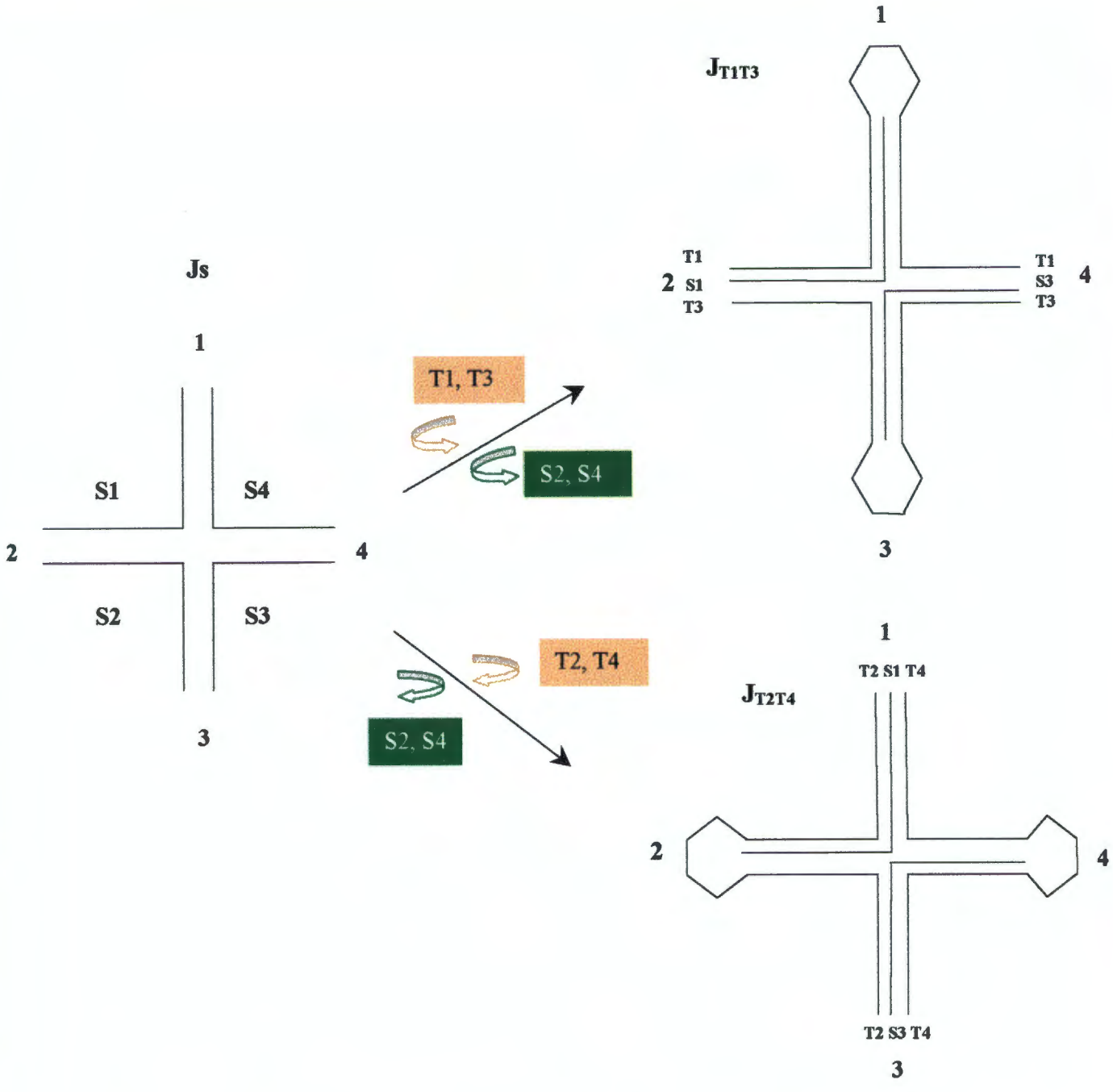

Figure 3.1: Schematic representations of Js and its triple helical analogues J_{T1T3} and J_{T2T4}. The triple-helical four-way junctions are made from the same sequences that make Js. The differences between the junctions are the positions of the loops. S1, S2, S3 and S4 represent the individual strands. Arabic numerals illustrate the arms. T1 and T3 of J_{T1T3} are made by extending the pyrimidine strands S2 and S4 at the 3' end. Similarly, extending S2 and S4 at the 5' end makes the T2 and T4 of J_{T2T4}.

To dissect the contribution of the different arms to the stability of the structure, four more junctions were constructed, labeled J_{T1} to J_{T4}. J_{T1} has the same Watson-Crick sequences as J_{T1T3} but contains only one extended homopyrimidine strand S4⇒T1 and thus forms a four-way junction with two triple helical arms (1 and 2) and two double-helical arms (3 and 4). The loop is positioned on arm 1. The same design principle is followed for the three other junctions respectively. In J_{T2}, the loop is on arm 2 and the triplex arms are 1 and 2 whereas the duplex arms are 3 and 4. In the case of J_{T3}, the loop is on arm 3 and the triplexes are in arms 3 and 4. For J_{T4}, the loop is on arm 4 and the triplexes in arm 3 and. It should be kept in mind that all the triple-helical junctions mentioned here contain the same core Watson-Crick double-helical four-way junction, Js.

3.2 Oligonucleotide synthesis and purification

The oligonucleotides listed below were synthesized on large scale (1000nm) on an Oligo 1000M DNA synthesizer (Beckmann Instruments) using sold-phase cyanoethyl phosphoramidite chemistry (Beacucage and Carothers, 1981). Samples were purified by an anion exchange HPLC using an acetonitrile gradient. The purity of the samples was further checked on the polyacrylamide gel electrophoresis. The concentrations of the oligonucleotides were determined spectrophotometrically in distilled water at 260nm and 90°C using extinction coefficients of 15400, 7400, 11500 and 8700 $M^{-1}.cm^{-1}$ for A, C. G and T respectively (Cantor et al., 1970). The following oligonucleotides were synthesized for this project:

D1 5' GAAAGGAGAA 3'
D2 5' TTCTTTTTTC 3'
D3 5' AGAAAGAAGG 3'
D4 5' TCTCTTCTCT 3'
D5 5' GAAAAAAGAA 3'

D6 5' AGAGAAGAGA 3'
D7 5' TTCTCCTTTC 3'
D8 5' CCTTCTTTCT 3'
S1 5' GAAAGGAGAAGAAAAAAGAA 3'
S2 5' TTCTTTTTTCCCTTCTTTCT 3'
S3 5' AGAAAGAAGGAGAGAAGAGA 3'
S4 5' TCTCTTCTCTTTCTCCTTTC 3'
LD1 5' TTCTCCTTTCCCCCCTTTCCTCTT 3'
LD3 5' CCTTCTTTCTCCCCTCTTTCTTCC 3'
T1 5' TCTCTTCTCTTTCTCCTTTCCCCCCTTTCCTCTTCTTTTTTCTT 3'
T2 5' CTTTCCTCTTCTTTTTTCTTCCCCTTCTTTTTTCCCTTCTTTCT 3'
T3 5' TTCTTTTTTCCCTTCTTTCTCCCCTCTTTCTTCCTCTCTTCTCT 3'
T4 5' TCTTTCTTCCTCTCTTCTCTCCCCTCTCTTCTCTTTCTCCTTTC 3'

Oligonucleotide	Extinction coefficient, ε, ($M^{-1}cm^{-1}$)
D1	138400
D2	84400
D3	138400
D4	81800
D5	146200
D6	138400
D7	81800
D8	81800
S1	284600
S2	166200
S3	276800
S4	163600
HS1	193200
HS2	193200
T1	359400
T2	362000
T3	359400
T4	276800

3.3. Osmium tetroxide modification reactions

Oligonucleotides were labelled at their 5'end termini with γ-^{32}P by T4 polynucleotide kinase (Boehringer). The purity of the labelled strands was checked by denaturing gel electrophoresis. Junctions were formed by annealing equimolar amounts of appropriate oligonucleotides in 10μl of 50mM Tris–HCl buffer (pH 5.0 or pH 8.0) at 90°C for 2 minutes which was followed by slow

cooling to room temperature. The Tris–HCl buffer contained both 10mM $MgCl_2$ and 100mM NaCl or no cations. Samples were consecutively incubated with 1mM OsO_4 and 1% pyridine in Tris-HCl buffer at 10°C (junctions) and 20°C (single strands) for 15 minutes. This was followed by cleavage with 1M piperidine at 90°C for 30minutes. Samples were ethanol precipitated, dried in vacuum and dissolved in 8µl of loading buffer ("blue juice"). Samples were heated to denature any secondary structure before loading on a 20% denaturing polyacrylamide gel. The gel was autoradiographed for 18 hours at 4°C.

3.4. Polyacrylamide gel electrophoresis

Gel electrophoresis was carried out in gels containing 20% acrylamide and 2% bis-acrylamide. TBE (89mM Tris, 89mM Boric acid and 0.5mM EDTA, pH 7.0) was the buffer used for the denaturing gels. Native gels were run with buffers containing 100mM Ammonium acetate, 10mM $MgCl_2$, and 100mM NaCl, pH 5.0 or pH5.5. Native gels were run for ~24hrs at 100V and 4°C. Buffers were circulated to maintain the specified pH values and the ionic strength. The gels were stained by "stains-all" dye (dissolved in equal amounts of water and formamide) and destained in distilled water.

3.5 Thermal denaturation monitored by UV absorbance

Absorbance at 260nm was measured as a function of temperature on a Pye-Unicam spectrophotometer equipped with a temperature controller interfaced to an analog to digital device (Oasis/4) and an IBM 386 computer. The temperature was increased at a heating rate of 1°C/min. The thermodynamic parameters were determined using a least square fitting procedure by means of the Levenberg/Marquardt algorithm.

3.6 Differential scanning calorimetry

The change in heat capacity as a function of temperature was recorded on a DASM-4 differential scanning calorimeter (Mashpriborintork, Moscow) interfaced to an analog to digital device (Oasis/4) and an IBM 386 computer. Data was collected at a rate of 1°C/min starting at 20°C ending at 100°C. Samples were rerun to ensure reproducibility and reversibility of the transitions.

DSC data was analyzed using MicroCal Origin Scientific plotting software (Microcal Inc., Northampton).

RESULTS

CHAPTER 4

4.1. The formation of the double –helical four-way junction, Js.

Js was combined from four separate 20-mer oligonucleotide strands (S1, S2, S3 and S4). S1 and S3 contain purines only whereas S2 and S4 consist of pyrimidines. The strands were designed that on mixing, a stable immobile four-way junction with four double helical arms is formed; **Figure 4.1**. Each arm contains 10 base pairs and is identified by the Arabic numerals. All arms of Js were also studied as isolated double helices to determine their individual contribution to the stability of the junction and to check whether base pairing is intact throughout the structure. (Hüsler and Klump, 1995; Marky et al., 1987). Binary complex D1D7, D2D5, D3D8 and D4D6 represent the arms 1, 2, 3 and 4 respectively.

4.1.1. Polyacrylamide gel electrophoresis

Four 20-mer oligonucleotides (S1, S2, S3 and S4) were mixed in a 1:1:1:1 ratio to form a complete double helical four-way junction, Js. The formation of the four-way junction has been examined using polyacrylamide gel electrophoresis under non-denaturing conditions. **Figure 4.2** shows the results of an electrophoretic separation on a 20% polyacrylamide native gel performed at 4°C in Tris-borate buffer containing 100mM Na^+ and 10mM Mg^{2+}. Lanes 1 to 4 contain single stranded oligonucleotides, S1, S2, S3 and S4 respectively. The binary combinations, S1S2, S1S3, S1S4, S2S3, S2S4 and S3S4 are present in lanes 5, 6, 7, 8, 9 and 10 respectively. Each combination runs as single band indicative of appropriate base pairing among the strands and the presence of only one type of species per lane (except S1S3 and S2S4). S1S3 and S2S4 complexes do not form base pairs but run as single bands because they are of the same size.

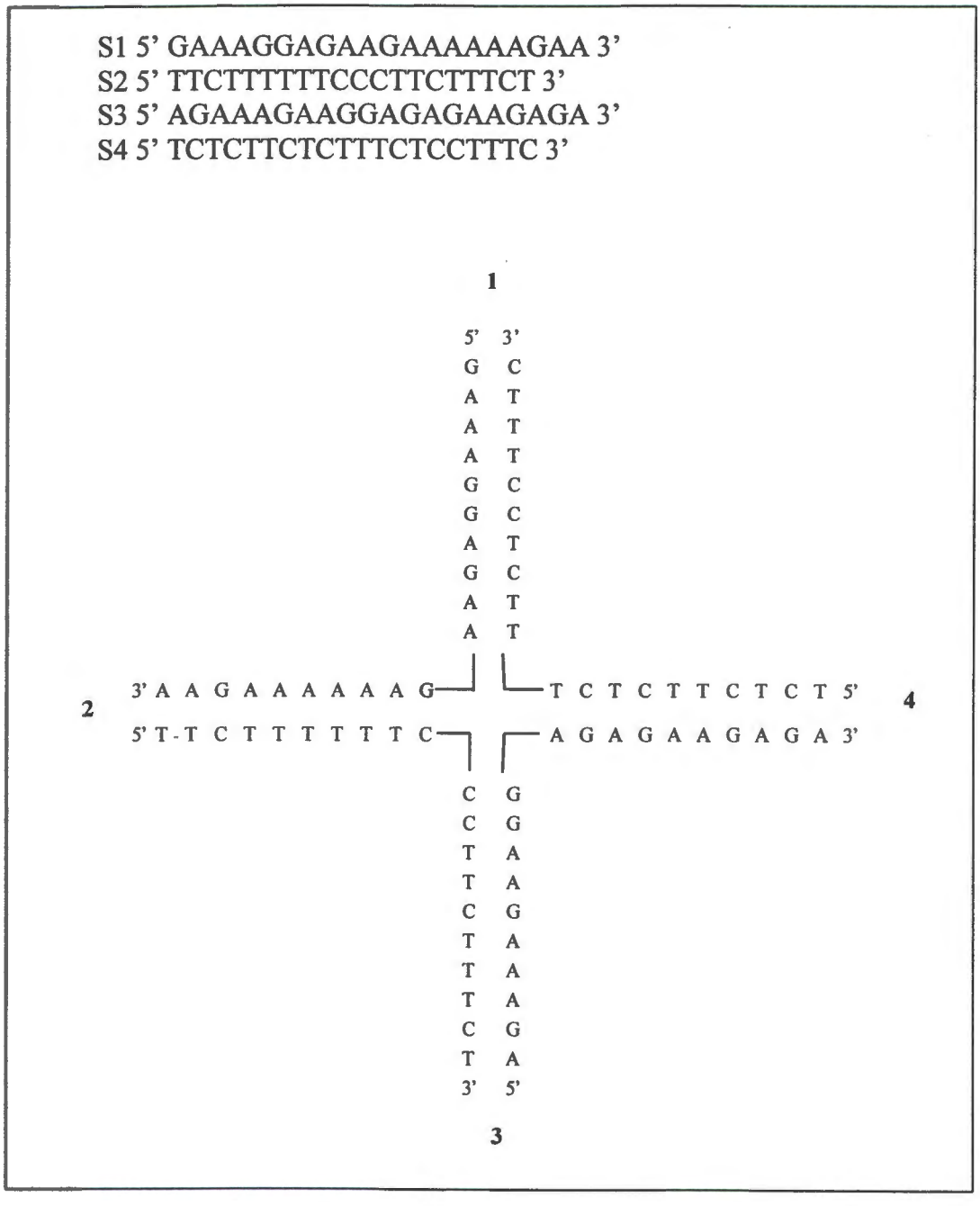

Figure 4.1: The sequence and the structure of the double-helical four-way junction, Js. The junction is composed of four 20-mer strands that are labelled S1, S2, S3 and S4. The arms are labelled by Arabic numerals.

The ternary complexes S1S2S3, S1S2S4, S1S3S4 and S2S3S4 are shown in lanes 11, 12, 13 and 14 respectively. The multiple bands observed in each of the lanes containing a set of three oligonucleotides suggest that the ternary complexes are of limited stability under the given conditions. The instability of ternary complexes was observed previously for other junctions (Chen et al., 1988). A single band with greatly reduced mobility in lane 15 represents the equimolar combination of S1, S2, S3 and S4. This combination represents Js and the single band confirms the formation of the complete double-helical four-way junction.

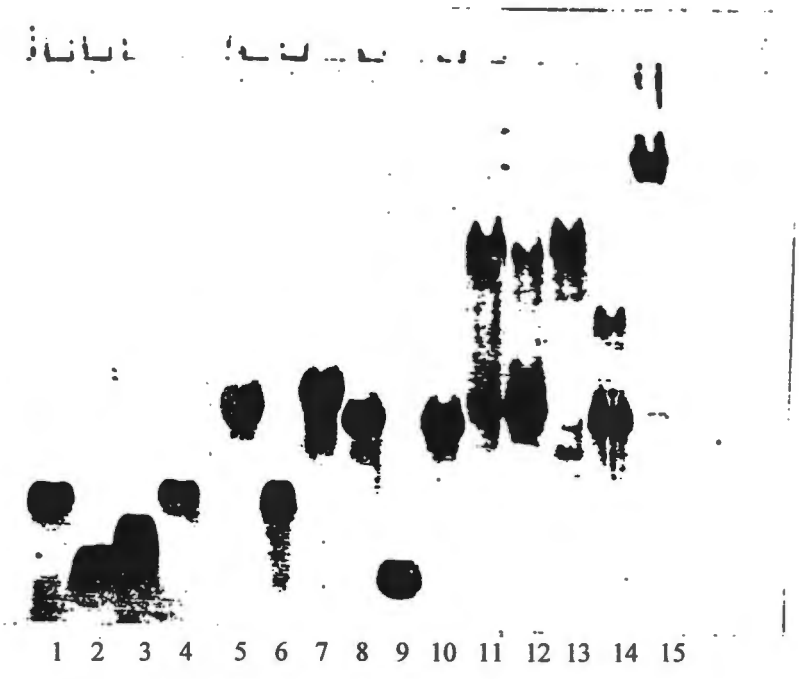

Figure 4.2: The structure of the double-helical four-way junction Js, and its arms subjected to gel electrophoresis. Illustrated on the figure are the equimolar amounts of all possible oligomer and various combinations of the strands. Lanes 1-4 contain the single strands S1, S2, S4 and S3 respectively. Lanes 5 – 10 contain the binary combinations S1S2, S1S3, S1S4, S2S3, S2S4 and S3S4 respectively. Lanes 11 – 14 contain the ternary complexes S1S2S3, S1S2S4, S1S3S4 and S2S3S4 respectively. Lane 15 contains the equimolar amounts of all the strands that form Js. The complete junction migrates as a single distinct band. Buffer contained 89mM Tris-borate, 100mM NaCl and 10mM $MgCl_2$.

4.1.2. Osmium tetroxide modifications of strands S2 and S4.

Figure 4.3. illustrates the electrophoretic mobility of radioactively labelled strands S2 and S4 after OsO_4 treatment and denaturation either on their own or as part of various junctions. The results serve to further illustrate the formation of the four-way junction and to check if base pairing also occur at the branch point. Lanes 1 to 4 represent fragments or the unmodified S4 and lanes 6 to 9 represent the fragments of S2 as well as the complete strand. The untreated S2 and S4 single strands (as references) are in lanes 1 and 6 respectively. Treated single strands S2 and S4 are in lanes 2 and 7 respectively. Lanes 3 and 8 contains treated junctions in the absence of salt and lanes 4 and 9 contain treated junctions in the presence of 10mM $MgCl_2$ and 100mM NaCl, pH8.0.

The S4 single strand is significantly cut from the 5' end, consistent with the assumption of the absence of any secondary structure formation (lane 2). In the absence of salt, S4 is also cut (lane 3) but the cleavage is not as strong as that observed for the single strand, (lane 2). Equally observable is the strong cleavage of the thymines at the branch point (lane 3). The weak cleavage observed in lane 3 suggests that although not very stable, the four-way junction does form without added Mg^{2+} and Na^{+}. The strong cleavage between the thymines at the branch point suggests that the structure is not properly folded. There is no cleavage of S4 in the presence of salt, lane 4. The absence of cleavage of S4 in the presence of salt suggests that the complete four-way junction forms and that the base pairs at the branch point are intact and stacked. The stacking of the bases is expected in the presence of Mg^{2+}. The strand S2 is similarly cleaved from the 5' end (lane 7). There is no cleavage in the presence and very little in the absence of salt, lanes 8 and 9. The absence of cleavage in the last two lanes suggests that S2 is fully base paired within the junction and that also the base pairs at the branch point are intact (lane 9). It is

difficult to conclude that the bases at the branch point are paired and stacked in the absence of salt because S2 does not have thymines at the branch point. The results obtained here further confirm the PAGE results.

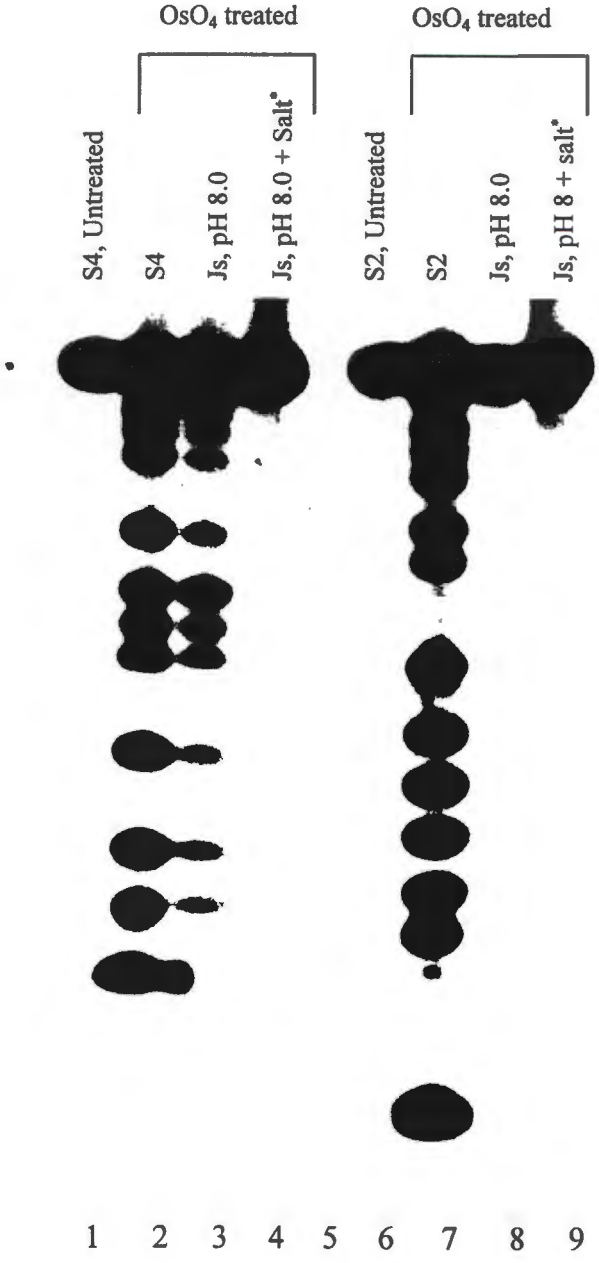

Figure 4.3: OsO_4 modification of the pyrimidine strands S2 and S4. Radioactively labelled S2 and S4 were reacted with 1mM OsO_4, 3% pyridine in Tris-borate buffer. The strands were modified as either single strands, lanes 2 and 7 respectively, or as part of junctions in the absence or presence of added cations. Lanes 1 and 6 contain untreated single strands as references.
* 10mM Mg^{2+} + 100mM NaCl.

4.2. Thermodynamic parameters of Js.

4.2.1. UV absorbance melting as a function of temperature.

The thermal denaturation of Js was monitored by measuring the UV absorbance at 260nm as a function of temperature. **Figure 4.4** (p43) shows the thermal melting profiles of Js and isolated arms in 20mM Na_3PO_4 and 1M NaCl, pH 7.0. The arms melt as monophasic transitions with the least stable arm melting at a Tm of 33.6°C (arm 2). This is expected as arm 2 has only two GC base pairs as compared to the other arms with four GC pairs each. Js appears to melt with a single transition at the Tm of 45.2°C, 4° C higher than its most stable isolated arm. The high Tm obtained for Js can be associated with the formation of the junction. It can be assumed at 1M Na^+ all the base pairs including those at the branch point are intact below the Tm. However, this might not be the case. A comparison of the calculated ΔH_{VH} of unfolding of the whole Js with the sum over individual arms results in a discrepancy. The thermodynamic parameters of Js and its isolated arms are listed in **Table 4.1**. The ΔH_{VH} calculated for Js is much smaller than the sum of ΔH_{VH} calculated for the individual arms. The discrepancy may be attributed to two things: either the thermal melting of Js does not follow a two-state melting behavior and then the method used to calculate the ΔH_{VH} is invalid or that some of the base pairs are not intact. The former is more likely because of the sequence composition (number of GC base pairs per arm) making up the individual arms.

Table 4.1: Thermodynamic parameters of Js and its isolated arms obtained from UV thermal melting data.

	Tm (°C)	ΔH_{VH} (kcal.mol^{-1})*	ΔS_{VH} (cal.mol^{-1}.K^{-1})
Js	45.2 ± 0.3	150.3 ± 2.2	472.4 ± 6.7
Arm 1 (D1D7)	37.1 ± 0.4	66.4 ± 2.4	214.0 ± 7.0
Arm 2 (D2D5)	33.6 ± 0.4	64.9 ± 2.0	211.4 ± 6.6
Arm 3 (D3D8)	40.2 ± 1.0	67.7 ± 0.4	216.0 ± 0.7
Arm 4 (D4D6)	41.4 ± 0.3	68.6 ± 0.	218.0 ± 1.9
Sum of arms		267.6	859.4

Buffer: 1M NaCl, 20mM Na_3PO_4, pH 7.0.
*1 cal = 4.18 J

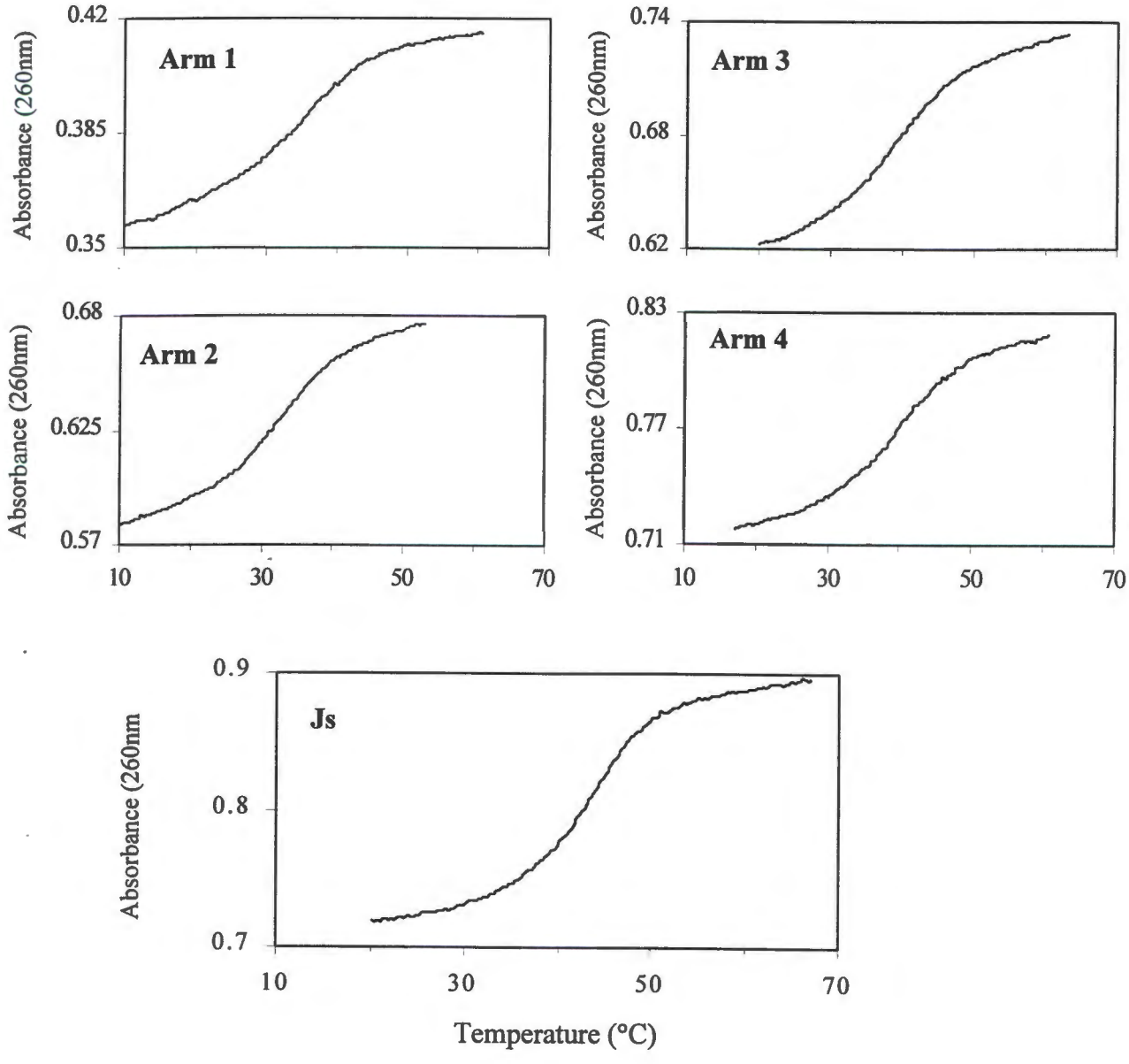

Figure 4.4: Thermal denaturation curves of Js and its arms obtained from the UV absorbance melting data. Buffer contained 20mM Na_3PO_4, 1M NaCl at pH 7.0. Total strand concentration: Arm 1 = 2.17μ, arm 2 = 3.55μM, arm 3 = 2.17μM, arm 4 = 3.67μM, Js = 14.05 μM.

4.2.2 Differential scanning calorimetry

Figure 4.5 shows the experimental and the fitted (orange) thermal melting profiles of Js in 1M Na^+ at pH 8.0. The underlying four peaks represent the deconvoluted four transitions of the arms (constructed from S1, S2, S3 and S4) of Js. Each of the arms of Js melts at a different temperature. The lowest transition that can be associated with the melting of arm 2 has a Tm of 46.8°C. The second transition occurs at 50.6°C, followed by the third at 51.8°C and the last one happening at 53.2°C. The Tm's obtained from DSC for the individual arms (**Table 4.2**) are higher than those from the UV thermal melting (**Table 4.1**). This is probably due to the much higher strand concentrations used in DSC experiments as compared to the UV melting experiments. The all-or-none melting behavior of Js and its arms can be verified by comparing the ΔH_{VH} and ΔH_{cal}. The data in **Table 4.1** and **4.2** reveal that the isolated duplex arms exhibit the two-state melting behavior. That is ΔH_{VH} (267.6 kcal/mol) = ΔH_{cal} (262.4 kcal/mol). However, the sum of ΔH_{cal} of the isolated arms (267.6 kcal/mol) is less than the ΔH_{cal} (358.6 kcal/mol) obtained for the complete junction. There is also a discrepency between the ΔH_{cal} (358.6 kcal/mol) and ΔH_{VH} (150.3 kcal/mol) obtained for the complete junction, suggesting that the melting of Js does not follow a two-state melting behavior.

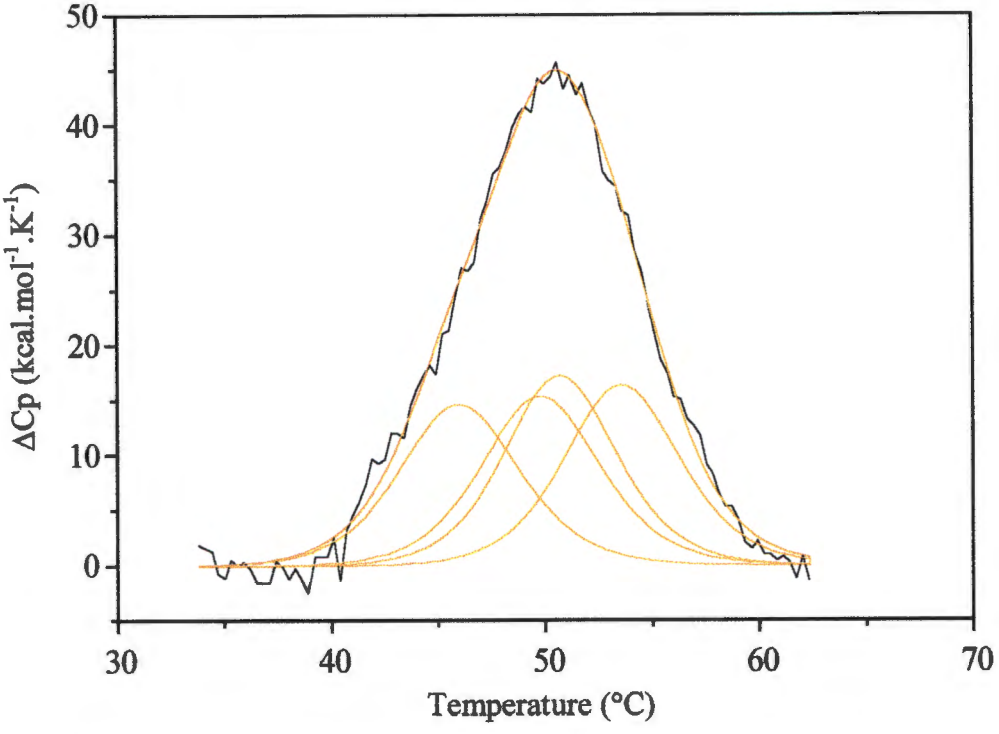

Figure 4.5: Excess heat capacity curve as a function of temperature for the double-helical four-way junction Js (designated by the solid black line) and the fitted curve (orange line). The underlying peaks represent the deconvoluted transitions of the arms of Js. Buffer: 20mM Na_3PO_4, 1M NaCl, at pH 8.0. Total strand concentration equals 140.5μM.

Table 4.2: Thermodynamic properties of double-helical four-way junction Js and its isolated arms. Data were obtained from DSC.

	Tm1	$^{a}\Delta H_{cal}1$	$^{b}\Delta S1$	Tm2	$^{a}\Delta H_{cal}2$	$^{b}\Delta S2$	Tm3	$^{a}\Delta H_{cal}3$	$^{b}\Delta S3$	Tm4	$^{a}\Delta H_{cal}4$	$^{b}\Delta S4$
Arm 1 (D1D7)	47.5	61.1	190.4									
Arm 2 (D2D5)	43.1	64.5	204.0									
Arm 3 (D3D8)	49.4	67.0	207.7									
Arm 4 (D4D6)	53.0	69.8	216.0									
Js (subtransitions)	46.8	91.1	284.7	50.6	102.0	315.1	51.8	82.2	253.0	53.2	83.3	255.2
Sum of duplex (isolated) arms			(ΔH^{a} = 262.4; ΔS^{b} = 818.1)									
Js			(ΔH^{a} = 358.6; ΔS^{b} = 1108.0)									

$^{a}\Delta H$ = units are kcal.mol^{-1}
$^{b}\Delta S$ = units are cal.K^{-1}.mol^{-1}
1 cal = 4.18 J
Error margins are less than 5%
DSC results were obtained using Microcal Origin plotting software

CHAPTER 5

THE STRUCTURE OF THE TRIPLE HELICAL FOUR-WAY JUNCTION, J_{T1T3} AND ITS COMPONENTS, JUNCTIONS J_{T1} AND J_{T3}.

5.1. The folding of oligonucleotides into the four-way junctions containing double- and triple-helical arms.

J_{T1} was constructed from 20-mers S1, S2, S3 and a 44-mer T1 (**Figure 5.1B**). The structure of J_{T1} is based on the structure of the double helical four-way junction, Js (**cf. Chapter 4**). J_{T1} has its strand S4 extended, now called T1. S4 was extended at the 3'-terminus by a segment of four cytosines to become a four-member loop followed by twenty pyrimidine bases. It is expected that at neutral pH the double helical four-way junction with dangling S4 3' extension will be formed. In lowering the pH, the first 10 bases following the cytosine loop are intended to bind to the purine strand of the Watson-Crick duplex (Arm 1) *via* Hoogsteen hydrogen bonding. The remaining 10 bases are complementary to the purine strand of the Watson-Crick duplex in arm 2 and will bind there. The loop allows the formation of the four-way junction containing two triple helical arms, arm 1 (capped with a loop) and arm 2, and two double helical arms, 3 and 4 (**Figure 5.1B,** Top). Since the loop is located at the end of arm 1 the structure formed is called J_{T1}.

J_{T3} was assembled by hybridizing 20-mers S1, S3, S4 and a 44-mer T3 (**Figure 5.1B,** Bottom). As in J_{T1}, Js forms the core double-helical four-way junction. In the case of J_{T3}, S2 is the extended strand (at the 3' terminus), renamed T3. Folding of the extension of T3 results in a four-way junction containing arm 1 and 2 as duplexes and arm 3 (capped with a loop) and arm 4 as triplexes. The cytosine loop is positioned at the end of arm 3 and accordingly the structure is named J_{T3}.

The elements of J_{T1} and J_{T3} can be combined into one triple-helical four-way junction containing one loop at the end of arm 1 and one at the end of arm 3. This structure is called J_{T1T3}. J_{T1T3} was assembled from the strands S1, T1, S3 and T3, **(Figure 5.1A)**. At neutral pH, J_{T1T3} forms a core double helical four-way junction like Js with dangling 3' T1 and 3' T3 extensions. At decreasing pH, the T1 extension forms the four-member cytosine loop and binds to the purine strand of the Watson-Crick helix in arm 1 and arm 2 *via* Hoogsteen hydrogen bonds. The T3 extension binds to the purine strand of the Watson-Crick of arm 3 and arm 4. Simultaneously this result in the triple-helical four-way junction containing two loops, on arm 1 and the other on arm 3 respectively as well as two blunt-ended triplexes.

5.1.1. pH titration

Triplexes containing the CG•C^+ triads form at acidic pH because of the need to protonate the N3 of cytosines in the third strand. UV absorption is a very sensitive indicator of base stacking effects in polynucleotides and the reduction in hyperchromicity as such has been used to monitor coil to helix transitions. Therefore, formation of the double stranded four-way junction and the subsequent pH-dependent folding of T1 or T3 into the triplex can be clearly monitored by recording UV absorbance. The helix to coil transition was investigated by measuring the absorbance at 260nm as a function of pH (Völker et al., 1993; Hüsler and Klump, 1995). The pH was lowered from 12 to 3 by adding successive aliquots of concentrated HCl (to minimize dilution) to the solution. The samples were allowed to equilibrate for 5 minutes before measuring the absorbance at 260nm and 18°C.

S1 5' GAAAGGAGAAGAAAAAAGAA 3'
S3 5' AGAAAGAAGGAGAGAAGAGA 3'
T1 5' TCTCTTCTCTTTCTCCTTTC CCCC CTTTCCTCTTCTTTTTTCTT 3'
T3 5' TTCTTTTTTCCCTTCTTTCT CCCC TCTTTCTTCCTCTCTTCTCT 3'

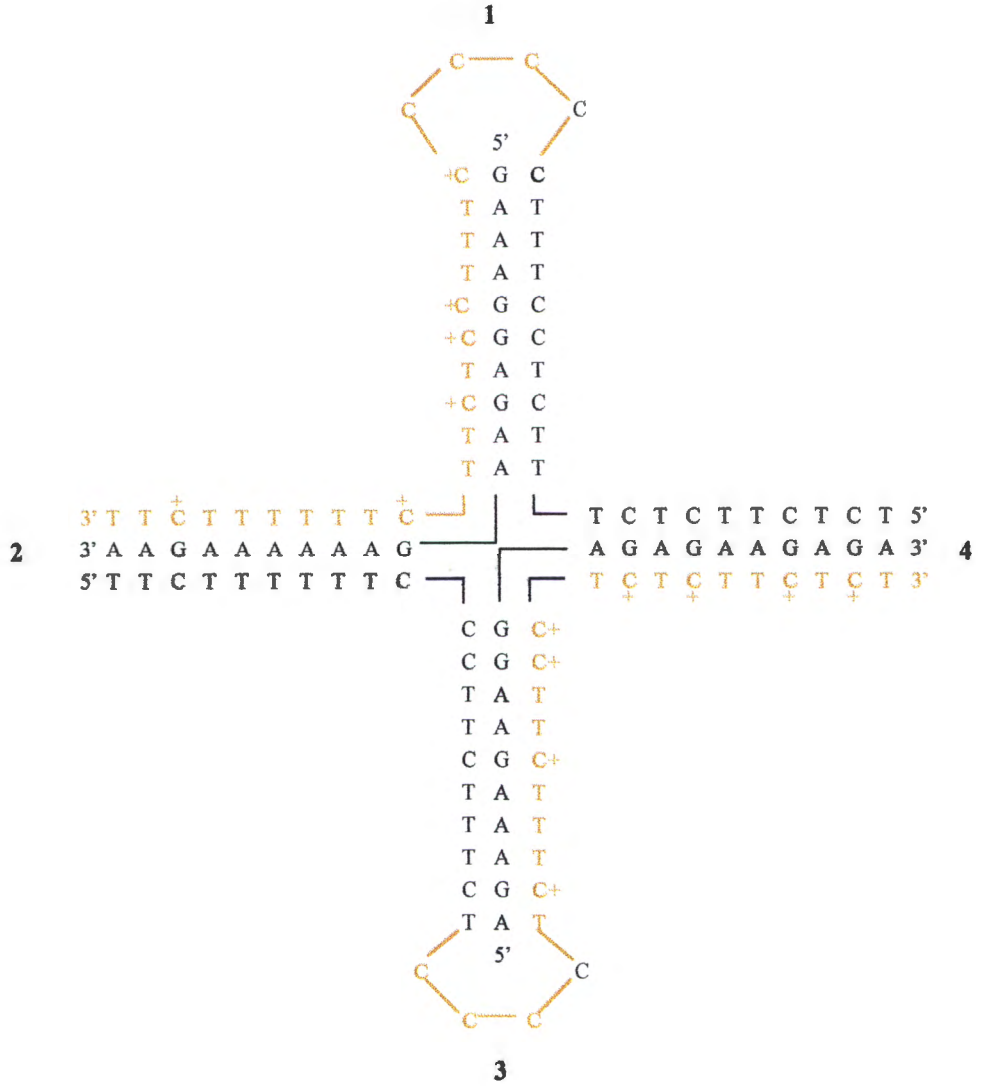

Figure 5.1A: schematic representation of J_{T1T3}. J_{T1T3} is constructed from the same sequences that forms Js. The S2 and S4 strands are extended at the 3'end with the four-member cytosine loop to form 44-mer T1 and T3 respectively. The loops are positioned on arms 1 and 3. The third strands (Hoogsteen) are shown in color

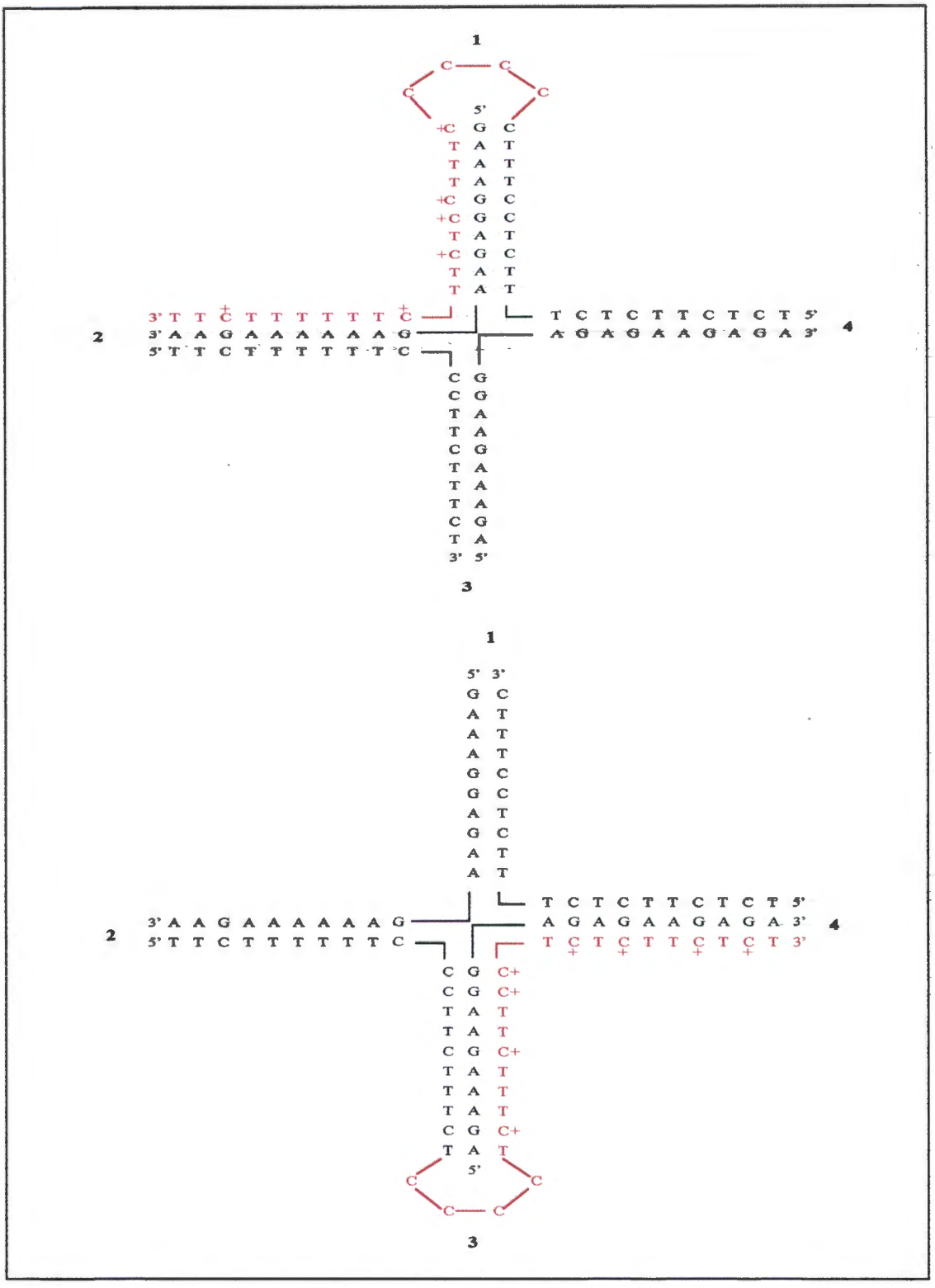

Figure 5.1B: Schematic representations of J_{T1} (Top) and J_{T3} (Bottom). J_{T1} and J_{T3} are simplified representations of J_{T1T3}. J_{T1} is assembled from S1, S2, S3 and T1 and J_{T3} is assembled from S1, S3, S4 and T3. The Hoogsteen strands are shown in color

Figure 5.2A shows the variation of absorbance at 260nm as a function of pH for J_{T1} (top graph). Between pH 12 and 10.8, there is no change in absorbance, suggesting that the strands are present as random coils. There is a decrease in absorbance below pH 10.5, denoting the formation of the ordered structure. This can be presumably associated with the presence of the double-helical four-way junction with dangling 3'end extension on arm 1. Lowering the pH further to 7 did not have any effect on the absorbance of the structure that is formed. There is a steep decrease in the absorbance between pH 7.0 and 4.7. The decrease in absorbance reflects the formation of the triplex, that is, the binding of the T4 3' extension to the duplex arms 1 and 2. The structure formed is stable until pH 3.5 after which, by lowering the pH further, it becomes destabilized. The same procedure was applied to equimolar amounts of S1, S3, S4 and T3 which were mixed together in a 1:1:1:1 ratio in the buffer (1M NaCl, 20mM $NaPO_4$, pH 12.0) to result in J_{T3}.

The pH was lowered stepwise from 12 to 2 by adding successive aliquots of concentrated HCl to the solution. The results are illustrated in **Figure 5.2A** (bottom graph). Between pH 12.0 and 10.0, the absorbance is maximal suggesting that the solution contains single strands as random coils. There is a gradual hypochromic shift between pH 10 and 7. This can be attributed to the formation of the double-helical four-way junction with a dangling T3 3' extension on arm 3. Lowering the pH further (pH 6 to 5.0) results in a steep hypochromic shift. This can be associated with binding of the T3 3' extension to the major grooves of arms 3 and 4 forming a four-way junction containing arms 3 and 4 as triplexes and arms 1 and 2 as duplexes. The change in absorbance plateaus at about pH 4.5 to 3.0 and increases afterwards as the pH is further lowered. The increase in absorbance is due to the dissociation of the triple-helical four-way junction into single strands.

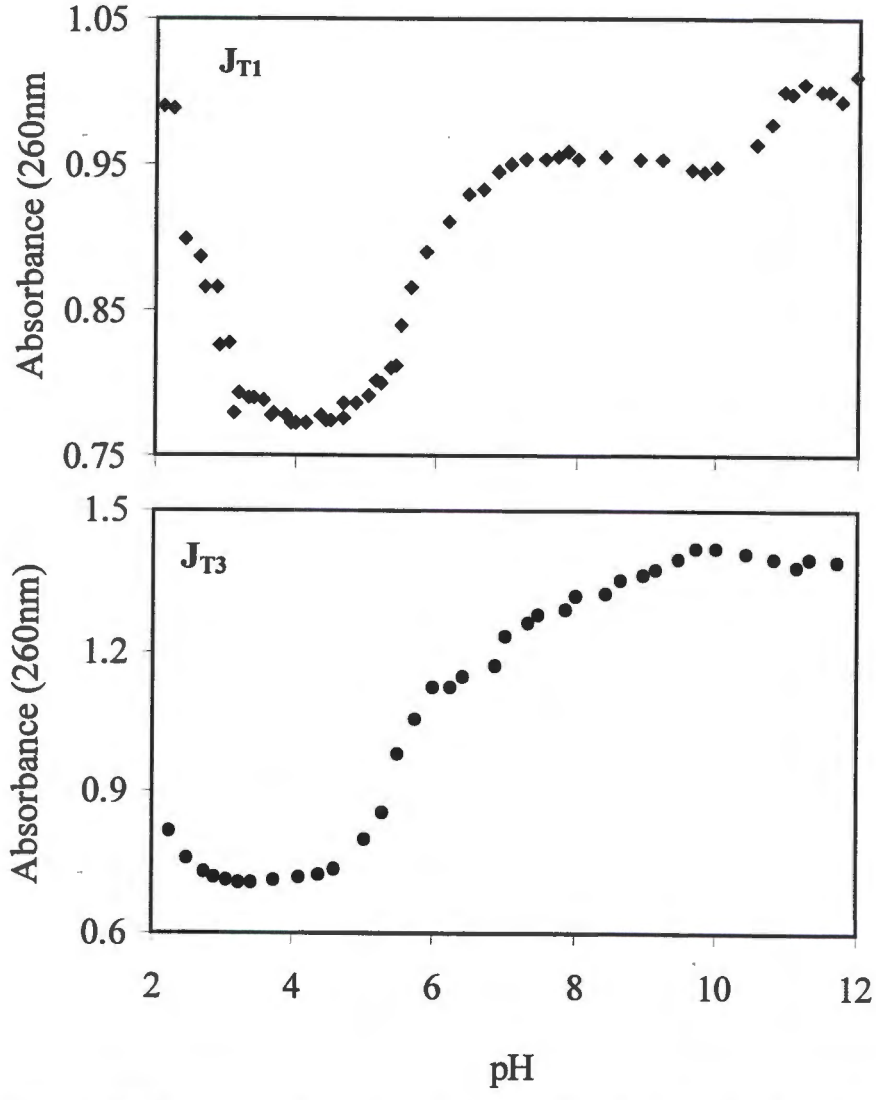

Figure 5.2A: pH titration curves of J_{T1} (TOP) and J_{T3} (BOTTOM performed in 20mM Na_3PO_4, 1M NaCl at 18°C. The total stran concentration of each junction is 14.05μM.

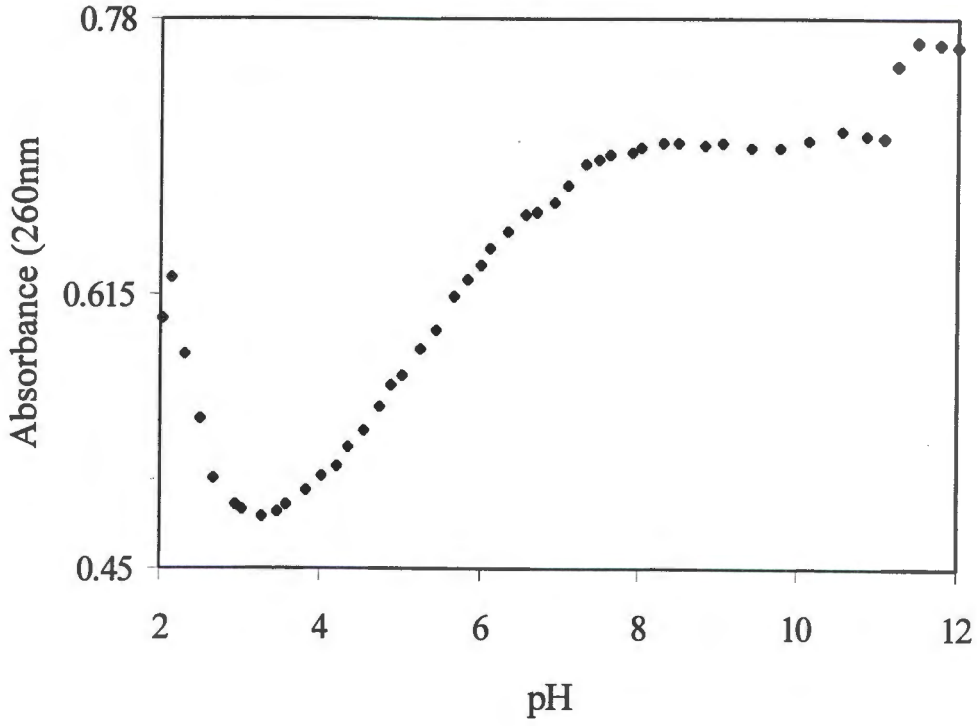

Figure 5.2B: pH titration of J_{T1T3} performed in 20mM Na_3PO_4 and 1 NaCl at 18°C. Total strand concentration equals 14.05μM.

The pH titration profile of J_{T1T3} as a function of pH is shown on **Figure 5.2B**. At pH 12 to pH 11, the absorbance is at its maximum. This corresponds to the mixture of single strands as random coils. Lowering the pH results in the decrease in the absorbance, suggesting the formation of the double helical structure as the first step. The absorbance remain constant between pH 9.5 to 7.5 after which it decreases and slightly levels off between pH 6.7 and 6.5. Lowering the pH further results in the decrease in the absorbance that reaches a minimum between pH 3.5 and 3.0. The decrease in absorbance signals the formation of the triplex structure, J_{T1T3}. The rapid increase in absorbance below pH 3.0 signifies the unfolding of the triplexes into single stranded random coils.

5.1.2. Polyacrylamide gel electrophoresis

The formation of the partial triplex structures J_{T1}, J_{T3} and the full structure J_{T1T3} were analyzed in 20% polyacrylamide gel electrophoresis. For J_{T1} and J_{T3}, single stranded oligonucleotides and complexes containing the strands that form the Hoogsteen bonds were subjected to electrophoresis. Only combinations containing either T1 of J_{T1} or T3 in the case of J_{T3} were run in the gels. Other combinations were omitted because their formation has been shown in gel electrophoresis of Js (cf. **Figure 4.2**).

Figure 5.3A: illustrates the native gel electrophoresis of J_{T3} in 100mM ammonium acetate, 100mM NaCl and 10mM $MgCl_2$ at pH 5.0. Lanes 1 to 4 contain single strands S1, T3, S3 and S4. Lanes 5 to 7 contain binary complexes S3T3, S1T3 and S4T3. The band in lane 6 shows reduced mobility as compared to the band in lane 5 and lane 7. This is because the S3T3 complex forms the triplex whereas the S1T3 complex forms the duplex. Lanes 8, 9 and 10 represent the ternary complexes S1S4T3, S1S3T3 and S3S4T3 respectively. Lane 11 contains an equimolar combination of S1, S3, S4 and T3 strands. The single band that has the lowest mobility indicates the presence of the complete junction (J_{T3}). The results of the native gel electrophoresis of J_{T1T3} are shown in **Figure 5.3B**. The first four lanes represent the single stranded oligonucleotides S1, T1, S3 and T3. Lanes 5 to 10 represent binary combinations S1T3, S1S3, S1T1, S3T3, T1T3 and S3T1 respectively. Each of the binary combinations form unique complexes that run as one band. S1S3 (lane 6) and T1T3 (lane 9) do not form base pairs but they run as single bands because they are of the same size. The S1T1 (lane 7) and S3T3 (lane 8) combinations form triplexes and thus migrate slower than the duplex combinations S1T3 (lane 8) and S3T1 (lane 6). Lanes 11 to 14 represent the ternary complexes S1S3T3, S1T1T3, S3T1T3 and S1S3T1 respectively. It can be seen from the gel that the ternary complexes do form but are

unstable. The band with the reduced mobility in lane 15 represents an equimolar mixture of the four oligonucleotides, S1, S3, T1 and T3. The single band indicates the formation of a complete structure, the triple-helical four-way junction J_{T1T3}.

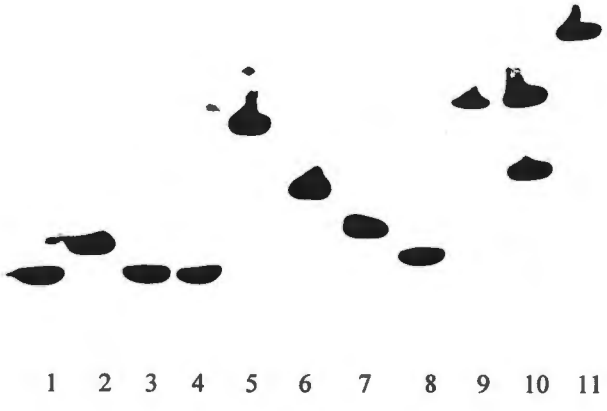

Figure 5.3. A. Polyacrylamide gel electrophoresis of J_{T3}. Note that only the combination containing T3 strand are subjected to electrophoresis. Buffers contained 100mM ammonium acetate, 100mM NaCl, 10mM $MgCl_2$ at pH 5.0. Lanes 1-4 contain single strands S1, S3, S4 an T3. Lanes 5 - 7 represent binary mixtures S1T3, S3T3 and S4 T3. Lanes 8 to 10 contain ternar complexes S1S3T3, S1S4T3 and S3S4T3 respectively. Lane 11 contains equimolar amounts of S1, S3 and T3. The single band represents the complete four-way junction J_{T3}. **B.** Native gel elctrophoresis of J_{T1T3}. Single strands S1, T1, S3 and T3 are in lanes 1 to 4 respectively. Binary complexes are in lanes 5 – 10 and ternary complexes in lanes 11 – 14. Th band in lane 15 represents the triple-helical four-way junction.

5.1.3. Osmium tetroxide (OsO_4) modifications (Chemical footprinting).

Osmium tetroxide modification of single strand DNAs has been used as a probe to determine stacking of bases at the branch point of three- and four-way junctions (Møllegaard et al., 1994; Duckett et al., 1988; Duckett and Lilley, 1990). In the presence of metal ions, the four-way junction folds into a completely stacked and base paired conformation with pairwise stacking of helical arms. In the absence of metal ions, the structure is open with the helical arms directed towards the corners of a square. In this conformation, the bases at the branch point are only partially stacked. The thymine residues immediately around the branch point are susceptible to modification by OsO_4. The reactivity is believed to results from the OsO_4 attack on the C5-C6 double bond of thymine thereby forming a *cis* ester. This modification is followed by cleavage with piperidine.

OsO_4 has been used to characterize the structure of J_{T1} in the absence or presence of magnesium and sodium chloride, **Figure 5.4A**. At pH 8.0 and no extra cations added, it is unlikely that the junction will form given the size of the arms and the overall negative charge of the phosphate groups along the Watson-Crick and the Hoogsteen strands. However, if it does form, it will be in its square planar conformation and highly unstable because of the repulsion of the negative charges on the phosphate groups of the four strands at the branch point. Addition of the salt at this pH will enable the formation of a double helical four-way junction with single-stranded extensions. At pH 5.0 and additional Na^+ and Mg^{2+} present, the complete four-way junction with two triple helical arms should form. It should be possible to distinguish between the conformation of the structures at pH 5 and 8 by means of the cleavage of the thymines located on the single-stranded extension. It should also be possible to show that base pairing occurs at the branch point and to some extend stacking of helical arms has occurred.

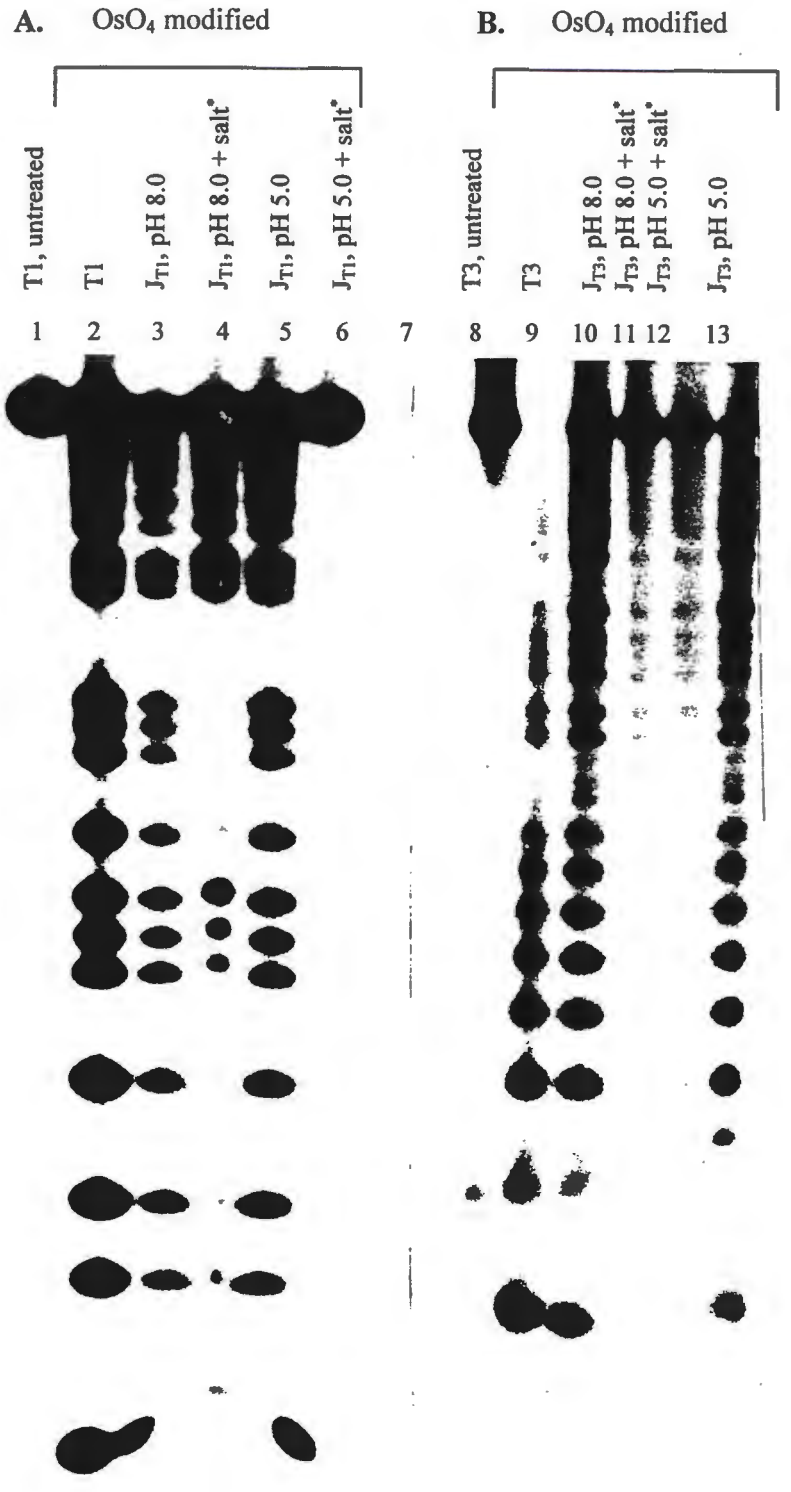

Figure 5.4: OsO_4 modifications of T1 (A) and T3 (B) strands. The strands are modified either a individual strands (lanes 2 and 9) or incorporated in their respective junctions. Radioactivel labelled strands were reacted with 1mM OsO_4 and 3% pyridine in the absence or presence of 100mM Na^+ and 10mM Mg^{2+} under different pH conditions. *100mM Na^+ and 10mM Mg^{2+}.

The J_{T1} junction was assembled from the appropriate oligonucleotides as described earlier (cf. **Chapter 5.1**). T1 was radioactively labelled at the 5'-terminus as it contains thymines at the point of strand exchange and more importantly, it forms the triplex on arms 1 and 2. Samples of J_{T1} were prepared in buffer solutions containing 100mM NaCl and 10mM $MgCl_2$ at pH 5.0 or pH 8.0. Samples of J_{T1} were also prepared in the absence of cations at pH 8.0 or pH 5.0. The junctions were modified by OsO_4 and subsequently cleaved with piperidine. Piperidine cleaves the OsO_4-thymine adducts starting from the 5'-terminus. The cleavage products were analyzed by denaturing gel electrophoresis and autoradiography.

The bands at the bottom of the gel represent the 5'-terminus of T1. The band in lane 1 represents single-stranded T1 that was not reacted with OsO_4. Lane 2 contains single stranded T1 reacted with OsO_4 in the absence of cations. Lane 3 contains the J_{T1} complex reacted with OsO_4 and piperidine in the absence of cations and at pH 8.0. Lane 4 contains the J_{T1} complex reacted with OsO_4 and cleaved by piperidine in the presence of 100mM NaCl and 10mM $MgCl_2$ at pH 8.0. Lane 5 contains the J_{T1} complex which has reacted with OsO_4 in the absence of cations, pH 5.0 and the band in lane 6 represents the J_{T1} complex reacted with OsO_4 in the presence of 100mM NaCl and 10mM $MgCl_2$ at pH 5.0. The many bands in lane 2 show that the single strand T1 was cleaved considerably as expected. In the absence of metal ions (lane 3), T1 is still cleaved but not as effectively as in lane 2. This is also the case at pH 5.0 in the absence of cations, lane 5. The reason for this might be that the junction does form in the absence of salt, but it is unstable in these conditions.

In the presence of 100mM NaCl and 10mM $MgCl_2$ at pH 8.0, the double helical four-way junction is formed, lane 4. This is shown by the absence of cleavage of thymine residues located on arms 4 and 1 respectively. The extended part of T1 strand that should form the triplex is

notably cleaved (lane 4, top part of the gel). Also very significant is the cleavage of three thymine bases located at the branch point. There are two possible reasons for the cleavage at the branch point. Firstly, although the double helical four-way junction is formed, the amount of cations present may be insufficient to induce folding of J_{T1} into a stacked structure hence the OsO_4 modification of thymine bases at the point of strand exchange. Secondly, the dangling 3' extension on arm 1 may destabilize that arm and perhaps prevents the junction from folding into the stacked structure which then results in cleavage of the unprotected bases located at the branch point. T1 was not cleaved in the presence of cations at pH 5.0, lane 6. The absence of cleavage of J_{T1} in 100mM NaCl and 10mM $MgCl_2$ at pH 5.0 signifies the formation of the complete triple helical four-way junction with stacked arms. This suggests that the amount of salt used is sufficient to induce complete folding.

Similarly, J_{T3} was subjected to the same OsO_4/pypiridine treatment as J_{T1}. The results are shown in **Figure 5.4B**. Lane 8 represents single-stranded T_3 that was not reacted with OsO_4 and lane 9 contains single stranded T3 reacted with OsO_4. Lane 10 represents modified J_{T3} in the absence of cations, pH 8.0. Lanes 11 and 13 contain modified J_{T3} in 100mM NaCl and 10mM $MgCl_2$ at pH 8.0 and 5.0 respectively. The 12^{th} lane represent modified J_{T3} in the absence of cations at pH 5.0. There is complete cleavage of single stranded T3. T3 is also cleaved in samples that contained no salt, lanes 10 and 13. The single band at the top of the gel confirms the presence of the triple-helical DNA four-way junction, lane 12.

It should be noted that the cleavage of thymines from the 5' end occurs first in the Watson-Crick strands followed by the cleavage on the Hoogsteen strands after the loop for both T1 and T3.

5.2 Thermodynamics of J_{T1}, J_{T3} and J_{T1T3} formation.

5.2.1. UV absorbance melting

Folding of nucleic acids into secondary and particularly into tertiary structures brings the negatively charged phosphate groups into close proximity. For instance, the complete structure of the double helical four-way junction is sensitive to the kind of cations chosen and the concentration of charges. Similarly, the formation of the triplex structures requires the presence of metal ions and/or acidic pH conditions. Therefore, it is reasonable to assume that incorporating third strands into arms of the four-way junction will result in relatively high charge density and possibly steric hindrance at the branch point due to crowding. Monovalent cations or polycations are required to compensate for the repulsive forces between negatively charged phosphate groups. The requirement for the protonation of the cytosines in the third strand to form Hoogsteen bonds poses yet another constrain on the formation and the maintenance of the four-way junction structure.

5.2.1.1. The effect of pH on the melting of J_{T1}, J_{T3} and J_{T1T3}.

The effect of pH on the melting of J_{T1} and J_{T3} were characterized by measuring the change in UV absorbance at 260nm as a function of temperature. The buffer contained 20mM Na_3PO_4 and 1M NaCl. **Figure 5.5** (top graph) depicts the first derivative melting curves ($\delta A_{260}/\delta T$) as function of J_{T1} at varying pH conditions. There is a monophasic transition at pH 7.0 with a Tm of about 45 °C. This Tm corresponds to the observed Tm of a double-helical four-way junction, Js. Therefore, the transition can be associated with melting of the double-helical core of J_{T1}. The transition shown at pH 6.0 is still monophasic although at this pH Hoogsteen hydrogen bonds are supposed to be formed between the Watson-Crick duplex and the single strand extensions.

Lowering the pH to 5.5 produces a shoulder at about 45°C and the appearance of the second high-temperature transition. It is therefore reasonable to treat the monophasic peak at pH 6.0 as two overlapping transitions. At pH 5.0 and 4.67 respectively, two distinct transitions appear. The lower transition temperature occurs to be pH independent as it remains invariant (Tmax = 47.0 ± 1.0 °C) under different pH conditions. The shifting of the upper transition to higher temperatures shows that it is associated with the pH-dependent structure formation.

The result obtained for J_{T3} follow the same pattern shown for J_{T1}, **Figure 5.5** (Bottom graph). That is, decreasing the pH of the solution results in the appearance of two distinct transitions. The first transition temperature (Tmax = 44.0 ± 1.0 °C) is pH independent whereas the second transition is highly dependent on pH. The first transition (pH 7.0) is in agreement with the melting of the double-helical four-way junction.

The thermal melting of J_{T1T3} is different from those of its analogues, **Figure 5.6**. At pH 7.0, a similar broad peak as obtained for J_{T1} and J_{T3} emerges with an approximate Tm of 45°C. The Tm peak should correspond to the unfolding of the double helical Js core of J_{T1T3} with dangling ends on arms 1 and 3. Decreasing the pH results in the shifting of the entire unfolding to higher temperatures. A shoulder emerges at the low temperature slope of the peak as the pH is decreased and shifts to higher temperature with the decrease in pH as much as the main peak shifts. Unlike its simplified complexes J_{T1} and J_{T3} that separate during unfolding into two distinct peaks, one of which is pH independent, J_{T1T3} unfolding is completely pH dependent as is expected. The thermodynamic parameters associated with the unfolding are listed in **Table 5.1** for J_{T1} and J_{T3} and **Table 5.3** for J_{T1T3}.

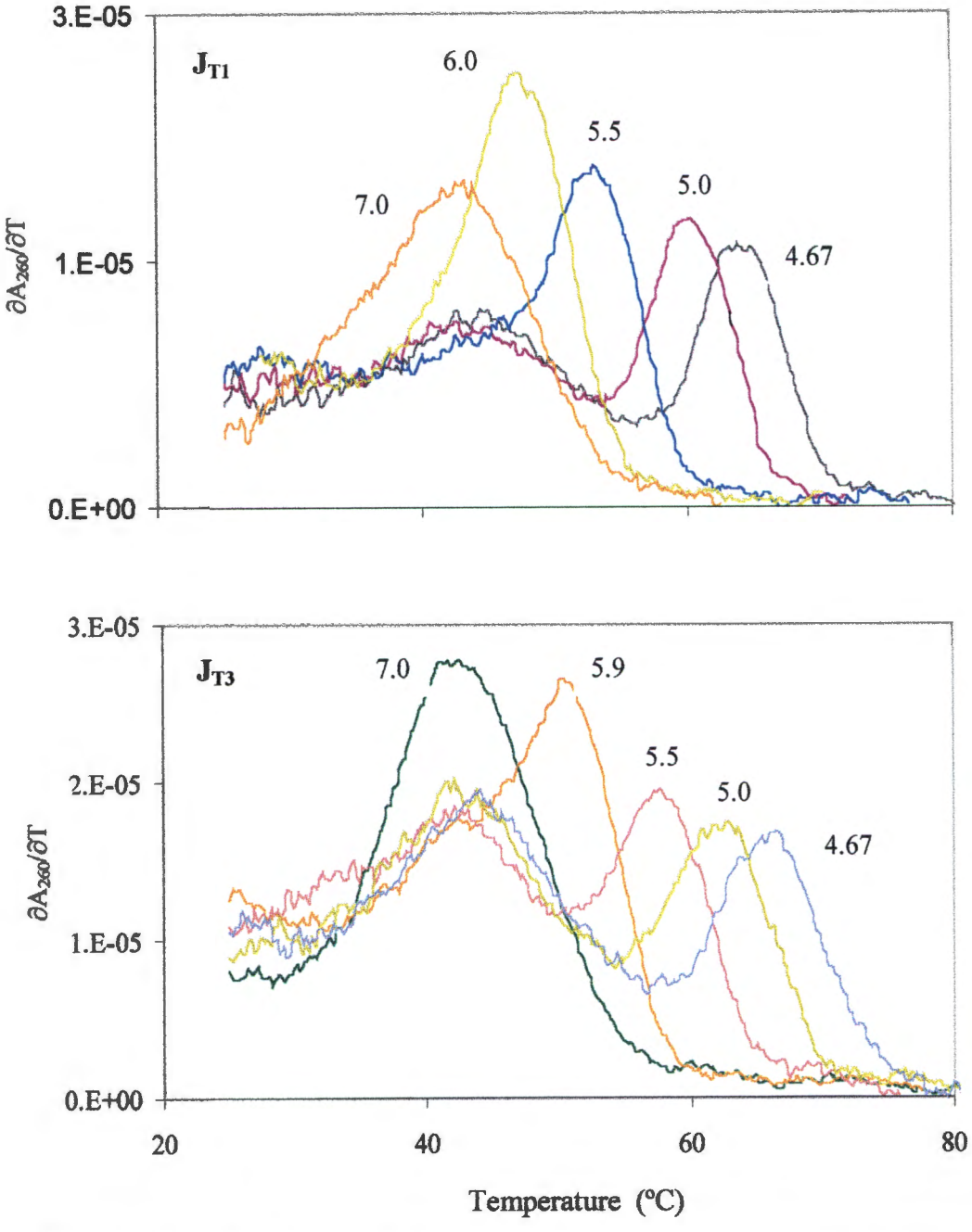

Figure 5.5: The first derivative melting curves ($\partial A_{260}/\partial T$) *versus* temperature of J_{T1} (top) and J_{T3} (bottom) obtained at different pH values. Buffer contained 20mM Na_3PO_4 and 1M NaCl. Total strand concentration per junction = 14.05μM.

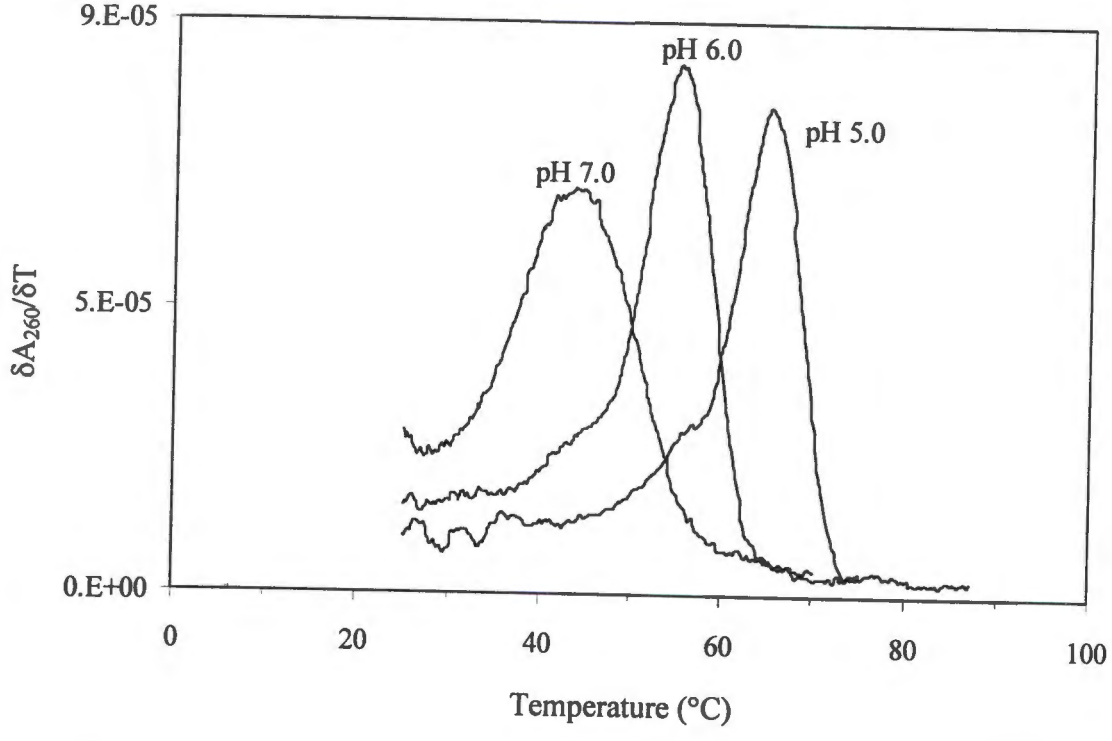

Figure 5.6: First derivative melting curves ($\partial A_{260}/\partial T$) of J_{T1T3} *versu* temperature obtained from UV thermal melting data. Buffer contained 20m Na_3PO_4, 1M NaCl. Total strand concentration equals 14.05μM.

The effect of pH on the thermal stability of J_{T1} and J_{T3} is further illustrated in the phase diagrams (Tm versus pH). It shows the boundaries of the areas in which the different conformations of the structures dominate (**Figure 5.7**). The first transition with a Tm of 46°C in both **Figures 5.7** (top and bottom graph) remains pH independent. This is indicated by the straight line almost parallel to the x-axis.

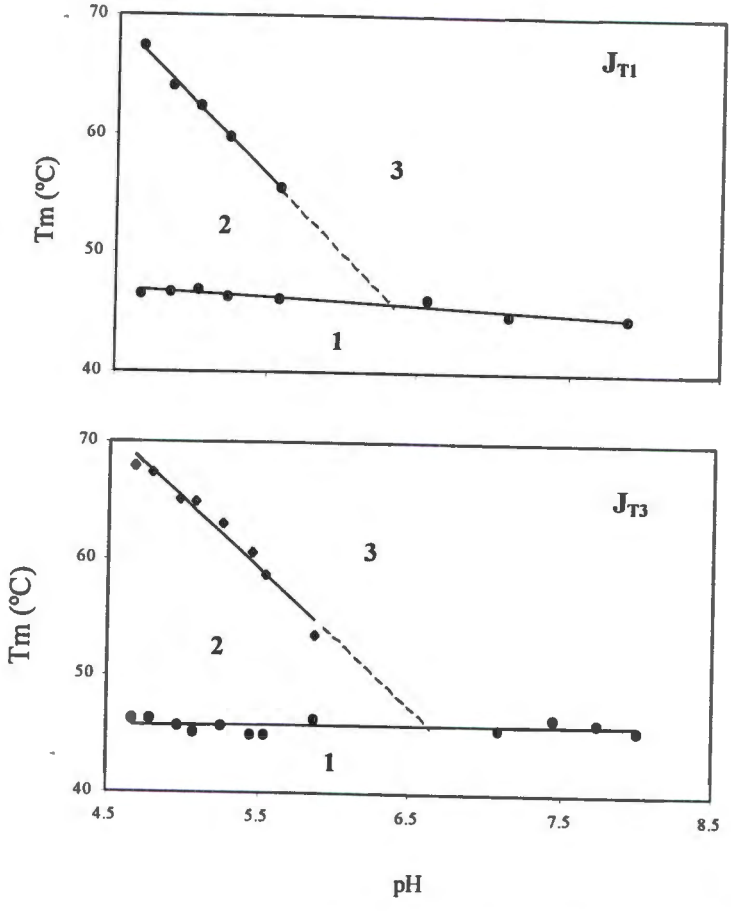

Figure 5.7: Phase diagram (Tm *versus* pH) for J_{T1} and J_{T3}. The Arabic numerals illustrate the areas within which the different conformations are stable. Th second boundary lines are extrapolated (dotted lines) to highlight th boundaries. 1. The complete four-way junction with two double helical and tw triple-helical arms. 2. The triplex structure intact and the duplexes melte (below pH 6.5). 3. Single strands.

The slopes ($\delta Tm/\delta pH$) reflect the dependence of the Tm on the pH and are obtained by linear least square curve fitting. The slope associated with this line is -0.17 for J_{T1} and -0.23 for J_{T3}. On the other hand, the second transition is pronounced pH dependent with the Tmax increasing linearly with the decrease in pH ($\delta Tm/\delta pH$ equals -12.77 for J_{T1} and -11.81 for J_{T3}). Because of the pH independent nature of the first transition in J_{T1}, this transition can be allocated to melting of arms 3 and 4. Likewise, the first transition in J_{T3} can be allocated to melting of arms 1 and 2. The second transition is assigned to arms 1 and 2 (J_{T1}) and arms 3 and 4 (J_{T3}) respectively since both arms contain Hoogsteen cytosines and their melting temperature should therefore be pH dependent. It should be noted that the arms in both junctions do not necessarily melt simultaneously as suggested by the presence of only two peaks. This should particularly hold for arm 2 of both junctions since it contains the least number of GC base pairs.

5.2.1.2. The effect of the ionic strength on the structural stability of J_{T1} and J_{T3} as reflected in the melting temperature.

The effect of the ionic strength on the structural transition of J_{T1} and J_{T3} was investigated by measuring the absorbance (260nm) as a function of temperature. The total strand concentration for each junction was 14.05μM. The buffer contained 20mM Na_3PO_4, NaCl concentrations ranged from 0.1M to 1.0M at pH 4.67. The thermal unfolding of J_{T1} and J_{T3} in both cases revealed two transitions that are dependent on the ionic strength.

The effect of the ionic strength on the Tm is summarized in the phase diagram of Tm versus -log [Na^+], **Figure 5.8**. The slope $\delta T_m/\delta log[Na^+]$ illustrates the relationship between the Tm and the ionic strength and it is generally higher for the triple helices (Plum et al, 1990; Wilson et al., 1994) than for the corresponding duplexes.

Figure 5.8 (top graph) shows that for both the first and second transitions the slope below 0.4M Na^+ is smaller than the slope above 0.4M Na^+. Below 0.4M Na^+, the slope for the first transition equals 6.5°C/log[Na^+] and that corresponding to the second transition equals 8.4°C/log[Na^+]. The slopes above 0.4M Na^+ equals 14.3°C/log[Na^+] for the first transition and 16.3°C/log[Na^+] for the second transition. This behavior, where the slope at lower salt concentration is smaller than the slope at high salt concentration, has been observed for other triplex structures before (Plum et al., 1990).

The same pattern is observed for J_{T3}. The slopes of the first and second transitions are less below 0.4M Na^+ and increases drastically above 0.4M Na^+. For the first transition, the slope below 0.4M Na^+ equals 8.1°C/log[Na^+] and the slope above 0.4M Na^+ is 13.8°C/log[Na^+]. The slopes corresponding to the second transition below and above 0.4M Na^+ are 5.8°C/log[Na^+] and 20.24°C/log[Na^+] respectively. The increase in the slope above 0.4M Na^+ is more pronounced in the second transition which corresponds to the melting of the triple-helical arms. It is expected that the protonation of cytosines will partially compensate the negative charges on the third strand and thus reduce the ionic strength dependency of the melting of the third strand. It is not clear whether it is the triplex structure that is more stabilized by the increase in the ionic strength or whether there is an increase in the stability of the whole junction. However, from the trends observed, it can be assumed at this stage that the ionic strength dependency has more to do with the four-way junction properties than with the stability of the triplex arms.

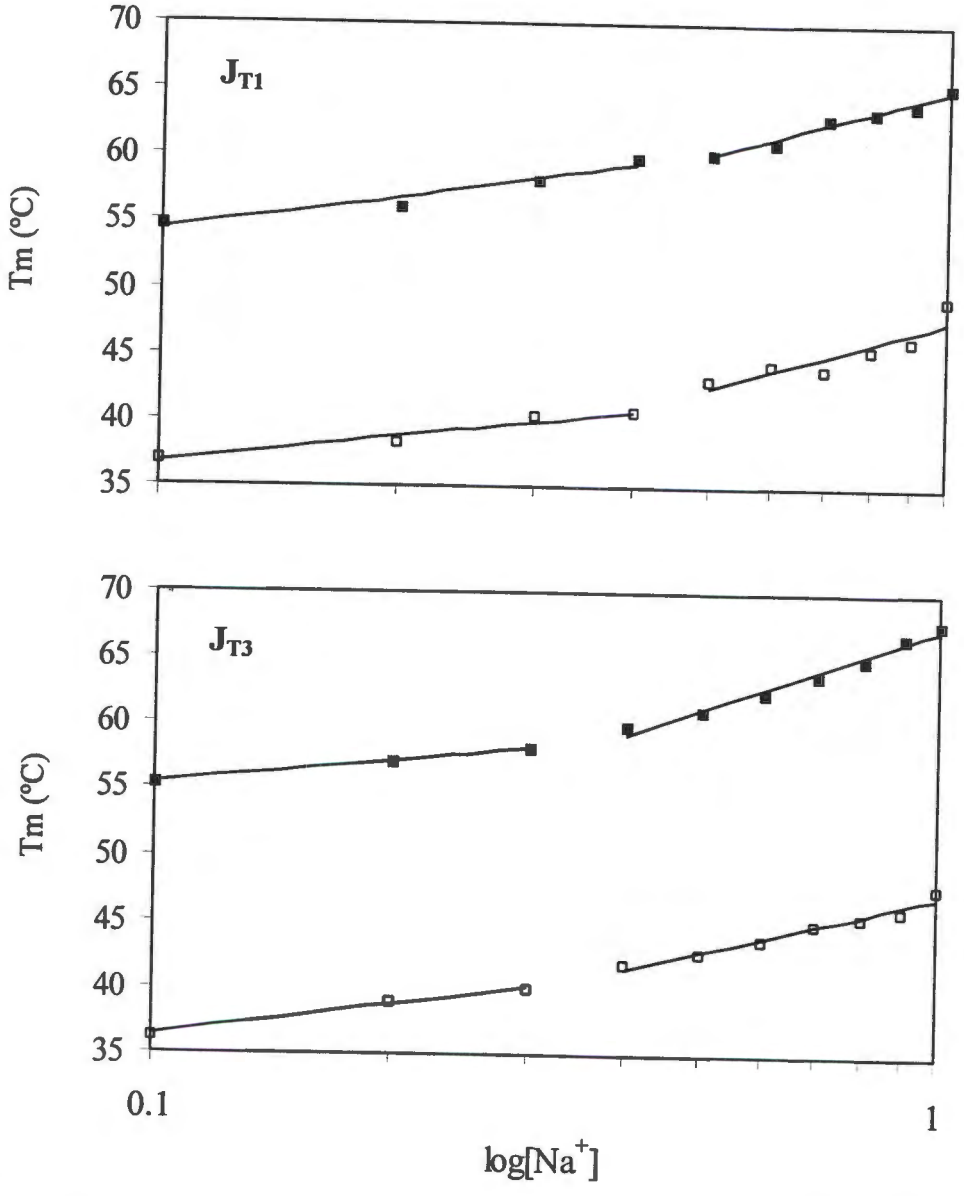

Figure 5.8: The plots of Tm as a function of log[Na^+] for J_{T1} (top graph) and J_{T3} (bottom graph). Open squares represent the first transition. Filled squares represent the second transitions.

5.2.2. Differential scanning calorimetry

Figure 5.9 depicts the experimentally observed excess heat capacity curve of J_{T1} (pH 5.0 and 4.79) and J_{T3} (pH 5.0 and 4.6). The corresponding plot for the complete triple-helical four-way junction J_{T1T3} is illustrated in **Figure 5.10**. Baselines were subtracted from the curves. All scans were reproducible to within less than 5% on second heating of the same sample. As observed for the UV melting experiments, the DSC reveals two transitions, one of them pH dependent and the other pH independent. Deconvolution of the curves using the Origin program yielded four transitions under all pH conditions. The areas under the graph represent the transition enthalpies of the individual arms. The thermodynamic parameters extracted this way are listed in **Table 5.2**. Each junction displays a set of different thermodynamic data and the implication of this will be discussed further down. For J_{T1} and J_{T3}, the first two transitions are pH independent. This confirms the UV absorbance melting data indicating that these transitions are associated with the melting of the double-helical arms of the junctions. J_{T1T3} surprisingly melts at higher temperature(s) than J_{T1} and J_{T3} (**Table 5.3**). A possible explanation for this observation is that the symmetrical folding and the two loops on opposite arms reduce the conformational entropy, resulting in a higher melting temperature.

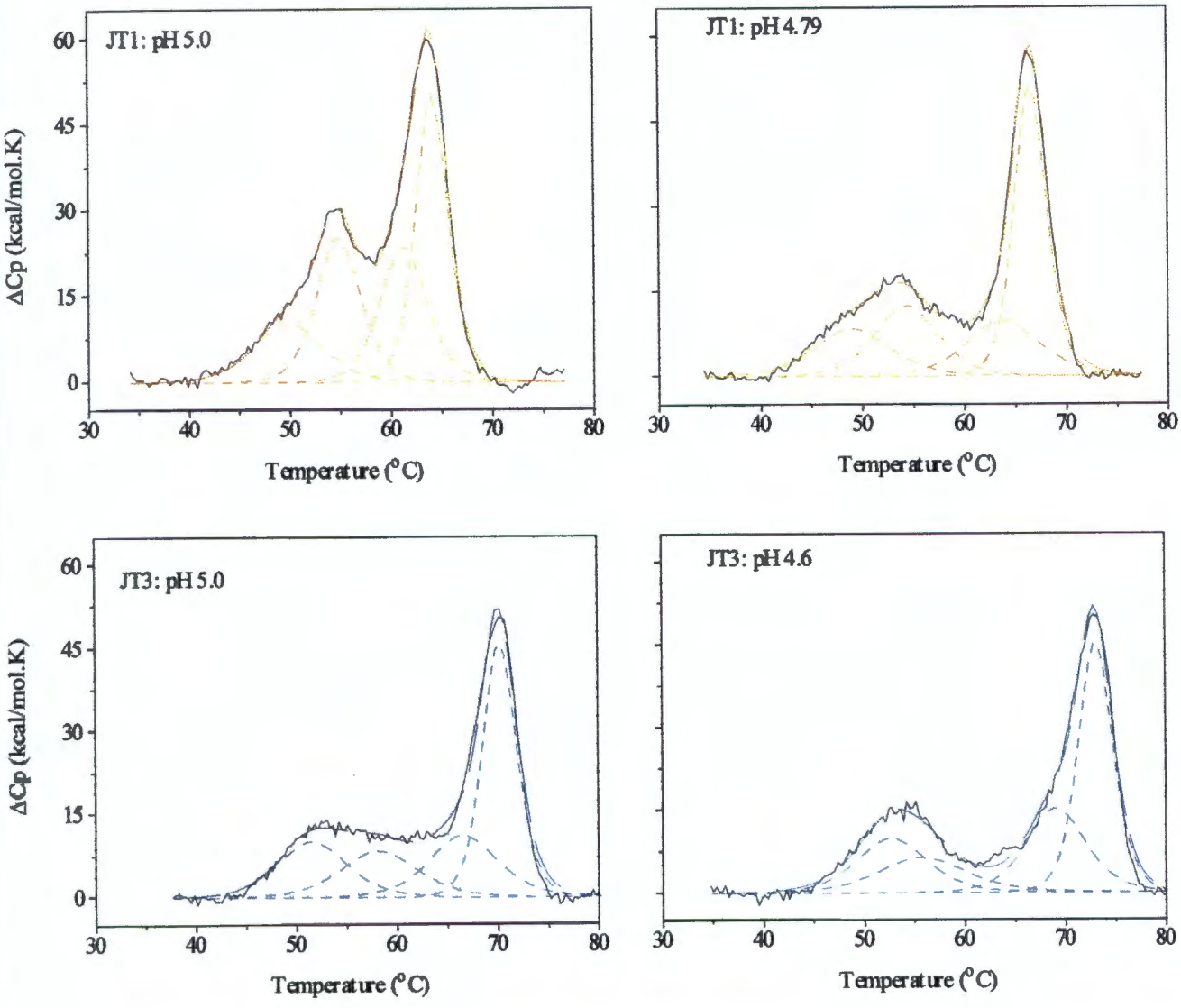

Figure 5.9: DSC curves of J_{T1} (Top) at pH 5.0 and pH 4.67. The bottom graphs represent the DSC curves of J_{T3} at pH 5.0 and 4.6. Total strand concentration for each junction is 140.5 μM. Measurements were carried out in 20mM Na_3PO_4, 1M NaCl. The solid black lines in all curves represent the experimental data. The solid orange (J_{T1}) and royal (J_{T3}) lines are the fitted curves and the underlying peaks represent the deconvoluted transitions.

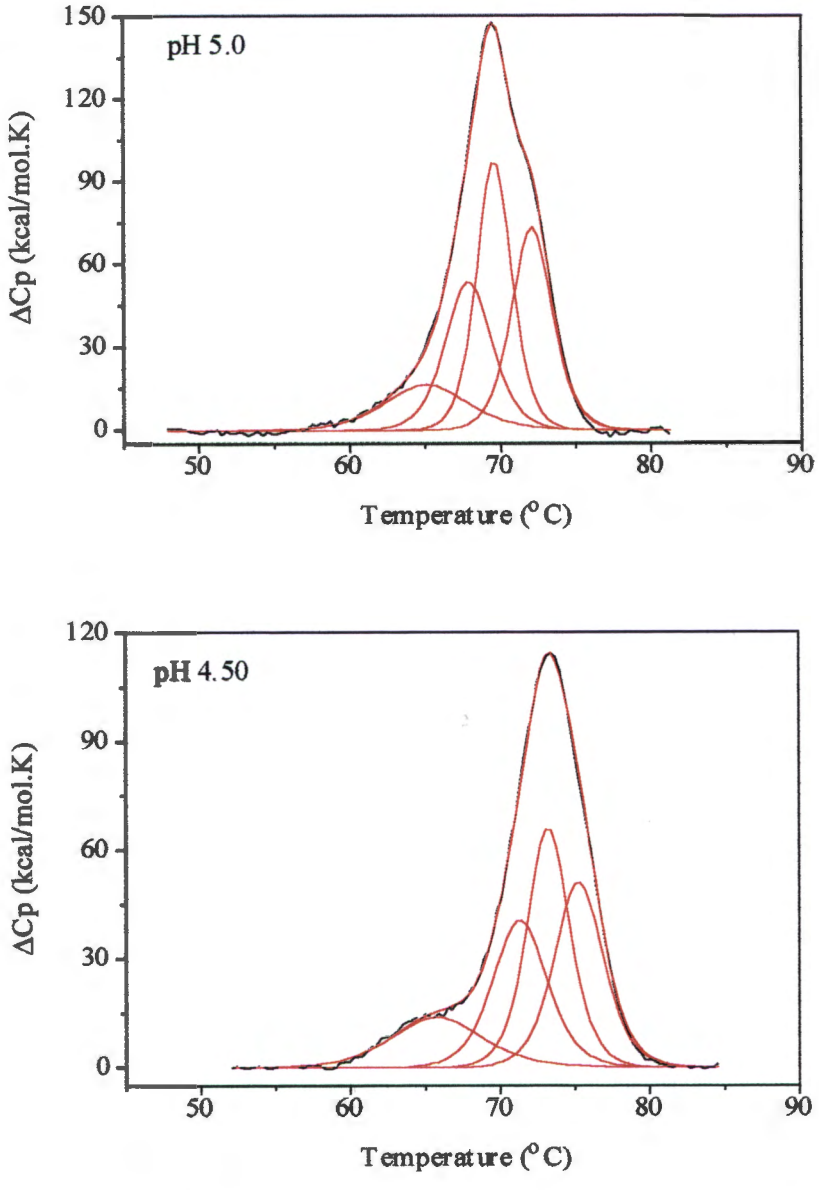

Figure 5.10: The excess heat capacity as a function of temperature curves (black lines) of J_{T1T3} obtained in 20mM Na_3PO_4 and 1M NaCl at pH 5.0 and 4.5 respectively. The red lines represent the deconvoluted enthalpy contributions of the individual transitions. The total strand concentration = 140.5μM.

Table 5.1: Thermodynamic parameters of J_{T1} and J_{T3} obtained from UV absorbance melting data.

	J_{T1}						J_{T3}					
pH	Tm1[a]	ΔH1[b]	ΔS1[c]	Tm2[a]	ΔH2[b]	ΔS2[c]	Tm1[a]	ΔH1[b]	ΔS[c]	Tm2[a]	ΔH2[b]	ΔS2[c]
5.5	47.0	171.9	537.0	55.3	435.5	1212.8	45.0	168.9	530.3	59.0	308.6	907.6
5.25	46.4	170.2	532.6	59.7	446.2	1280.4	43.7	168.2	528.1	62.3	300.1	899.6
5.0	46.9	170.7	533.4	62.7	433.8	1291.6	45.1	168.8	530.4	64.2	303.5	904.0
4.6	46.8	170.3	533.2	66.7	440.0	1307.0	45.2	168.8	531.3	68.0	310.4	909.7
pH 5.0	ΔH1 + ΔH2 = 604.5			ΔS1 + ΔS2 = 1825.0			ΔH1 + ΔH2 = 472.3			ΔS1 + ΔS2 = 1434.4		
pH 4.6	ΔH1 + ΔH2 = 610.3			ΔS1 + ΔS2 = 1840.2			ΔH1 + ΔH2 = 479.2			ΔS1 + ΔS2 = 1441.0		

[a] Tm units = °C
[b] ΔH_{VH} units = kcal.mol^{-1}
[c] ΔS_{VH} units = cal.mol^{-1}.K^{-1}
1cal = 4.18 J
Buffer contains 20mM Na_3PO_4, 1M NaCl.

Table 5.2: Thermodynamic parameters of J_{T1} and J_{T3} obtained from DSC data.

Junction	pH	Tm1[a]	ΔH1[b]	ΔS1[c]	Tm2[a]	ΔH2[b]	ΔS2[c]	Tm3[a]	ΔH3[b]	ΔS3[c]	Tm4[a]	ΔH4[b]	ΔS4[c]
J_{T1}	5.0	50.4	85.5	263.7	54.5	110.0	336.0	61.5	120.5	358.0	64.0	205.3	602.2
	4.79	49.6	69.0	213.8	53.3	99.8	306.0	64.4	108.0	319.6	66.5	220.7	656.4
J_{T3}	5.0	52.8	95.8	294 .0	59.0	79.3	208.6	66.6	109.6	305.8	70.2	209.7	608.0
	4.6	52.8	100.6	320.8	59.8	81.2	237.8	68.7	105.9	360.0	72.8	208.0	589.0

J_{T1}: pH 5.0 $\Delta H1 + \Delta H2 + \Delta H3 + \Delta H4 = 520.8$ $\Delta S1 + \Delta S2 + \Delta S3 + \Delta S4 = 1416.4$

: pH 4.79 $\Delta H1 + \Delta H2 + \Delta H3 + \Delta H4 = 497.5$ $\Delta S1 + \Delta S2 + \Delta S3 + \Delta S4 = 1495.8$

Average = 509.2 Average = 1456.1.0

J_{T3}: pH 5.0 $\Delta H1 + \Delta H2 + \Delta H3 + \Delta H4 = 494.4$ $\Delta S1 + \Delta S2 + \Delta S3 + \Delta S4 = 1371.8$

: pH 4.6 $\Delta H1 + \Delta H2 + \Delta H3 + \Delta H4 = 495.7$ $\Delta S1 + \Delta S2 + \Delta S3 + \Delta S4 = 1507.6$

Average = 495.0 Average = 1440.0

[a]Tm units are °C

[b]ΔH units are $kcal.mol^{-1}$

[c]ΔS units are $cal.K^{-1}.mol^{-1}$

1 cal = 4.18J

Buffer contains 20mM Na_3PO_4, 1M NaCl at pH 5.0 or 4.5.

Table 5.3: Thermodynamic parameters of J_{T1T3} obtained from UV absorbance melting and DSC data

pH	Tm1[a]	ΔH1[b]	ΔS1[c]	Tm2[a]	ΔH2[b]	ΔS2[c]	Tm3[a]	ΔH3[b]	ΔS3[c]	Tm4[a]	ΔH4[b]	ΔS4[c]
❶5.0	65.0	111.3	328.7	67.7	160.8	471.0	69.5	117.3	346.4	72.1	225.4	650.8
❶4.6	65.6	112.3	331.5	71.2	160.5	466.0	73.1	119.8	324.6	75.1	224.3	644.0
❷5.0	56.4	228.6	693.8	64.9	351.6	1040.2						
❷4.56	60.0	173.4	520.5	69.4	361.0	1054.0						

❶5.0 ΔH1 + ΔH2 + ΔH3 + ΔH4 = 615.0
❶4.6 ΔH1 + ΔH2 + ΔH3 + ΔH4 = 616.9
Average = 616.0

ΔS1 + ΔS2 + ΔS3 + ΔS4 = 1797.0
ΔS1 + ΔS2 + ΔS3 + ΔS4 = 1765.5
Average = 1781.2

❷5.0 ΔH1 + ΔH2 = 580.6
❷4.5 ΔH1 + ΔH2 = 534.4
Average = 557.5

ΔS1 + ΔS2 = 1734.0
ΔS1 + ΔS2 = 1574.5
Average 1654.0

[a]Tm units are °C
[b]ΔH units are kcal.mol^{-1}
[c]ΔS units are cal.K^{-1}.mol^{-1}
❶ Data obtained from DSC experiments
❷ Data obtained from UV absorbance melting experiments
Buffer contained 20mM Na_3PO_4, 1M NaCl at pH 5.0 or 4.6.

CHAPTER 6

THE STRUCTURE OF THE TRIPLE HELICAL FOUR-WAY JUNCTION, J_{T2T4} AND ITS COMPONENTS, JUNCTIONS J_{T2} AND J_{T4}.

The triplex four-way J_{T2T4} is formed by annealing S1, T2, S3 and T4, **Figure 6.1A**. To enable the interpretation of data, J_{T2T4} is represented by two simplified junctions J_{T2} and J_{T4} **(Figure 6.1B)** which allow to study certain features of J_{T2T4} independently. Hybridizing 20-mers S1, S3, S4 and T2 results in J_{T2}. T2 is a 44mer generated by extending the 20mer S2 at the 5'end by a four cytosine spacer and twenty pyrimidine bases. At appropriate buffer conditions, the underlying double-helical four-way junction Js should form followed by the annealing of the 5' extension of T2 onto arms 2 and 1. This will result in a four-way junction containing two triple-helical arms (1 and 2) and two double-helical arms (3 and 4).

J_{T4} is formed by hybridizing S1, S2, S3 and T4 where T4 is the extension of S4. Folding of T4 onto arm 4 and 3 will result in the formation of four-way junction with arms 1 and 2 as double helices and arms 3 and 4 as triple-helices. The difference between the strands forming J_{T1T3} and J_{T2T4} is that in J_{T1T3} (**cf Chapter 5**). S2 and S4 are extended from the 3'end whereas in J_{T2T4} they are extended from the 5'end.

S1 5' GAAAGGAGAAGAAAAAAGAA 3'
S3 5' AGAAAGAAGGAGAGAAGAGA 3'
T2 5' CTTTCCTCTTCTTTTTTCTT CCCC TTCTTTTTTCCCTTCTTTCT3'
T4 5' TCTTTCTTCCTCTCTTCTCT CCCC TCTCTTCTCTTTCTCCTTTC 3'

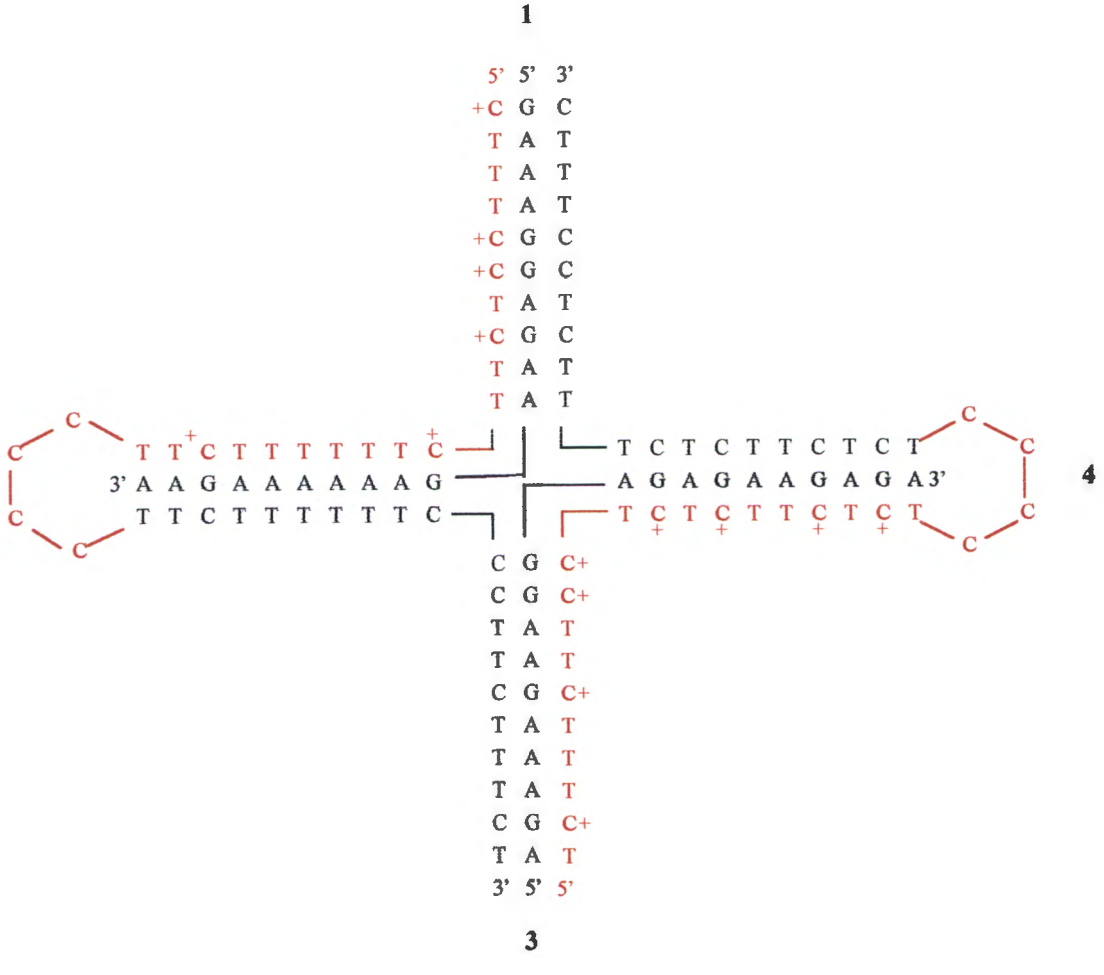

Figure 6.1A: Schematic representations of the sequences contributing to the structure of J_{T2T4}. J_{T2T4} is assembled from S1, T2, S3 and T4. S2 and S4 (from Js) are extended at the 5' with a four-member cytosine spacer to form T2 and T4 respectively. The loops are located on arms 2 and 4. Special features of J_{T2T4} can be studied with the help of J_{T2} and J_{T4} (next page), named according to the position of the C4-loops. The Hoogsteen strands are shown in red color.

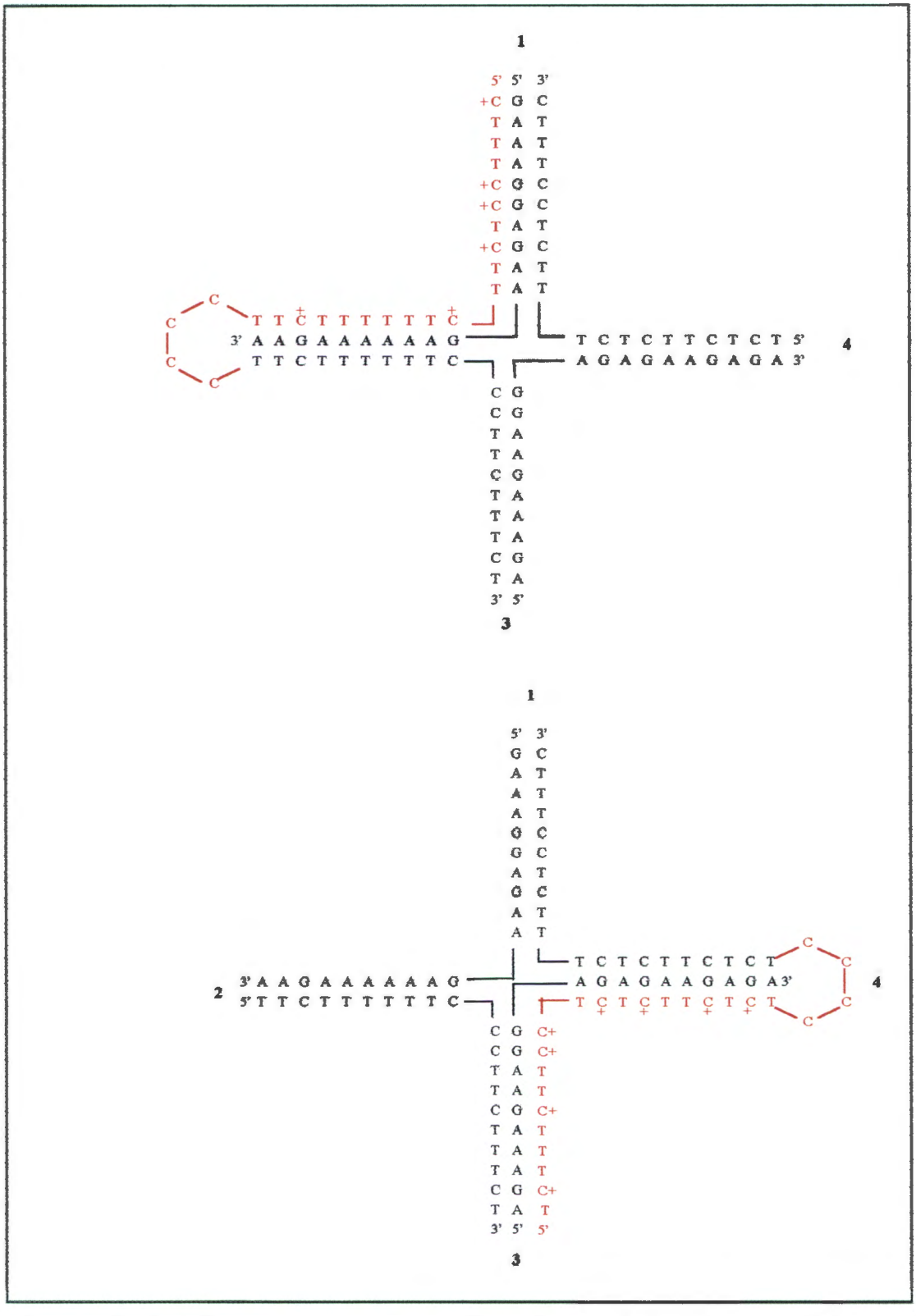

Figure 6.1B: Schematic representation of J_{T2} (Top) and J_{T4} (Bottom). Each junction forms part of the complete triple-helical four-way junction, J_{T2T4}. The Hoogsteen strands are shown in red color.

6.1 The formation of J_{T2T4} and its simplified representations J_{T2} and J_{T4}.

6.1.1 pH titration

Figure 6.2 shows the pH dependent folding patterns for J_{T2}, J_{T4} and J_{T2T4} as monitored by the absorbance at 260nm *versus* pH. The titrations were performed in 20mM Na_3PO_4 and 1M NaCl at 18°C (260nm). The pH was lowered from 12 to 2 using minute amounts of concentrated HCl (to minimize the dilution effects). At pH 12 to pH 11, the oligonucleotides forming J_{T2} (**Figure 6.2A**: open triangles) remain in a single-stranded coil form as is shown by the constant maximal absorbance. The absorbance decreases as the pH is lowered between 11 and 10. This signifies the formation of the double-helical species, most likely the core double-helical four-way junction Js with dangling 5'extension on arm 2. The absorbance remains constant between pH 10 and 7.0 indicating that no further folding occurs. A small but significant change in absorbance is observed between pH 7 and pH 6.5. This may be linked to the binding of the third strand to the helix in arm 2. This is likely because arm 2 contains the highest number of the TA•T triads. The complete formation of the triplex structure in arm 2 and its stability at this pH can be attributed to the hairpin loop that reduces the conformational entropy. It is likely that already at this pH, the binding of the third strand takes place. The resulting triple helical four-way junction may still increase in stability with further decrease in pH. Dropping the pH results in a further decrease of the absorbance. This can be assigned to the complete formation of the four-way junction. The absorbance reaches a minimum at about pH 4 to pH 3.5. It increases from this point as the pH is increasingly lowered indicating an unfolding of the four-way junction.

The pH dependent folding of J_{T4} follows the same pattern as observed for J_{T2} (**Figure 6.2B**: crosses). The absorbance is maximal and constant between pH 12 and 10.7. Lowering the pH decreases the absorbance, signaling the formation of the double-helical four-way junction. The

absorbance is constant between pH 9.8 and 6.9. Dropping the pH further results in the decrease in the absorbance, suggesting the binding of the third strand to the duplex arms 1 and 4 as part of the folding of the complete structure.

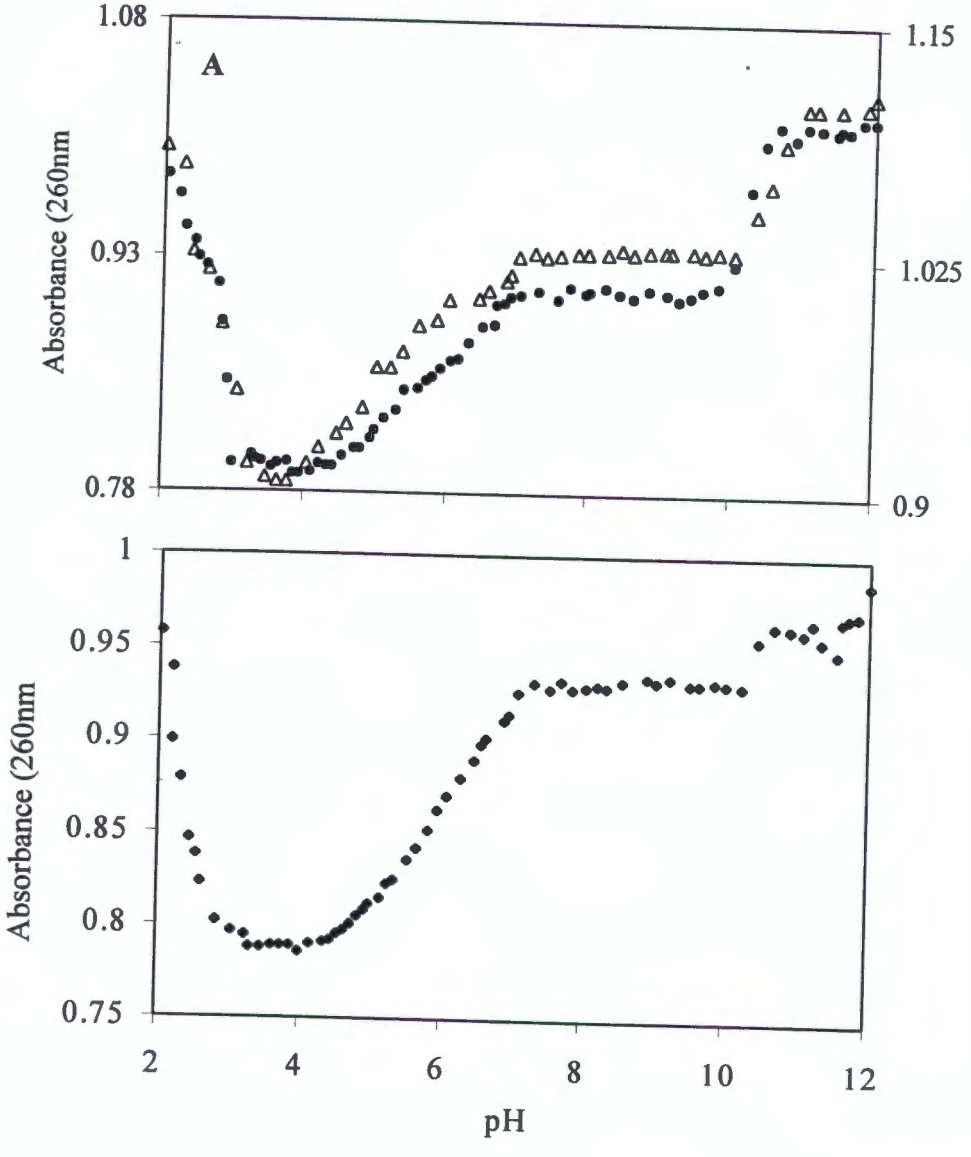

Figure 6.2: **A.** pH titration curves of J_{T2} (open triangles) and J_{T4} (crosses). **B.** pH titration curve of J_{T2T4}. The absorbance readings were recorded at 260nm and 18° C. Buffers contained 20mM Na_3PO_4 and 1M NaCl. The total strand concentration per junction = 14.05μM.

The pronounced decrease in absorbance between pH 7 and 6.5 observed in J_{T2} titration is not observed with J_{T4}. The absorbance reaches a minimum at about pH 4 and 3.25 and increases steadily again with the decreasing pH.

Figure 6.2B shows the pH titration curve obtained for J_{T2T4} under similar conditions. The general folding pattern resembles that of J_{T2} and J_{T4}. The oligonucleotides remain in a random coil conformation between pH 12.0 and pH 10.5 as illustrated by the maximal absorbance. Dropping the pH to 10.0 is accompanied by the decrease in absorbance, an effect associated with the formation of the double-helical four-way junction with dangling 5' extensions on arms 2 and 4. The absorbance remains invariant between pH 10.0 and 7.0. This is the pH range where the DNA duplex Js is stable. There is a marked decrease in the absorbance between pH 7.0 and 4.5. This suggests the binding of the third strands to their corresponding duplex arms, resulting in the triple-helical four-way junction J_{T2T4}. The absorbance reaches a minimum between pH 4.0 and 3.25. Decreasing the pH below 3.0 results in the increase in the absorbance. The increase in absorbance is attributed to the unfolding of the triple-helical junction into single strands again.

6.1.2. Polyacrylamide gel electrophoresis

The migration patterns of single-stranded oligonucleotides and the various corresponding equimolar combinations were analyzed in a 20 % polyacrylamide gel at 4°C (Buffer contained 100mM Ammonium Acetate, 10mM $MgCl_2$, 100mM NaCl, pH 5.0). The results are illustrated in **Figure 6.3**. In the native gel containing J_{T2} and its components (**Figure 6.3A**), single strands S1, S3, S4 and T2 are loaded in the last four lanes (8 – 11). Binary complexes S3T2, S4T2 and S1T2 are present in lanes 5, 6 and 7 respectively. S1T2 migrates much slower than other binary complexes because part of it forms a triplex with a loop.

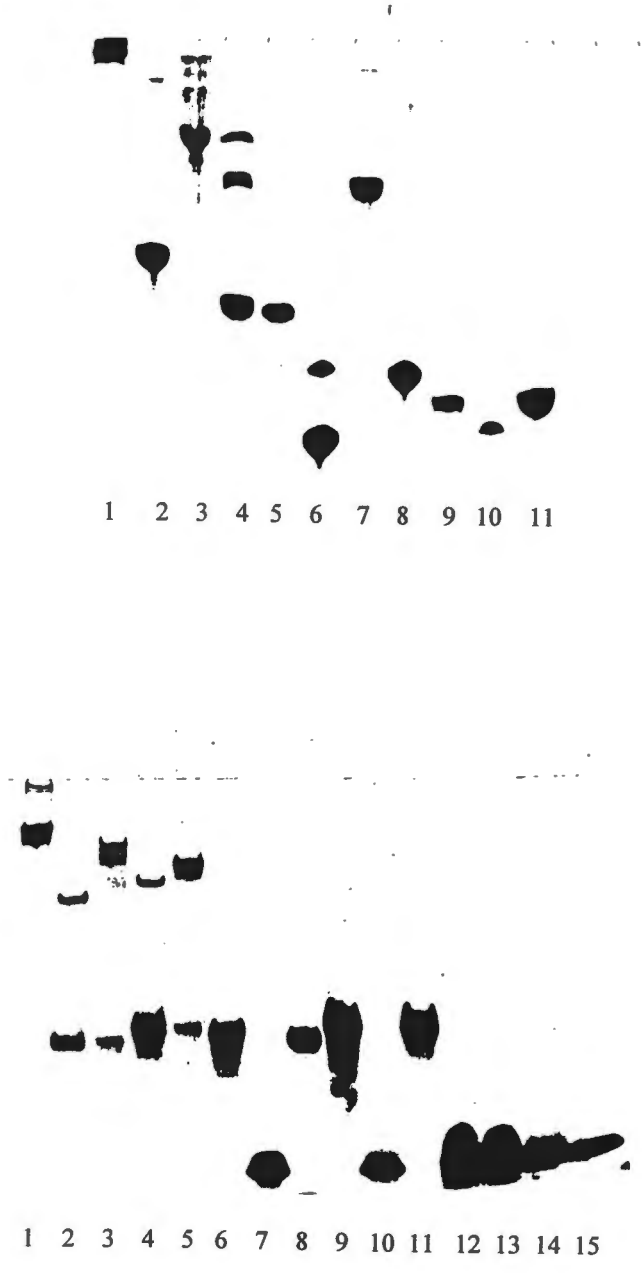

Figure 6.3. A. Polyacrylamide gel electrophoresis of J_{T2}. Buffers contained 100mM ammonium acetate, 100mM NaCl, 10mM $MgCl_2$ at pH 5.0. The last four lanes contain single strands S1, S3, S and T2. Lanes 5, 6 and 7 represent binary mixtures S3T2, S4T2 and S1T2 respectively. Lanes 2 to 4 contain ternary complexes S3S4T3, S1S4T2 and S1S3T2 respectively. The band in lane 1 represents the quartenary complex, J_{T1}. **B.** Native gel elctrophoresis of J_{T2T4}. Single strands S1, T2, S3 and T4 are in lanes 12 to 15 respectively. Binary complexes are in lanes 6 – 11and ternary complexes in lanes 2 – 5. The band in lane 1 represents the triple-helical four-way junction J_{T2T4}.

The presence of a single band in lanes 5 and 7 signifies the formation of one species. S4 and T2 are both pyrimidine strands and thus do not form a pair, lane 6. The ternary complexes, S3S4T2, S1S4T2 and S1S3T2 are run in lanes 2, 3 and 4 respectively. S3S4T2 and S1S4T2 form single species whereas the ternary complex S1S3T2 is unstable. The single band in lane 1 represents the equimolar mixture of S1, S3, S4 and T2. The slower migration relative to binary and ternary complexes illustrates that the four-way junction (J_{T2}) has been formed.

Figure 6.3B represents the polyacrylamide gel electrophoresis of J_{T2T4}. The bands in lanes 15 and 13 represent the 20-mers S1 and S3 and bands in lanes 12 and 14 represent 44-mers T2 and T4 respectively. Bands in lanes 6 to 11 represent the binary complexes S3T4, T2T4, S3T2, S1T4, S1S3 and S1T2 respectively. Each lane contains a single band, suggesting the formation of only one species (except for bands in lanes 7 and 10 which each represents the migration of two species of the same length). Bands in lanes 2 to 5 represent the ternary complexes S1S3T2, S3T2T4, S1S3T4 and S1T2T4 respectively. The ternary complexes are unstable as shown by two bands in those lanes. The lower bands migrate with the same mobility as binary complexes in lanes 8, 9 and 11. The top bands can be assigned to the complete ternary structures. That is, the ternary complexes seem to be in equilibrium with the binary complexes. The full triple helical four-way junction runs slightly higher (lane 1) than the ternary complexes S3T2T4 and S1T2T4. The appearance of the single band in lane 1 confirms the formation of the complete triple-helical four-way junction J_{T2T4}.

6.1.3. Osmium tetroxide modifications

T2 and T4 were radioactively labelled at the 5'-terminus respectively. Samples of J_{T2} and J_{T4} were prepared in buffer solutions containing 100mM NaCl and 10mM $MgCl_2$ at pH 5.0 or pH 8.0. The same samples were also prepared in the absence of cations at pH 8.0 or pH 5.0. The junctions were modified by OsO_4 and subsequently cleaved with piperidine. The products were analyzed by denaturing polyacrylamide (20%) gel electrophoresis. The results of the OsO_4 modifications performed on J_{T2} and J_{T4} are shown in **Figure 6.4**.

Figure 6.4A illustrates the OsO_4 modification results for J_{T2}. Lane 1 contains the untreated T2 strand. The single stranded T2 strand is cleaved predominantly from the 5'end (bottom of the gel), Lane 2. Lane 3 contains J_{T2} at pH 8.0 with no salt added. T2 strand is again cleaved considerably suggesting that the junction did not form under these conditions. Addition of 50mM Na^+ and 20mM Mg^{2+} at pH 8.0 results in the different cleavage pattern. T2 is partially cleaved (lane 4). The observed cleavage is markedly reduced or completely abolished when the pH is dropped to 5 (cf. lanes 5 and 6) indicative of the formation of the intact four-way junction J_{T2}.

Figure 6.4B shows the OsO_4 modifications results of J_{T4}. Untreated single stranded T4 is present in lane 8 followed by the treated T4 in lane 9. T4 is cleaved at pH 8.0 and in the absence of salt, lane 10. This is also the case at pH 5.0 in the absence of salt, lane 12. There is minimal cleavage on arm 4 at pH 8 in the presence of salt, lane 11. Similar results were obtained for J_{T3} where at pH 8 and in the presence of salt where there is minimal cleavage of the third strand. This is surprising because it is expected that the third strand will be cleaved at pH 8.0. The third strands in J_{T3} and J_{T4} are on arms 3 and 4. The difference is the position of the loop. At pH 5 and in the presence of salt, there is no cleavage anywhere in the junction, lane 13. This illustrates the formation of a complete four-way junction with two triple-helical arms.

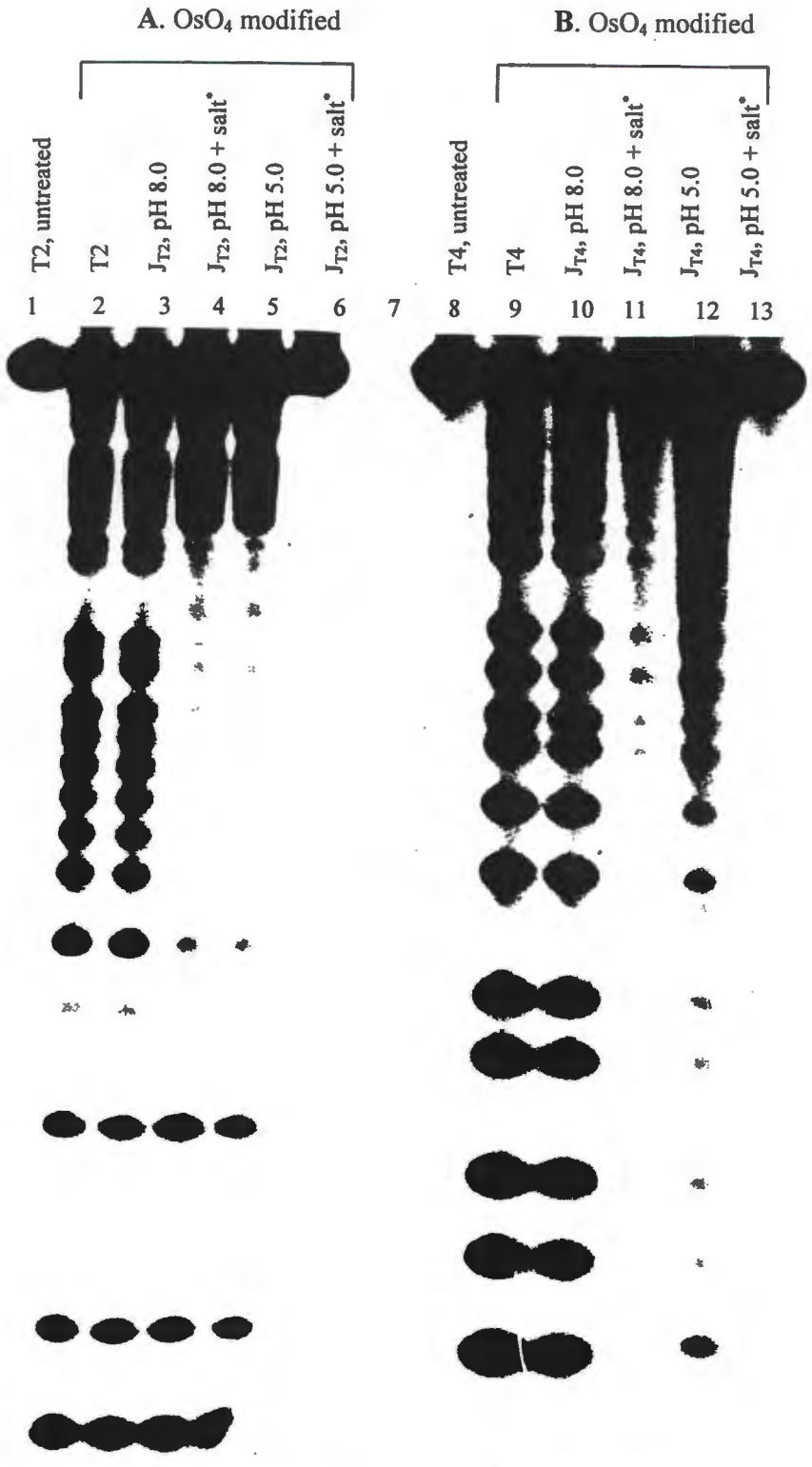

Figure 6.4: OsO_4 modifications of strands T2 and T4. Lanes 1 and 8 contain unmodified single strands T2 and T4 respectively. Lanes 2 and 9 contain modified single strands. In lanes 3 – 6 (T2) and 10 – 13 (T4), the strands are incorporated in their respective junctions. Radioactively labelled strands were reacted with 1mM OsO_4 and 3% pyridine in the absence or presence of 100mM Na^+ and 10mM Mg^{2+} under different pH conditions.

*100mM Na^+ and 10mM Mg^{2+}.

6.2. Thermodynamics of J_{T2}, J_{T4} and J_{T2T4} unfolding.

6.2.1. Thermal melting of J_{T2} and J_{T4} as a function of pH.

The thermal unfolding of J_{T2} and J_{T4} respectively were determined at different pH conditions in the buffer containing 20mM Na_3PO_4 and 1M NaCl. Shown in **Figure 6.5A** (top graph) are the first derivatives of melting profiles of J_{T2} at different pH conditions. At pH 6.6 a monophasic but broad transition (gold curve) emerges with a Tmax of about 49.0°C. The broad peak could be the result of four unresolved superimposed transitions. Between pH 5.5 and 4.6, a clear biphasic melting transition is observed. In addition to the transition at about 49°C a second transition emerges which exhibits a higher Tm. It shifts to even higher temperature as the pH is decreased. The bottom graph in **Figure 6.5A** illustrates the thermal unfolding of J_{T4}. At pH 7.0, there is a single peak (gold) corresponding to the unfolding of the double-helical four-way junction. There is a small pre-transition at about 28°C. Lowering the pH to 6.5 results in the appearance of a shoulder on the low temperature side (green curve). At pH 6.0, the two transitions are completely merged (grey curve). Lowering the pH further separates the peak into two distinct transitions (pink and black curves). The first transition is pH independent, with a Tmax of 45.3 ± 0.8 °C. The Tm of the second transition is pH dependent. The Tm increases with the decrease in pH. The results obtained here are similar to the results obtained for J_{T1} and J_{T3}. However, there is a difference in Tm's obtained for each of the junction. For instance, it was expected that the Tm for the first transitions of J_{T1} and J_{T2} should be equal because the same arms (arms 3 and 4) are melted. This is not the case; the first transition for J_{T2} (Tmax = 51.8°C) is at a higher temperature than the first transitions of the complementary arms of J_{T1}. This is likely to do with the loop which, depending on its position within the junction, renders three of the arms interlinked. The sequence composition also contributes to the discrepancies. In case of J_{T1}, arm 2 is made from

two separate strands and it contains the least amount of GC base pairs. This will have a destabilizing effect on arm 3 and thus lower the Tm of the first transition. However, in J_{T2} arm 2 is capped by a loop and its transition can be viewed as intramolecular. It is therefore possible to suggest that the stabilizing effect by the loop on arm 2 (J_{T2}), which is the least stable in the whole junction, is more pronounced as compared with other arms capped with a loop. In case of J_{T3} and J_{T4}, there is a very small difference in the Tmax of the first transition (44°C and 45.3°C respectively).

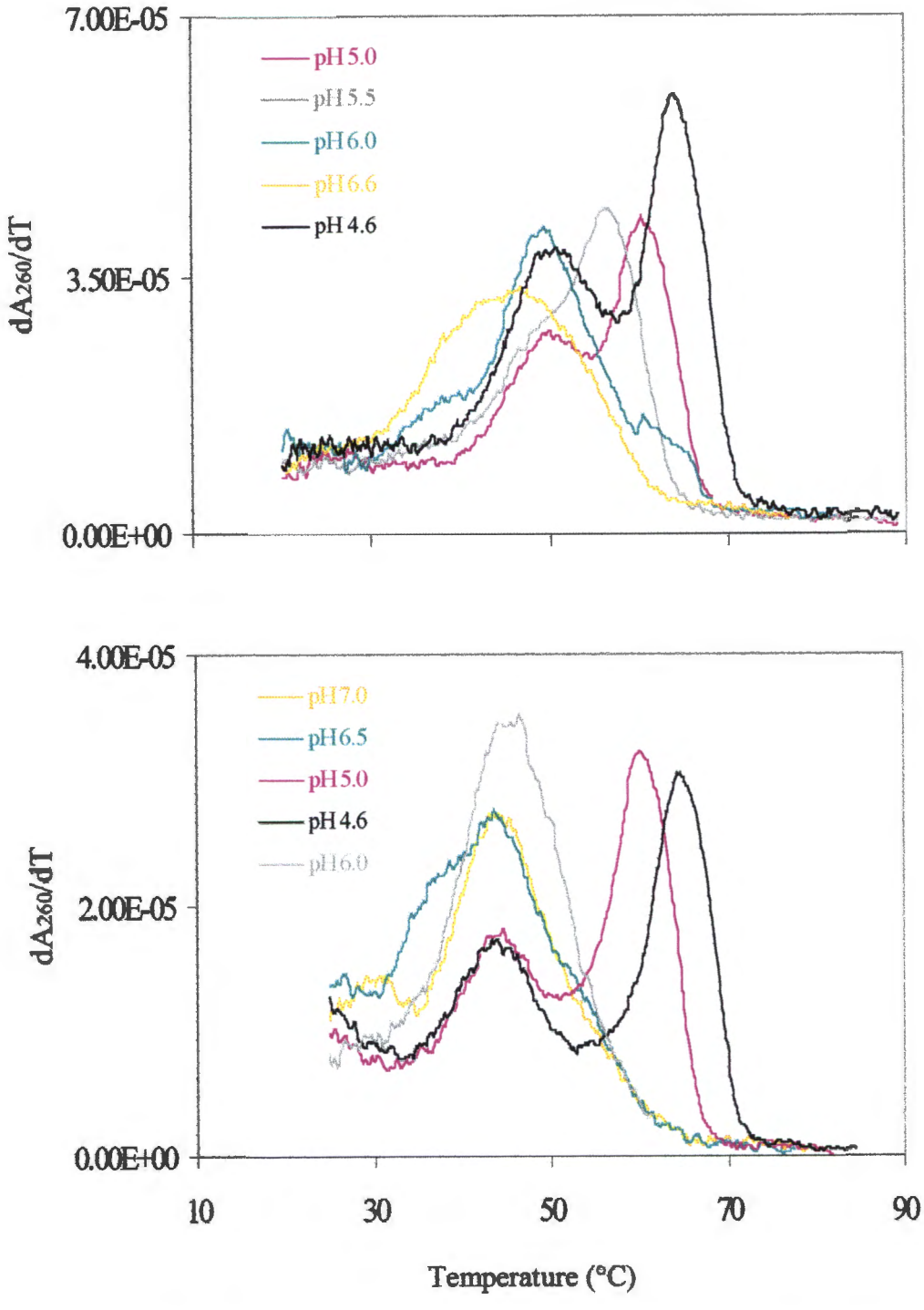

Figure 6.5A: First derivative ($\delta A_{260}/\delta T$) melting profiles of J_{T2} (top graph) and J_{T4} (bottom graph) obtained in 20mM Na_3PO_4 and 1M NaCl under varying pH conditions. The total strand concentration per junction equals 14.05μM.

Figure 6.5B represents the thermal denaturation curves of the triple-helical four-way junction J_{T2T4} recorded in 20mM Na_3PO_4, 1M NaCl and varying pH conditions. At pH 7.0, a single broad peak (gold curve) with a Tmax of about 55°C appears. There is a pronounced asymmetry on the low temperature side of the transition, indicating non-cooperative unfolding such as unstacking of single strands. The transition is assigned to the unfolding of the double-helical four-way junction with dangling 5' extensions.

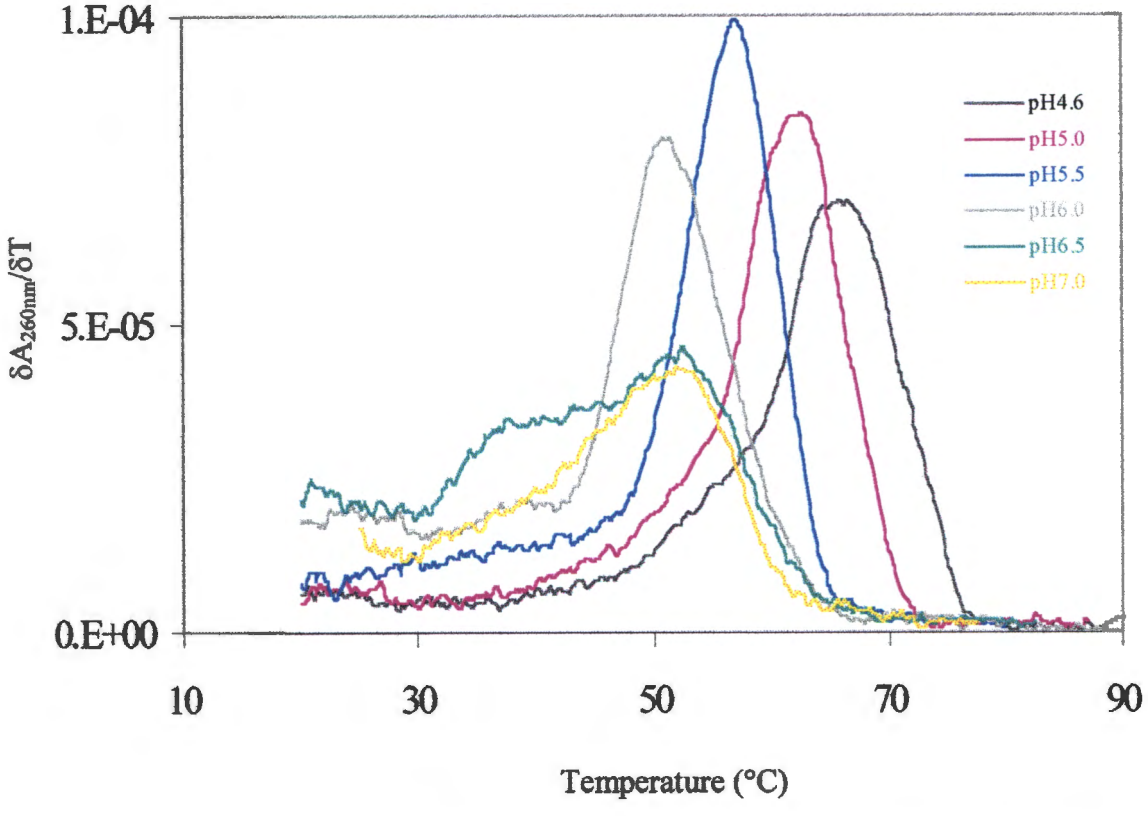

Figure 6.5B: First derivative ($\delta A_{260}/\delta T$) melting profiles of J_{T2T4} obtained in 20mM Na_3PO_4 and 1M NaCl under varying pH conditions. The total strand concentration equals 14.05μM.

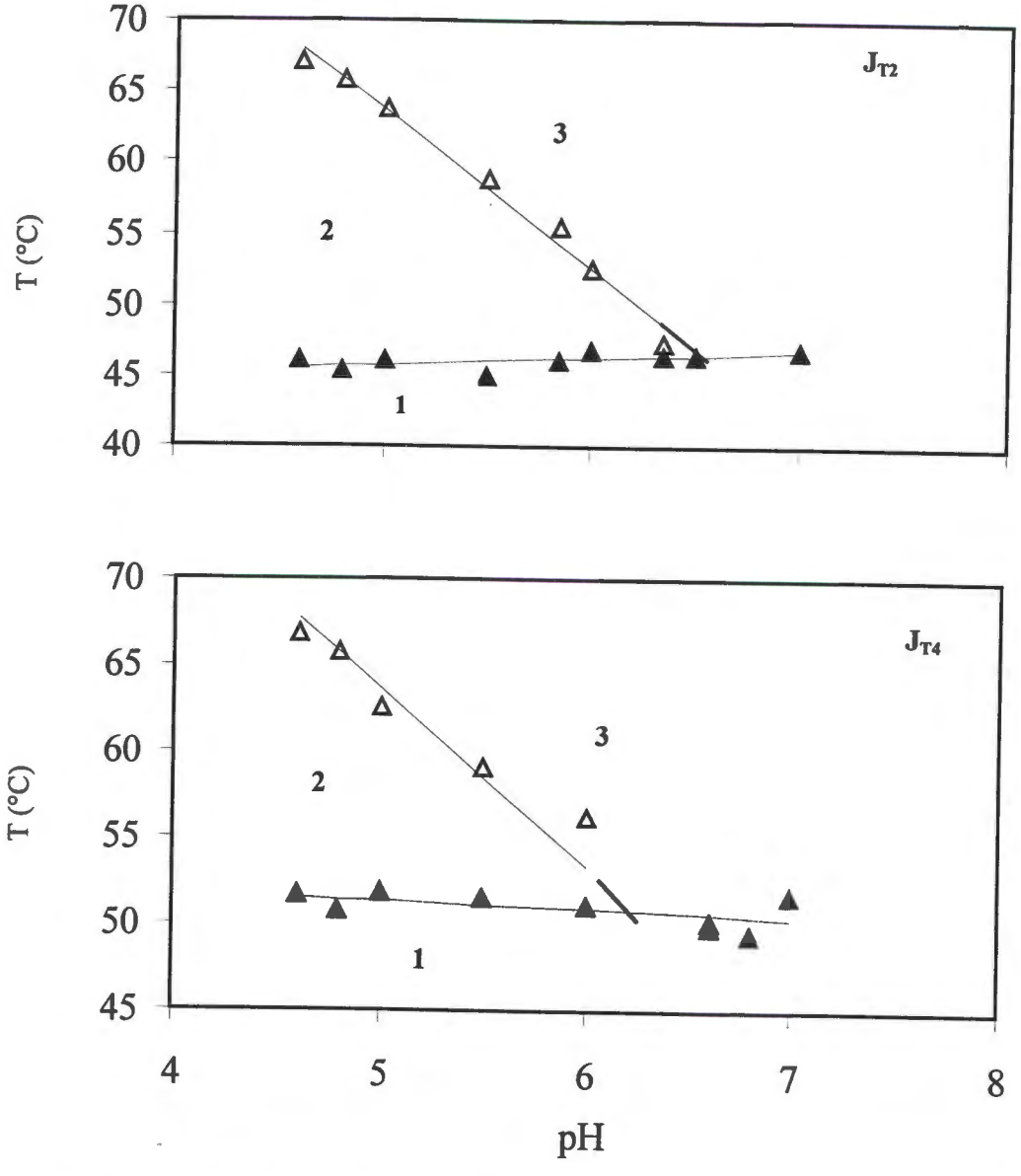

Figure 6.6: Phase diagram of J_{T2} and J_{T4}. The Arabic numerals represent the areas where the different conformations are dominant. 1: the complete four-way junction with two double-helical and two triple-helical arms. 2: The triplex arms, intact and the double helices unfolded. Above pH 6.5, the melting temperature of th structures increases with the decrease in pH. 3: single strands.

Lowering the pH results in the appearance of a pre-transition (green curve) at a lower Tmax (41°C). At pH 6.0, the main transition has become almost symmetric and only a small pre-transition remained. The transitions shift to higher temperature with a further decrease in pH. Between pH 5.0 and 4.6, yet a shoulder appears at about the position of the Tm of the pH 6.0 peak. It is slightly pH dependent. It is very difficult at this stage to assign the individual transitions to any particular structure element because of the overlapping transitions. The thermodynamic data obtained from UV absorbance melting curves are listed in **Table 6.1.**

Figure 6.6 illustrates the plots of Tm as a function of pH in the form of phase diagrams for J_{T2} and J_{T4}. It is clear from both plots that the Tm of the first transitions (▲) is independent of the pH between 7.0 and 4.5. The slopes corresponding to the transitions are -0.18 °C/pH for J_{T2} and -0.21 °C/pH for J_{T4}. The absence of pH dependence (shown by the marginal slope) indicates the unfolding of double helical arms 3 and 4 (J_{T2}) and arms 1 and 2 (J_{T4}). Similar results were obtained for J_{T1} and J_{T3} **(cf. Chapter 5.).** The second transitions show the linear pH dependency (dTm/dpH = -10.3°C/pH for J_{T2} and -10.98 °C/pH for J_{T4}) expected from the dissociation of a third strand which contains cytosines. The slopes are also in the same range as those obtained for J_{T1} and J_{T3}. The effect of the loop on the δTm/δpH will be discussed later.

6.2.2. The effect of the ionic strength on the stability of the folded structures of J_{T2} and J_{T4}.

The effect of the ionic strength on the melting temperatures of J_{T2} and J_{T4} is shown **Figure 6.7.** The ionic strength dependency of both the first and the second transitions of J_{T2} resemble that of the junctions J_{T1} and J_{T3} **(cf. Chapter 5)**. The slope ($\delta Tm/\delta$ (log[Na^+]) = 10.6°C) above 0.4M Na^+

is more pronounced than the slope ($\delta Tm/\delta$ ($\log[Na^+]$) = 7.8°C) below 0.4M Na^+ for the first transition. This is also the case for the second transition where the slope below 0.4M Na^+ equals 7.3°C/$\log[Na^+]$ and the slope above 0.4M Na^+ equals 15.4°C/$\log[Na^+]$. The Tm *versus* $[Na^+]$ series of J_{T4} produces three transitions, all of which are dependent on the Na^+ concentration. The second transition appears as a shoulder on the lower temperature site of the main transition. The two transitions are not as clearly separated in the Tm *versus* pH plots as in the Tm *versus* $\log[Na^+]$ plots. The value for the slope corresponding to the first transition is 8.14°C/$\log[Na^+]$. The second transition has a steeper slope of the value 11.0°C/$\log[Na^+]$. The high temperature transition of J_{T4} display different behavior. The Tm dependence on sodium ion concentration (($\delta Tm/\delta$ ($\log[Na^+]$) = 5.4°C/$\log[Na^+]$) is smallest. Also evident is its higher thermal stability as compared to the other junctions at the same Na^+ concentration range. This probably has to do with the sequence composition of arms 3 and 4 and the arrangement of cytosines on the third strands.

6.2.3 Differential scanning calorimetry.

The DSC profiles of the unfolding of J_{T2}, J_{T4} and J_{T2T4} are illustrated in **Figures 6.8** and **6.9**. For J_{T2}, the same general behavior was observed as was recorded for the unfolding of other junctions. There are two main transitions, one pH dependent and the other pH independent. J_{T4} displays a different pattern at pH 4.6 where only one transition at the lower temperature is observed. The main peak can be deconvoluted into three transitions. This suggests a different unfolding pattern for J_{T4} at pH 4.6. Deconvolution of all the curves yielded four transitions (shown by colored lines) under all pH conditions. The areas under the graph represent the sum of all transition

enthalpies. They were determined by using Origin scientific plotting software. The thermodynamic parameters are listed on **Table 6.2.**

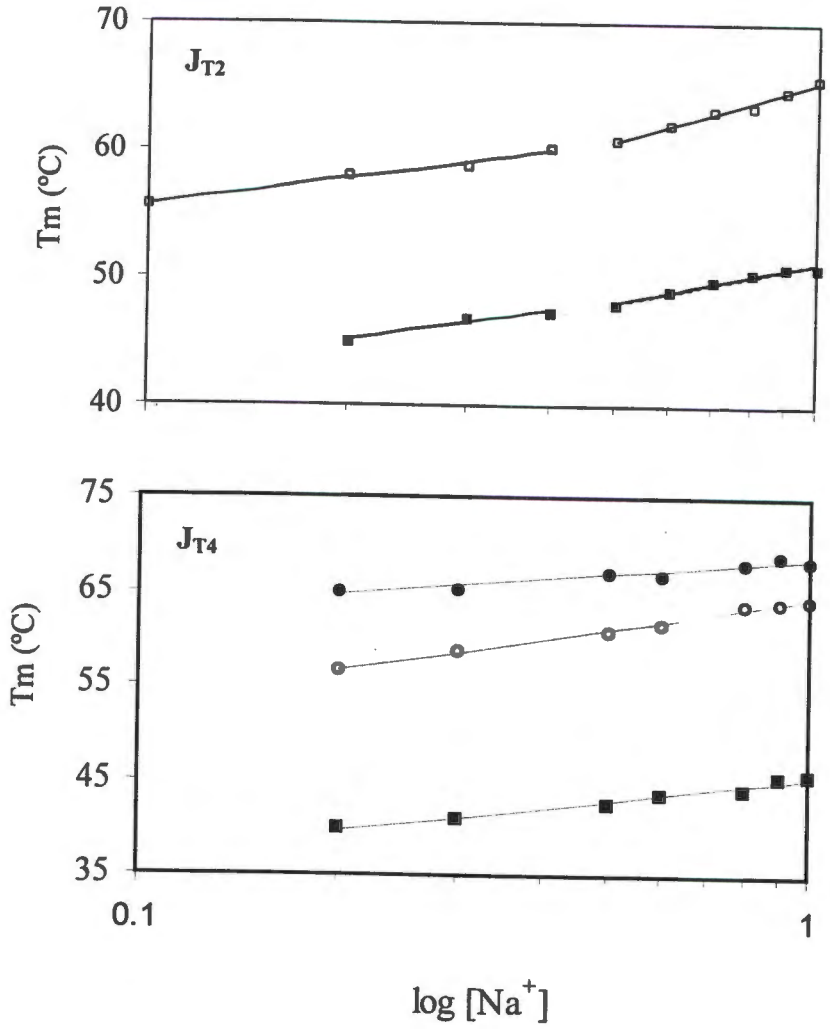

Figure 6.7: Phase diagram Tm *versus* log [Na^+] for J_{T2} (top graph) and J_{T4} (bottom graph). Total strand concentration for each junction = 14.05μM. Buffer contains 20mM Na_3PO_4, pH 4.6.

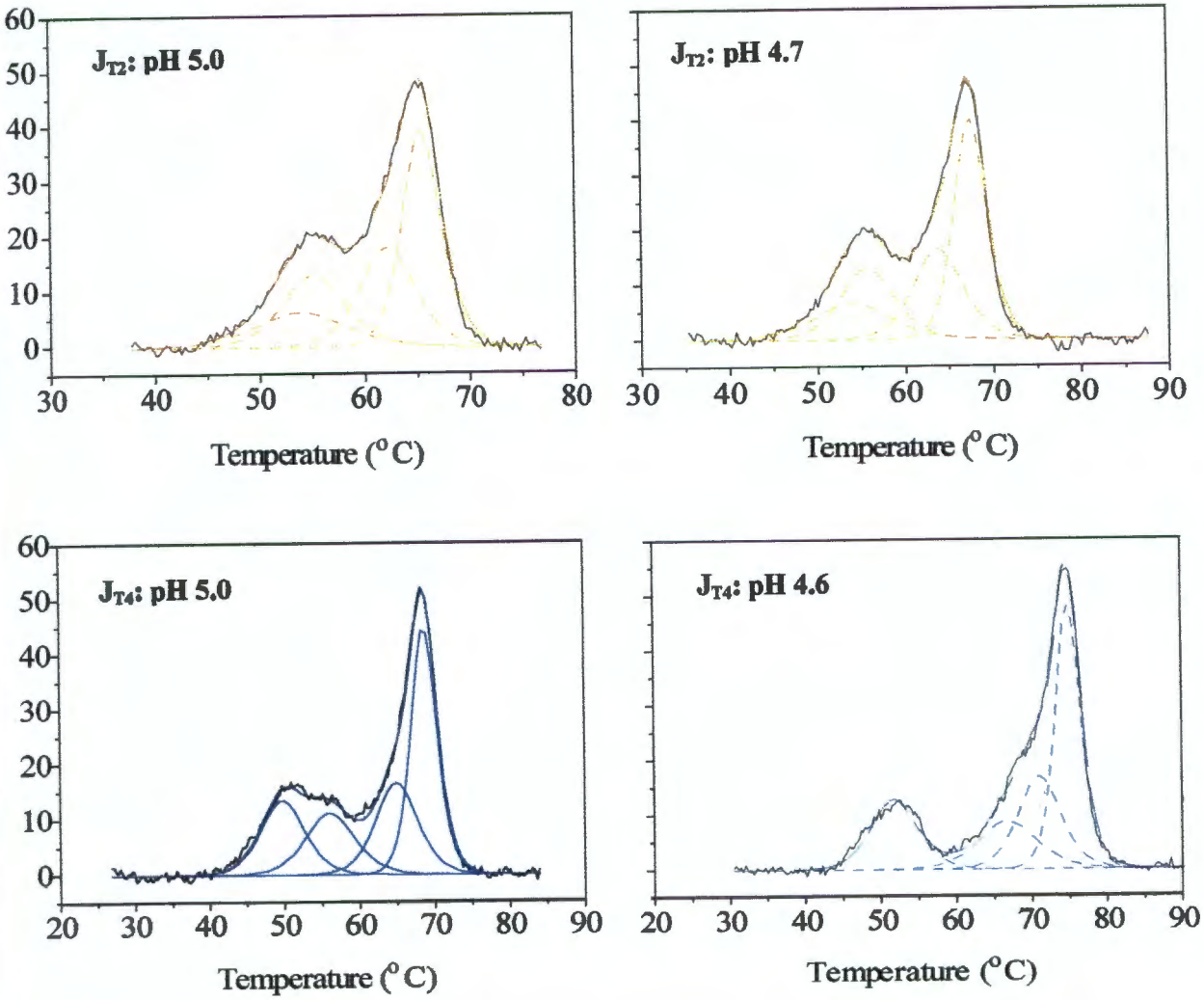

Figure 6.8: Excess heat capacity versus temperature plots (black lines) of J_{T2} (top graphs) and J_{T4} (bottom graphs) in 20mM Na_3PO_4 and 1M NaCl. The strand concentration per junction = 140.5μM. The colored peaks represent the deconvoluted subtransitions.

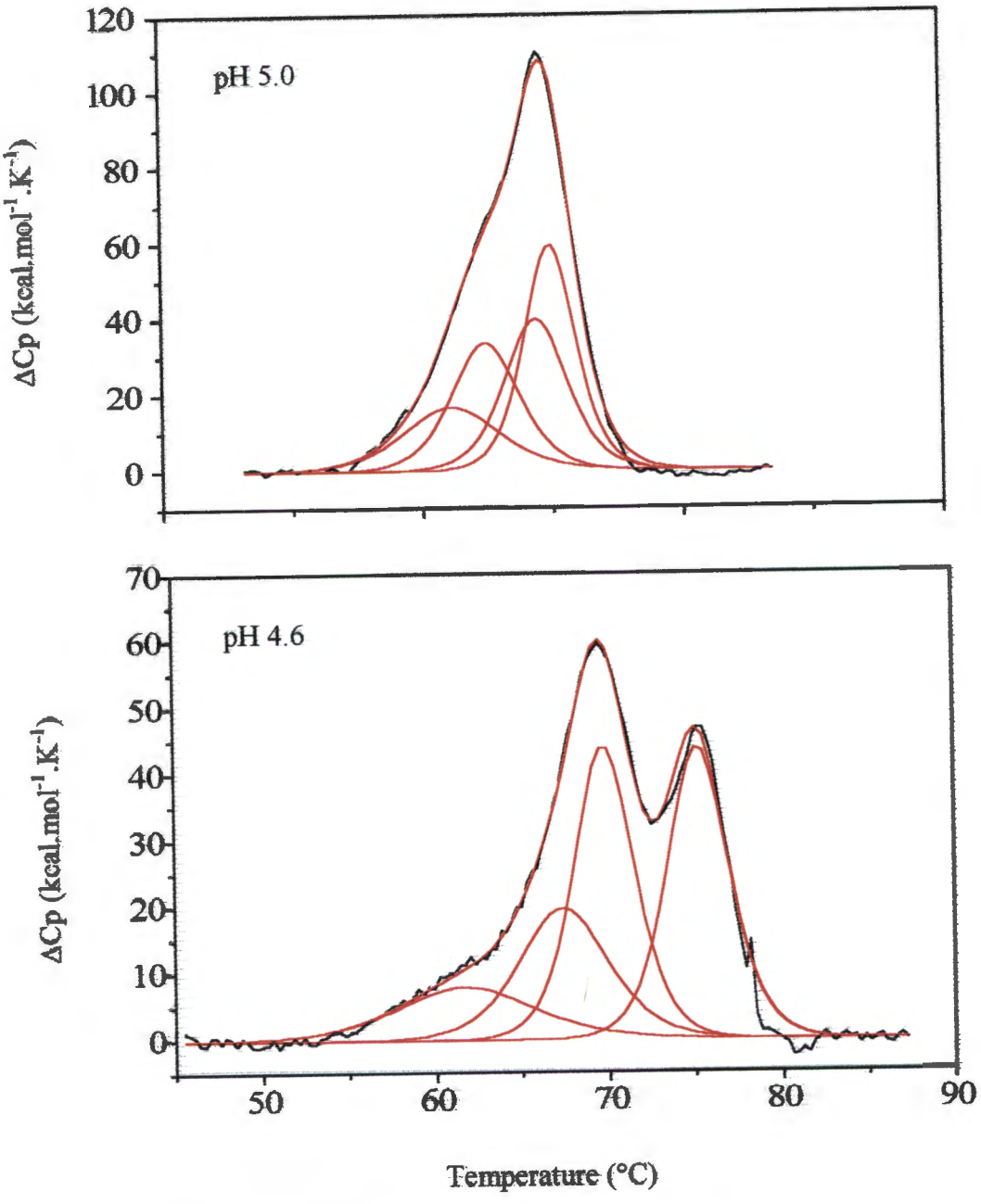

Figure 6.9: DSC profiles of J_{T2T4} at pH 5.0 and pH 4.60. The black line represents the excess heat capacity as a function of temperature. The red peaks represent the deconvoluted substructures.

Table 6.1: Thermodynamic parameters of J_{T2} and J_{T4} obtained from UV absorbance melting data.

	J_{T2}						J_{T4}					
pH	Tm1[a]	ΔH1[b]	ΔS1[c]	Tm2[a]	ΔH2[b]	ΔS2[c]	Tm1[a]	ΔH1[b]	ΔS1[c]	Tm2[a]	ΔH2[b]	ΔS2[c]
5.5	51.5	171.4	524.6	59.1	400.9	1230.0	45.0	185.8	584.0	58.7	414.4	1228.0
5.0	52.9	170.0	521.6	62.6	402.6	1200.0	46.1	205.9	645.0	63.7	412.6	1224.0
4.6	51.6	162.3	500.0	66.8	385.2	1133.2	46.0	187.8	588.0	67.0	420.0	1234.6

pH 5.0	ΔH1 + ΔH2 = 562.6	ΔS1 + ΔS2 = 1721.6	ΔH1 + ΔH2 = 618.5	ΔS1 + ΔS2 = 1869.0
pH 4.6	ΔH1 + ΔH2 = 547.5	ΔS1 + ΔS2 = 1633.2	ΔH1 + ΔH2 = 600.4	ΔS1 + ΔS2 = 1822.6
Average +				

[a]Tm units = °C
[b]ΔH_{VH} units = kcal.mol^{-1}
[c]ΔS_{VH} units = cal.mol^{-1}.K^{-1}
1cal = 4.18 J
Buffer contains 20mM Na_3PO_4, 1M NaCl

Table 6.2: Thermodynamic parameters of J_{T2} and J_{T4} obtained from DSC data.

Junction	pH	Tm1[a]	ΔH1[b]	ΔS1[c]	Tm2[a]	ΔH2[b]	ΔS2[c]	Tm3[a]	ΔH3[b]	ΔS3[c]	Tm4[a]	ΔH4[b]	ΔS4[c]
J_{T2}	5.0	51.4	73.6	225.7	55.0	107.0	326.0	62.0	128.0	384.5	65.2	190.0	560.0
	4.79	51.7	76.1	227.4	55.6	107.8	328.2	63.6	120.6	354.1	67.2	189.2	556.1
J_{T4}	5.0	50.2	95.7	296.0	55.8	86.8	264.0	64.8	116.0	341.4	68.5	201.5	590.0
	4.6	51.3	97.3	302.8	65.0	83.4	278.1	70.4	120.5	350.4	74.6	208.0	598.2

J_{T2}: pH 5.0 $\Delta H1 + \Delta H2 + \Delta H3 + \Delta H4 = 498.6$ $\Delta S1 + \Delta S2 + \Delta S3 + \Delta S4 = 1496.2$
: pH 4.6 $\Delta H1 + \Delta H2 + \Delta H3 + \Delta H4 = 493.7$ $\Delta S1 + \Delta S2 + \Delta S3 + \Delta S4 = 1465.8$
Average = 496.2 Average = 1481.0

J_{T4}: pH 5.0 $\Delta H1 + \Delta H2 + \Delta H3 + \Delta H4 = 502.0$ $\Delta S1 + \Delta S2 + \Delta S3 + \Delta S4 = 1491.4$
: pH 4.6 $\Delta H1 + \Delta H2 + \Delta H3 + \Delta H4 = 509.4$ $\Delta S1 + \Delta S2 + \Delta S3 + \Delta S4 = 1541.5$
Average = 505.7 Average = 1510.5

[a]Tm units are °C
[b]ΔH units are kcal.mol^{-1}
[c]ΔS units are cal.K^{-1}.mol^{-1}
1 cal = 4.18J
Buffer contains 20mM Na_3PO_4, 1M NaCl at pH 5.0 or 4.5

Table 6.3: Thermodynamic parameters of J_{T2T4} melting obtained from UV absorbance melting and DSC data

pH	Tm1[a]	ΔH1[b]	ΔS1[c]	Tm2[a]	ΔH2[b]	ΔS2[c]	Tm3[a]	ΔH3[b]	ΔS3[c]	Tm4[a]	ΔH4[b]	ΔS4[c]
❶5.0	60.9	120.5	242.7	63.5	184.3	547.4	66.5	135.3	400.0	67.4	209.0	614.0
❶4.5	62.1	118.6	256.7	67.4	170.3	508.0	69.7	140.0	403.6	75.2	203.3	568.4
❷5.0	62.0	193.7	693.8	67.9	415.4	1218.0						
❷4.56	65.6	249.0	736.4	73.1	470.2	1358.0						

❶5.0 ΔH1 + ΔH2 + ΔH3 + ΔH4 = 649.1
❶4.6 ΔH1 + ΔH2 + ΔH3 + ΔH4 = 632.5
Average = 640.8

ΔS1 + ΔS2 + ΔS3 + ΔS4 = 1804.1
ΔS1 + ΔS2 + ΔS3 + ΔS4 = 1836.4
Average = 1820.3

❷5.0 ΔH1 + ΔH2 = 609.1
❷4.5 ΔH1 + ΔH2 = 719.2
Average = 664.2

ΔS1 + ΔS2 = 1911.8
ΔS1 + ΔS2 = 2094.4
Average = 2002.7

[a]Tm units are °C
[b]ΔHunits are $kcal.mol^{-1}$
[c]ΔS units are $cal.K^{-1}.mol^{-1}$
❶ Data obtained from DSC experiments
❷ Data obtained from UV absorbance melting experiments
Buffer contained 20mM Na_3PO_4, 1M NaCl at pH 5.0 or 4.6

DISCUSSION
CHAPTER 7

7.1. Evidence for the formation of the four-way junction containing triple-helical arms

The pH titration (**Figures 5.2 and 6.2**) results show that the oligonucleotides anneal and fold in a sequential manner to form first double helical four-way junctions and subsequently complete triple helices. The pH titration results were confirmed by the results obtained by the non-denaturing polyacrylamide gel (**Figure 5.3 and 6.3**). The individual strands, the binary, the ternary complexes as well as the quartenary complex (representing the junction) were subjected to gel electrophoresis under specified buffer conditions. The observation of the single species migrating with the vastly reduced mobility on the native gel provides convincing evidence that the complete junctions are formed. Furthermore, the increased hyperchromicity (18.75%) observed when the double helical four-way junction Js was formed as compared to that observed for the individual arms (~7.5% each) suggests that indeed the complete four-way junction is formed. Another evidence is the even higher hyperchromic change associated with the unfolding of J_{T1T3} and J_{T2T4}.

The OsO_4-piperidine modification results indicate the conformations the junctions assume under different pH and salt conditions (**Figure 4.3, 5.4 and 6.4**). At pH 8.0 and in the absence of salt, all the single-stranded pyrimidine strands were cleaved substantially, confirming the instability of these junctions and/or the random coil-state of the extended strands. The reactions were also performed in the presence of salt. The pyrimidine strands were cleaved as well. At pH 8.0 and in the presence of salt, the pyrimidine strand is incorporated into the junction and formed the double-helical four-way junction. The less pronounced cleavage of thymines (particularly in S2 and S4 strands of Js, (**Figure 4.3**)) in the absence of salt suggests that although not completely

stable, the four-way junction does form. The 3' or 5' extension of J_{T1}, J_{T2}, J_{T3}, and J_{T4} were cleaved, indicating the presence of the double-helical four-way junction with the dangling 3' or 5' extension. The absence of cleavage of thymine residues in each junction at pH 5.0 and in the presence of salt again confirmed the formation of the intact four-way junction with double-helical and/or triple-helical arms. The generalized folding pathway of oligonucleotides (forming J_{T1}, J_{T2}, J_{T3}, and J_{T4}) from random coils *via* a double-helical four-way junction intermediate into the triple helical four-way junction can therefore be proposed, **Figure 7.1**. The figure indicates possible isomerization between A and B conformers with the latter being the most preferred. That is, the 1/2 and 3/4 (A/B, C/D) stack

7.2. Thermodynamic data

7.2.1.1 Effect of pH on the melting temperatures of J_{T1}, J_{T2}, J_{T3}, and J_{T4}:

The UV absorbance melting and the DSC plots illustrate that varying pH does not have an effect on the Tm of double helices i.e. arms 1 and 2 of J_{T3} and J_{T4} and arms 3 and 4 of J_{T1} and J_{T2} respectively. This is also illustrated in the phase diagram of Tm *versus* pH **(Figs 5.7 and 6.6)**. The melting temperatures display minimal pH dependency expressed in the slopes (J_{T1} = –0.17°C/pH; J_{T2} = –0.18°C/pH; J_{T3} = –0.23°C/pH and J_{T4} = –0.21°C/pH). The lower melting temperatures obtained for the arms suggest that arms 1 and 2 of J_{T3} and J_{T4} and arms 3 and 4 of J_{T1} and J_{T2} respectively melt before the arms which are locked in triplex structures. However, the unfolding patterns or the order of the melting of the individual arms might not necessarily be the same for each junction. The thermal melting pattern will firstly depend on the position of the C4-loop and secondly on the sequence composition of the arms. Decreasing the pH of the solution has a stabilizing effect on all the triple helical arms (**cf. Figure 5.5, 5.6, 6.4** and **6.5**).

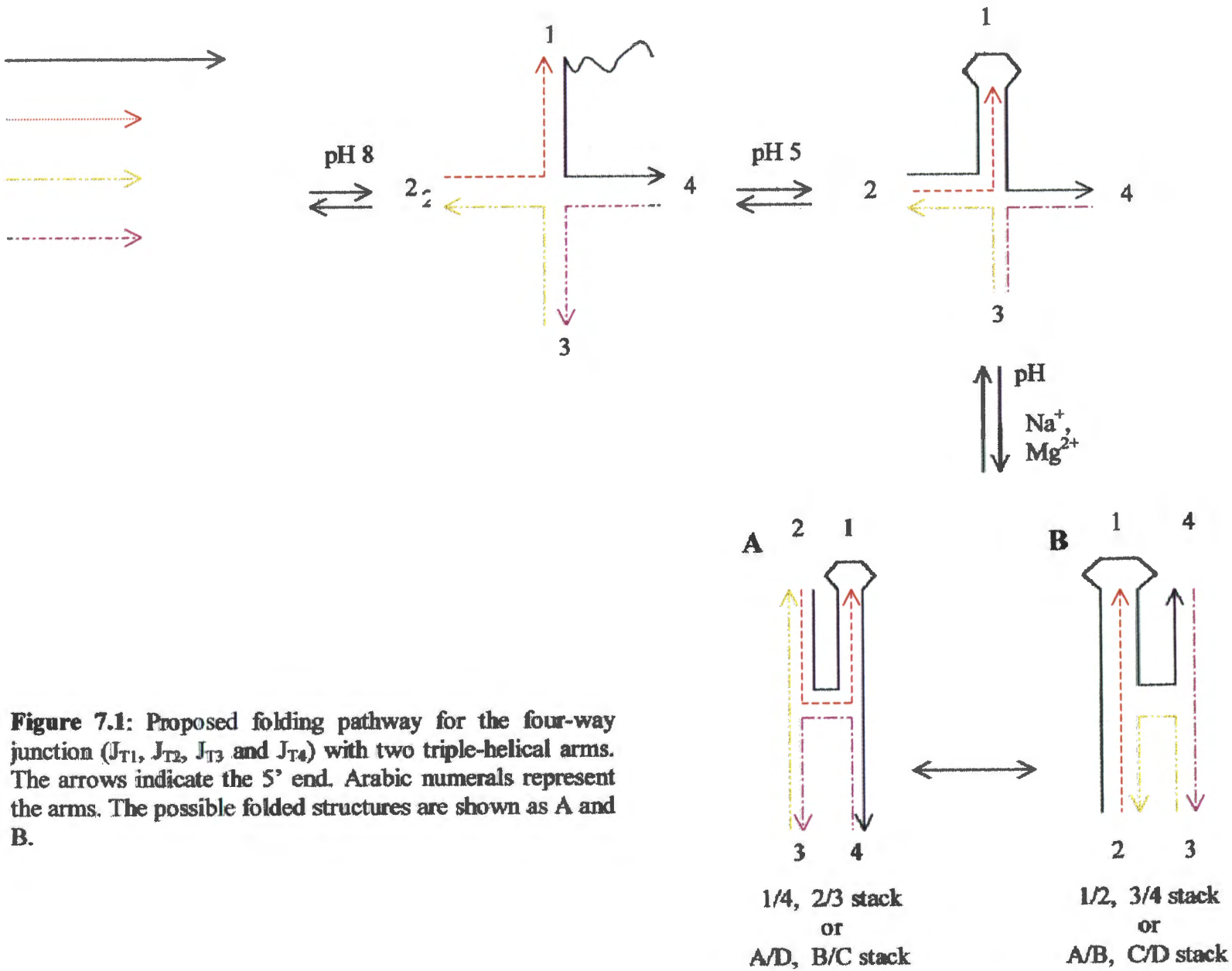

Figure 7.1: Proposed folding pathway for the four-way junction (J_{T1}, J_{T2}, J_{T3} and J_{T4}) with two triple-helical arms. The arrows indicate the 5' end. Arabic numerals represent the arms. The possible folded structures are shown as A and B.

The triple helical arms of J_{T1} and J_{T2} (arm 1and arm 2) have almost the same melting temperature. The difference is only 1°C (**Table 5.2 and 6.2**).

The melting temperatures assigned to the melting of arms 3 and 4 of J_{T3} and J_{T4} respectively also differ only marginally (about 2°C) (**Table 5.2 and 6.2**). J_{T1} and J_{T2} have the same third strand sequence. They differ only in the position of the loop. This also holds for J_{T3} and J_{T4}.

By contrast, the triple helical arms of J_{T3} and J_{T4} are thermally more stable than those of J_{T1} and J_{T2} respectively. As noted above, J_{T1} and J_{T2} may be destabilized by arm 2. Capping arm 2 with a loop should optimize the binding of the third strand and subsequently increase the melting temperature. Depending on the environmental conditions such as pH and ionic strength, the thermal stability of the triple helix increases linearly with the number of cytosines in the third strand if the third strand cytosines are separated by intervening thymines (Völker and Klump, 1994; Lee et al., 1984). However, it has been shown that in the case of intramolecular triplexes the destabilizing effect of the adjacent CG•C^+ triads is less significant at acidic pH as in the case of intermolecular complexes (Völker and Klump, 1994; Lee et al., 1984). The inspection of the third strand sequences of arm 1 (J_{T1}) and arm 3 (J_{T3}) suggests that the arms should melt at the same temperature because of the arrangement of the cytosines in the third strand. This is actually observed for the isolated arms of both junctions (**Table 7.1**). Within the junction, the triple helix in J_{T3} is thermally more stable than the triple helix in J_{T1}. Melting the third strand of arm 2 (J_{T1}), for instance, will affect the stability of arm 1 and *vice versa* and this will probably results in the decrease of the melting temperature of, in this case, arm 1. This may explain why the melting temperatures assigned to third strand melting of J_{T1}/J_{T2} and J_{T3}/J_{T4} respectively are the same. The results are also in line with the assumption of the presence of the folded structure **B** in **Figure 7.1. Table 7.1** shows that the most stable triplex occurs in arm 4 (J_{T4}). It should be noted that the

increased thermal stability of arm 4 as compared to other arms has more to do with the cytosine positions in the third strand than the presence of the loop. The loop should contribute to the stability of each junction equally (Wang et al., 1994; Booher et al., 1994).

Another observation related to adjacent CG•C^+ triads is that the J_{T3}/J_{T4} junctions are thermally more stable than the J_{T1}/J_{T2} junctions although the J_{T3}/J_{T4} junctions contain two consecutive cytosines at the branch point. The OsO_4 modification results do not suggest that the adjacent CG•C^+ triads destabilize the branch point and/or the arms they are positioned in. Thymines (both in the Watson-Crick and Hoogsteen strands) situated at the branch point of J_{T4} (arm 4) are not cleaved at pH 5 and in the presence of salt. In case of J_{T3}, the pyrimidine strand of the Watson-Crick does not have thymines at the branch point. The band corresponding to the cleavage of thymine in arm 4 (Hoogsteen strand) occurs higher up in the gel. It is difficult to comment on it and explain the observation. However, as in all other junctions, there is no cleavage at pH 5 and in the presence of salt. Thus, it seems that the adjacent CG•C^+ triads at the branch point have little or no effect on the melting temperatures of J_{T3} and J_{T4}. The order of thermal stability observed is $J_{T4} \geq J_{T3} > J_{T2} \geq J_{T1}$.

7.2.1.2 The effect of pH on the unfolding enthalpy, ΔHcal

The transition enthalpies obtained for each junction under pH conditions ranging from 6 to 4.5 turn out to be pH independent. This means that the stabilizing effect due to acidic pH is not enthalpic in origin. This supports the OsO_4 modification results that demonstrate that protonation of cytosine in the third strand does not induce folding of the triple-helical four-way junction into the stacked structure. The slight differences in the ΔHcal values can be attributed to the large temperature range over which these transitions occur. This points to a small but finite ΔΔCp.

Table 7.1: Thermodynamic parameters of the thermal melting of separate triple helical arms of different junctions (in brackets)

Arm	[a]Tm1	[b]ΔH1	[c]ΔS1	[a]Tm2	[b]ΔH2	[c]ΔS2
Arm1 (J_{T1})	35.4	52.4	169.4	60.4	66.8	198.5
Arm2 (J_{T1})	30.3	48.8	158.4	46.3	57.4	208.8
Arm1 (J_{T2})	33.9	55.4	179.2	57.4	78.5	236.6
Arm2 (J_{T2})	31.3	50.3	165.4	56.4	58.9	179.0
Arm3 (J_{T3})	36.4	54.1	174.7	61.0	61.4	182.6
Arm4 (J_{T3})	-	-	-	45.8	145.0	454.8
Arm3 (J_{T4})	34.3	65.5	213.0	59.6	87.0	261.5
Arm4 (J_{T4})	-	-	-	65.6	167.5	494.5

[a]Tm = °C
[b]ΔH = kcal.mol^{-1}
[c]ΔS = cal.mol^{-1}K^{-1}
1 kcal = 4.18 kJ

7.2.2. Influence of [Na^+] on the melting temperatures of J_{T1}, J_{T2}, J_{T3}, and J_{T4}.

The melting temperatures of the first and second transitions (obtained from UV absorbance melting curves) of all the junctions studied increase with the increase in Na^+ concentration. The slope ($\delta T_m/\delta log[Na^+]$) of such a plot demonstrates the effect Na^+ has on the melting temperature. It is clear from the plot of Tm versus [Na^+] that the salt has an overwhelming effect on the structural stability of the junctions. Except for J_{T4}, the plot of Tm versus [Na^+] of the other junctions shows that the slopes are different at ionic strength of less than 0.4M Na^+ and above 0.4M Na^+.

Comparing J_{T1} and J_{T2}: If it is assumed that both junctions are equally affected by the Na^+ concentration, then arms 3 and 4 of J_{T1} and J_{T2} respectively should have the same thermal stability. Arms 3 and 4 of J_{T1} and J_{T2} comprise the same sequences. Therefore, the observed differences in thermal stability between these junctions must come from the contribution of the triple-helical arms. The $\delta T_m/\delta log[Na^+]$ values, **Table 7.2**, corresponding to the melting of the double helical arms 3 and 4 in J_{T1} are different from the values of the same arms in J_{T2}. A possible explanation for these differences is that, as mentioned previously, arm 2 may have a destabilizing effect on the adjacent arms particularly in J_{T1}. The melting of J_{T1} and J_{T2} involves the removal of strand S3 which is base paired to strand S2(J_{T1})/T2(J_{T2}) in arm 3. In J_{T1}, strand S2 forms the "intermolecular" arm 2. In J_{T2}, strand S2 is replaced by T2, which positions the loop at this arm. The slightly lower slope, $\delta Tm/\delta log[Na^+]$, (6.5°C/log[$Na^+$] for J_{T1}, and 7.8°C/log[Na^+] for J_{T2}) of the first transition suggest that the binding of S3 in J_{T1} is less dependent on the ion concentration as compared to the binding of S3 in J_{T2}. It is possible that at lower ionic strength base pairing is incomplete in arm 2 of J_{T1}, hence the lower slope. Things are different, however, at higher salt concentration where the binding of S3 in J_{T1} displays a higher ionic strength dependency than expected.

Comparing J_{T3} and J_{T4}: J_{T3} displays a similar behavior as observed for J_{T1} and J_{T2} in so far as the slopes at lower salt concentration are less than the slopes at higher salt concentration. The slopes of the first transitions are marginally different from those observed for J_{T1} and J_{T2}. On the other hand, J_{T4} melting yields three sub-transitions, which clearly suggests a different melting pattern for this junction. Among the four junctions, the stability of the third strand in arm 4 should be the most pronounced one with or without the loop capping this arm. This should be the consequence

of the arrangement of cytosines. Nevertheless, one would expect to see a difference in thermal stability of arm 4 when capped with a loop and when lacking one. Although the loop contributes equally to the stability of each arm it is attached to, it seems that stabilizing the already stable arm 4 by means of a loop has some additional effects on the melting of the junction. For J_{T3} and J_{T4} which have the same third strand sequences, the differences in the melting patterns observed can be explained by the position of the loop.

Comparing J_{T1}, J_{T2}, J_{T3} and J_{T4}: The melting characteristics displayed by J_{T1}, J_{T2} and J_{T3}, i.e. the slope at lower salt concentration is less than the slope at higher salt concentration, has been linked to the presumed presence of a specific low and a different high salt conformation. It is known that in the absence of sufficient cations the four-way junction adopts the extended or square planar conformation, similar to tRNA in the absence of Mg^{2+}, with a pseudo-four-fold symmetry. On addition of sufficient cations, the four-way junction folds further by pairwise stacking of helical arms to yield a stacked X-structure (Duckett et al., 1990). It is possible that below 0.4M Na^+, J_{T1}, J_{T2} and J_{T3} are less folded and/or adopt a particular conformation, in this case, the square planar conformation. It should be noted that at 0.1M Na^+ and pH 4.6, the duplexes as well as the triplexes are formed in all junctions investigated here. Increasing the salt concentration to values above 0.4M Na^+ stabilizes the structures and apparently alters the conformation which is dominant below 0.4 M Na^+ into a more compact conformation. This compact conformation may well be a fully stacked X-structure. The deconvolution of the main transition of J_{T4} into three transitions does not necessarily mean it does not adopt a high salt conformation. The three transitions observed only demonstrate that there is different melting pattern of an already stacked structure. In fact, the results suggest that the triple helical arms of

J_{T1}, J_{T2} and J_{T3} melt from triplex to duplex and finally to random coil. On the other hand, the triple helical arms of J_{T4} melt as if they are part of a monomolecular structure.

The changed slopes obtained at low and high salt concentrations respectively for triplexes have only been seen for the triplex to hairpin transitions (Völker, 1993; Plum et al., 1990). Between pH 5.5 and 4.5, the same triplexes (Völker, 1993) melt from triplex to coil without a duplex intermediate and the slopes obtained remain the same at low and high salt concentrations. The thermal melting experiments as functions of $[Na^+]$ in this study were performed at pH 4.6. The triple-helical arms of J_{T1}, J_{T2}, and J_{T3} may not necessarily, at this pH, melt from triplex to coil. This is likely given the fact that removal of the strand forming the duplex part of the junction leaves behind two dangling strands, one on each of the remaining triple-helical arms. The dangling strands may either stabilize or destabilize the triplex arms they are attached to.

Table 7.2: The sodium concentration dependence ($dTm/d(\log[Na^+])$) values obtained from the plots of Tm versus $\log[Na^+]$.

	$dTm/d(\log[Na^+])$ first transition		$dTm/d(\log[Na^+])$ second transition	
	<400mM Na^+	>400mM Na^+	<400mM Na^+	>400mM Na^+
J_{T1}	6.5	14.3	8.4	16.3
J_{T2}	7.8	10.6	7.3	15.4
J_{T3}	8.1	13.8	5.8	20.2

	first transition	second transition	third transition
*J_{T4}	8.14	11.0	5.4

*J_{T4} unlike other junctions, has three transitions
Buffer contains 20mM Na_3PO_4, pH4.6.

7.2.3. The comparison of the calorimetric and van't Hoff transition enthalpies.

i. ***The double-helical four-way junction, Js***: The calculated enthalpy change (ΔH_{HV}) and the experimentally obtained calorimetric enthalpy (ΔHcal) (Table **4.1 and 4.2**) data obtained for the unfolding of the double-helical four-way junction Js show that the junction's melting does not follow a two-state melting behavior. In contrast, the melting of the isolated arms of the same junction can be described by a two-state model. Also apparent is that the sum of the ΔHcal of the isolated arms is far less than the ΔHcal obtained for the complete junction. The discrepancy can only be understood if it is assumed that the increased calorimetric enthalpy results from a contribution of pairwise stacking of helices in the complete junction. Because of the sequence composition of arm 2 of Js, it is reasonable to assume that this arm will be the first to be disrupted during melting. This will result in a structure with three arms intact and the fourth in the form of dangling ends. At this stage, no strand will be released into the solution. The dangling ends may have a stabilizing effect by adding some stacking interactions to the remaining duplexes. The influence of single strand extensions on the stability of the DNA duplex has been demonstrated by Senior et al. (1988). The authors have shown that the thermal stability and the transition enthalpy of double helices increased when dangling thymine residues are attached either at the 3' or 5' end. The 5'end extension is more effective in increasing the stability than the 3' end extension. It is, however, difficult to determine with confidence the exact contribution ((ΔΔT, ΔΔH, ΔΔS; Senior et al., 1988)) of the dangling strands to the stability of each arm because of the complex nature of the structure investigated here. Furthermore, it is difficult to assign the transitions to the individual arms (particularly arm 1 and arm 3) as they contain almost identical base sequences. The ΔΔT, ΔΔH and ΔΔS refer to the differences between the melting temperature, enthalpy and entropy changes observed for each isolated arm

and the corresponding arm in the complete junction. The overall estimated contribution to the transition enthalpy calculated for the junction from other sources amounts to 96-kcal mol^{-1} ($\Delta Hcal_{junction} - \Delta Hcal_{arms}$).

ii. ***Comparing J_{T1}, J_{T2}, J_{T3} and J_{T4}***: The enthalpy changes recorded for the first and second transitions of J_{T1} are similar to the enthalpy changes for the first and second transitions of J_{T2} respectively (**Tables 5.2 and 6.2**). This confirms the assumption that the first two transitions in either J_{T1} or J_{T2} correspond to the melting of the same double-helical arm 3 and arm 4 respectively. Likewise, the enthalpy changes associated with the third and fourth transitions of J_{T1} are similar to the enthalpy changes of the third and fourth transitions of J_{T2} respectively. These transitions are assigned to the melting of the triple-helical arm 1 and arm 2. Inspection of results listed in **Tables 5.2** and **5.3** reveals the same pattern for the junctions J_{T3} and J_{T4}. These results confirm the earlier assumption that the loop contributes equally to the stability of any arm it is capping. The transitions corresponding to the double helical arms of Js cannot be compared directly to the double–helical arms of J_{T1}, J_{T2}, J_{T3} and J_{T4} by comparing the corresponding melting temperatures. However, the transition enthalpies obtained for the arms of Js are well in agreement with the transition enthalpies of the double–helical arms of J_{T1}, J_{T2}, J_{T3} and J_{T4}.

7.3 Comparing thermal melting of J_{T1T3} and J_{T2T4}.

7.3.1 The effect of pH on the melting of J_{T1T3} and J_{T2T4}:

The effect of the pH on the thermal melting of J_{T1T3} and J_{T2T4} is well illustrated in the excess heat capacity versus temperature plots. It is clear that the two junctions unfold differently from each other (**Figures 5.6 and 6.5**). Inspection of the results in **Tables 5.3** and **6.3** shows that the thermal stability of both junctions increases with the decrease in pH. It is apparent that the

junctions are very stable, when compared with their underlying substructures (J_{T1}, J_{T2}, J_{T3} and J_{T4}). However, the results from the Absorbance (260nm) as a function of pH (**Figures 5.2A,B** and **6.2 A, B**) suggest that at 1M NaCl and pH 4.6, the triplexes in J_{T2T4} as well as the triplexes in the substructures J_{T1}, J_{T2}, J_{T3}, and J_{T4} are fully formed. This is not the case with J_{T1T3} where there is still the decrease in absorbance below pH 4.6. This may mean that the triplex structure is not completely formed or there is a "fast" equilibrium between the two or more conformers (conformers ≡ 1/2 and 3/4 stack or 1/4 and 2/3 stack or the square planar) (Grainger et al., 1998). The presence of the single band in the native polyacrylamide gel at pH 5.0 (**Figure 5.3**) rules out the incomplete formation of the triplex.

As observed for their respective components, the transition enthalpies of J_{T1T3} and J_{T2T4} are not affected by the change in pH. Therefore, the stabilizing effect of pH on the structures (as indicated by the increase of the Tm) is not enthalpic in origin.

7.3.2 Effect of Na^+ concentration on the stability of J_{T1T3} and J_{T2T4}:

The effect of [Na^+] on the stability of J_{T1}, J_{T2}, J_{T3} and J_{T4} revealed that at 0.1M Na^+, these structures are formed but they are not as stable as when the [Na^+] is higher than 0.4M. **Figure 7.2** shows that the junctions do form even in the absence of added salt. It is apparent from J_{T1T3} and J_{T2T4} phase diagrams (Tm *versus* [Na^+]) that at low salt concentrations, the transitions are separated from one another. Increasing the salt concentration does not only shift the transitions to higher temperatures but also results in merging of the transitions. The persistent transition, occurring with the lower melting temperature, which is also observed in absorbance *versus* temperature plots (pH series, cf. **Figures 5.6** and **6.5B**) as well as in the DSC curves, is assumed to correspond to the melting of arm 2. The merging of transitions probably signals the

interconnection of the unfolding of different arms. The results show that sufficient [Na^+] is required to stabilize the structures and eventually induces folding into a stacked X-conformer. The presence of [Na^+] is essential for shielding the negatively charged phosphate groups in the Watson-Crick and Hoogsteen strands, particularly at the branch point. It is not known if the adjacent cytosines in the third strand destabilize or stabilize the structures as it is in any case impossible to determine the extend at which certain domains of the structures are destabilized.

7.3.3 The effect of the loop on the structural stability of J_{T1T3} and J_{T2T4}:

The four-member cytosine loops have been introduced into the junctions, firstly, to facilitate triplex structure formation. Secondly, they are incorporated to maintain the number of strands participating in junction formation (molecularity) at four (i.e. not adding extra strands for the triplexes). For these reasons, the loops were designed to be all of the same size and sequence. As such, the contribution of each loop to the stability of the individual junctions should be the same. This has been shown to be the case with J_{T1}, J_{T2}, J_{T3} and J_{T4}. Inspecting **Tables 5.3** and **6.3** shows that J_{T1T3} is thermally more stable than J_{T2T4}. Since all loops have the same stabilizing effect on each junction, the question arises as to what contributes to the additional thermal stability of J_{T1T3}. One aspect to consider is that the specific positions of the loops yield two types of triple-helices, the 3' 5' 5' (J_{T2T4}) and the 5' 3' 3' (J_{T1T3}) triplex. Several studies conducted on these type of structures (conventionally termed H-y3 and H-y5) have shown that they have similar stabilities (Roberts and Crothers, 1996; Booher et al., 1994; Wang et al., 1994). However, this is not exactly the case with the junctions studied here (J_{T1T3} and J_{T2T4}). **Tables 5.3** and **6.3** show that the first three sub-transitions of J_{T1T3} are thermally more stable than the corresponding first three of J_{T2T4}.

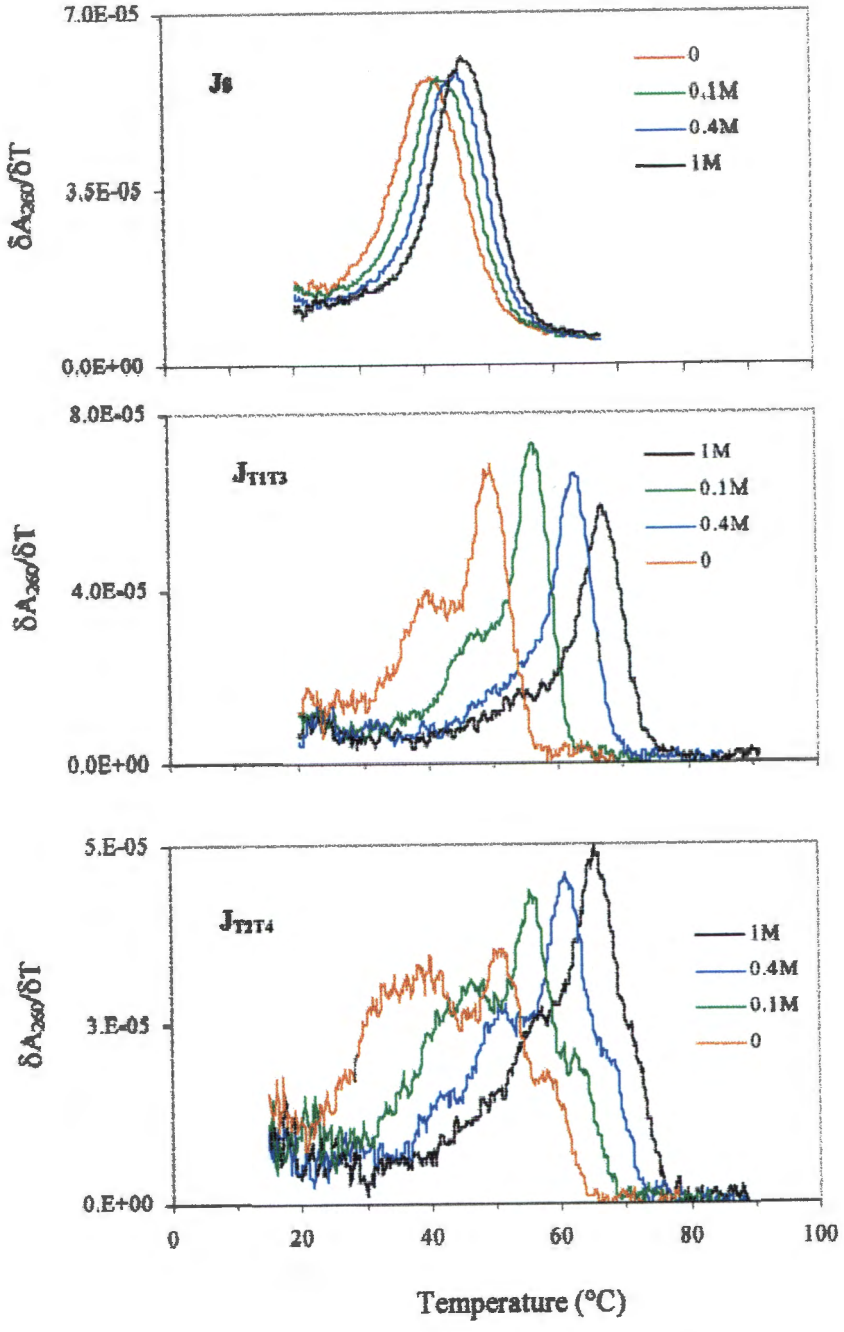

Figure 7.2: First derivative melting profiles ($\delta A_{260}/\delta T$) for J_{T1T3} and J_{T2T4} at various NaCl concentrations. Buffers contained 20mM Na_3PO_4 at pH 4.6 or pH 8.0 for Js. The total strand concentration per junction = 14.05 μM.

The last i.e. the fourth transitions of both junctions have similar melting temperatures at pH 4.6. Accordingly, the difference in thermal stability between J_{T1T3} and J_{T2T4} is associated with the first three transitions.

7.3.4 The calorimetric and van't Hoff transition enthalpies associated with the thermal melting of J_{T1T3} and J_{T2T4}:

The thermal melting of J_{T1T3} or J_{T2T4} does not follow a two-state model. The task of determining the thermodynamic data from UV melting curves (ΔH_{VH}) is complicated by the pronounced overlap of the sub-transitions. Therefore, reliable transition enthalpies corresponding to the melting of J_{T1T3} and J_{T2T4} were determined by calorimetry. **Figures 5.10** and **6.9** illustrates the melting of J_{T1T3} and J_{T2T4} at pH 5.0 and 4.6. It is obvious that the first three transitions for both junctions "look" the same and perhaps corresponds to the melting of the same sub-structures. The fourth (last) transition in J_{T2T4} is well separated from the first three and thus shows a different behavior. If the first three transitions observed in J_{T2T4} are the same, as the first three in J_{T1T3}, then their transition enthalpies and entropies are expected to match. This in turn should also hold for the complementary transition enthalpies and entropies associated with the melting of J_{T1}, J_{T2}, J_{T3} and J_{T4} respectively. The computed calorimetric enthalpies for the four individual transition of each junction are listed in **Tables 5.3** and **6.3** respectively. The first transitions observed in both junctions yield similar transition enthalpies. They match the third transition in **J_{T2} (Table 5.2)** (the third transition in J_{T1} is associated with the melting of the Hoogsteen strand). It was suggested in **section 7.2.2**, (Comparing J_{T1}, J_{T2}, J_{T3} and J_{T4}), that the triple-helical arms of J_{T1}, J_{T2}, and J_{T3} respectively melt consecutively first from triple helices to duplex structures and finally from double helices into random coils. Accordingly, the first transition observed for J_{T1T3}

and J_{T2T4} respectively can be associated with the melting of the Hoogsteen strand in arm 1 and arm 2. Melting of this strand in J_{T1T3} creates J_{T3} with a dangling strand on arm 1. Similarly, the melting of the same Hoogsteen strand in J_{T2T4} results in J_{T4} with the dangling strand extending from arm 2. The second transition separated out in the deconvoluted unfolding pattern of J_{T1T3} and J_{T2T4} is shown to be very similar in energy. The slight differences might be attributed to the effect of the dangling strand attached to arm 2. This transition can be compared to the melting of the double-helical arms of J_{T3} and J_{T4} respectively. The remaining transitions are assigned to the remaining arms of J_{T1T3} and J_{T2T4}. They behave very similar to the triple helical arms in J_{T3} and J_{T4} respectively. This is underlined by the very similar transition enthalpies for the third and fourth subtransitions.

The sum of all calculated partial transition enthalpies of J_{T2T4} is slightly higher than that obtained for J_{T1T3} by about 20.0 kcal mol^{-1}. Given the size of the structure and the order of magnitude of all enthalpies involved in thermal melting of these structures, the discrepancies are negligible and well within the experimental error margin (less than 5%). This implies that the formation of either J_{T1T3} or J_{T2T4} is not dependent on pH, sodium ion concentration, loop position or the polarity of the Hoogsteen strands. Comparing the thermodynamic parameters of J_{T1T3} with its components J_{T1} and J_{T3} suggests that J_{T1} and J_{T3} are properly formed and no defects like unpairing or unstacking are detected throughout the structure. The same can be concluded for the junction J_{T2T4} and its components J_{T2} and J_{T4}.

7.3.5: The effect of the third strand on the preferred stacked X-conformer

The double-helical DNA four-way junctions (4H junctions) (Lilley et al., 1996; Altona , 1996) are classified into six groups depending on the bases abutting the branch point. The double-

helical four-way junction used in this thesis, Js, is characterized by the central CGTA bases which form part of class 4-2 (Altona, 1996). The junctions in this class display exclusive preference for the A/B – C/D type coaxial stacked X-conformer e.g. junction 1 (L1) studied by Duckett (Duckett et al. 1988). Translated to Js, this means coaxial stacking of arms 1 and 2 and 3 and 4, that is, the A/B and C/D stacked conformer.

It is apparent from the melting data that the incorporation of the third strand on the double-helical four-way junction does not alter this conformation (**Sections 7.2.1.1 and 7.3.4**). That is formation of the 1/4, 2/3.stack conformer with two dangling ends may only allow triplexes in the continuos strands but not in either one or both of the crossover strands (**Figure 7.1 A and B**). the formation of the 1/4, 2/3 stack conformer will be hindered firstly by the sequence (base arrangement) at the branch point. Secondly, the stacked x-conformer may have to unfold to the square planar before all the arms become triplexes and this will then open the structure for attack by OsO_4.

CONCLUSION

CHAPTER 8

8.1 CONCLUSION

Viewing the results from the chemical and physical measurements it can be concluded that the formation of J_{T1T3} and J_{T2T4} as well as their substructures, J_{T1}, J_{T2}, J_{T3} and J_{T4}, shows the same dependence on pH, $[Na^+]$, loop position or the polarity of the HG strands. J_{T1T3} and J_{T2T4} form triple-helical four-way junctions that by design differ only in the position of the loops and/or polarity of the Hoogsteen strands. J_{T1}, J_{T2}, J_{T3} and J_{T4} are four-way junctions containing two double helical and two triple helical arms. Each of these four junctions is included either in J_{T1T3} or in J_{T2T4} as a substructure. Common to all these six structures is the underlying double-helical four-way junction, Js.

It can be demonstrated that the oligonucleotides designed for this study fold to form double-helical four-way junctions and subsequently triple helices when possible under varying pH conditions and at 1M Na^+. One characteristic of the four-way junctions is that in the presence of sufficient metal ions, the structures eventually fold into the so-called "stacked X-structure". The results obtained in this thesis can only indirectly illustrate this phenomenon. If it is assumed that the four-way junctions do fold into such conformations, it was not possible to determine the stacking patterns of the arms (whether arm 1 and arm 2 stack etc.). However, there is proof that these junctions do change from one conformation to another as the ionic strength (Na^+) is increased to more than 0.4M. Firstly, from the OsO_4-piperidine modification results, it seems reasonable to conclude that the junctions fold into a compact conformation. The amount of cleavage under a given set of buffer conditions differs slightly from junction to junction. The conclusions made based on the cleavage patterns imply that at pH 5.0 and in the presence of salt

(10mM Mg^{2+} and 100mM Na^{+}) all the junctions are completely formed and folded in a conformation that protects them from modification by OsO_4. It is also apparent that the protonation of third strand cytosines alone does not bring about the assumed stacked structure. The junctions are cleaved to some extend at pH 5.0 and in the absence of any cations. It appears that there is an interdependence of the pH and the cation concentration to bring about an uniterrupted triple-helical four-way junction.

Secondly, the change from one conformation to the other has been demonstrated in the phase diagram of the melting temperature *versus* log [Na^{+}]. Below 0.4M Na^{+}, the structures (as illustrated by J_{T1}, J_{T2}, and J_{T3}) adopt a "low-salt' conformation as indicated in the moderate slopes ($\partial Tm/\partial \log[Na^{+}]$. Above 0.4M Na^{+}, the slopes changes drastically. This may illustrate the presence of the structure with a different conformation.

The sequence chosen for the arms of Js allows the arms to melt separately from one another. This is also the case for the triple helical junctions although their melting patterns are slightly different from one another. The J_{T1}, J_{T2}, J_{T3} and J_{T4} thermal melting shows two separate transitions. The first transition is pH-independent while the higher temperature transition is pH-dependent. The thermal melting of J_{T1}, J_{T2}, J_{T3} and J_{T4} illustrates that during the melting process, the double helical arms within these junctions are the first to unfold followed by the triple helical arms. J_{T3} and J_{T4} are thermally more stable than J_{T1} and J_{T2}. This can be attributed to the sequence composition of the arms. At the same strand concentrations and buffer conditions, J_{T1}, J_{T2}, J_{T3} and J_{T4} turn out to be thermally more stable than the corresponding double-helical four-way junction, Js.

The impact of the loop on the stability of the individual arms is equal, but it gives rise to a different melting pattern of the different junctions due to the presence of the loops on the particular arms.

Comparison of the calorimetric transition enthalpy with the van't Hoff enthalpy of Js shows that the thermal melting of the junction cannot be described by a two-state model. In contrast, its isolated four arms each melt in a two-state manner. The sum of the transition enthalpy of the isolated arms is considerably less than the transition enthalpy of the complete junction. The increased transition enthalpy of Js is attributed to the contribution from the stacking of the four double helices.

The complete triple-helical four-way junctions, J_{T1T3} and J_{T2T4}, are highly sensitive to pH and Na^+ concentration. Each junction exhibits four sub-transitions during melting. J_{T1T3} and J_{T2T4} show a slightly increased thermal stability as compared to their substructures J_{T1}, J_{T2}, J_{T3} and J_{T4}. This implies that the third strands have a stabilizing effect on the arms of the four-way junction. The calorimetric transition enthalpies related to J_{T1T3} and J_{T2T4} melting are comparable to those associated with the melting of their substructures J_{T1}, J_{T2}, J_{T3} and J_{T4}.

We wish to acknowledge the fact that the deconvolution of DSC data is a complex procedure when overlapping peaks are involved. The success of the procedure in our case may simply reflect the limitations posed by the set of parameters used in the four-domain model.

Nevertheless, the results illustrate that the formation of the junctions is not restricted by the pH, $[Na^+]$, sequence composition of the arms, the loop position or the polarity of the backbone of the Hoogsteen strands. However, the loops, $[Na^+]$ and the sequence composition can have synergistic effects on the (un)folding of the junctions.

Finally, besides their role in genetic recombination branched DNA structures can be used as model systems to study protein-DNA interactions (Angelov et al., 1999). Other functions include the formation of zeolite-like lattices, development of drug delivery systems for therapeutic molecules (Zhang and Seeman, 1992).

DNA triple helices are considered promising candidates for pharmaceutical applications in controlling genetic expression. Combining triple helix formation and DNA branch formation therefore represents a novel approach, which allows simultaneous study of two related fields of DNA research.

To date the most challenging problems associated with both triplex structures and branched molecules have been the optimization of the poor cellular uptake as well as their stability *in vivo*. Questions may be answered if we have more physical properties of these structures.

8.2 REFERENCES

Altona C., Pikkemaat J. A., Overmars F.J.J., (1996) Three- and four-way junctions in DNA: a conformational viewpoint. *Curr. Opin. Struct. Biol.* **6** (3): 305-316.

Altona C., (1996) Classification of nucleic acid junctions. *J. Mol. Biol.* **2630**: 568 – 581.

Angelov D., Novakov E., Kochbin S., Dimitrov S., (1999) Ultraviolet laser footprinting of histone H1°-four-way junction DNA complexes. *Biochemistry* **38**: 11333 – 11339.

Antao V.P., Lai S. Y., Tinoco I. Jr., (1991). A thermodynamic study of unusually stable RNA and DNA hairpins. *Nucleic Acids Res.* **19**: 5901-5902.

Beal P.A., and Dervan P. B., (1991). Second structural motif for recognition of DNA by oligonucleotide directed triple-helix formation. *Science* **251**: 1360 – 1363.

Blake R.D. and Delcourt S.G., (1998) Thermal stability of DNA. *Nucleic Acids Res.* **26**: 3323-3332.

Blommers M. J. J., Walters J. A. L. I., Haasnoot C. A. G., Aelen J. M. A., van der Marel G. A., van Boom J. H., Hilbers C. W., (1989). Effects of base sequence on the loop folding in DNA hairpins. *Biochemistry* **28**: 7491-7498.

Booher M.A., Wang S., Kool E. T. (1994). Base-pairing and steric interactions between pyrimidine strand bridging loops and the purine strand in DNA pyrimidine-purine-pyrimidine triplexes. *Biochemistry* **33**: 4645 – 4651.

Breslauer K. J., Frank R., Blöker H., Marky L. A. (1996) Predicting DNA duplex stability from the base sequence. *Proc. Natl. Acad. Sci. USA.* **83**: 3746 – 3750.

Broker T. R., and Lehman I. R. (1971) Branched DNA molecules: Intermediates in T4 recombination. *J. Mol. Biol.* **60**: 131-149.

Cantor C. F., Warshaw M.M., Shapito H. (1970) Oligonucleotide interaction. III.circular dichroism studies of the conformation of deoxyoligonucleotides. *Biopolymers* **9**: 1059 – 1077.

Carlström G. and Chazin W., (1996) Sequence dependence and direct measurement of crossover isomer distribution in model Holliday junctions using NMR spectroscopy. *Biochemistry* **35** (11): 3534- 3544.

Cate J. H., Gooding A. R., Podell E., Zhou K., Golden B. L., Kundrot C. E., Cech T. R., Doudna J. A. (1996a). Crystal structure of a group I ribozyme domain: principles of RNA packing. *Science* **273**: 1678-1685.

Cate J. H., Hanna R. L., Doudna J. A. (1997) A magnesium ion core at the heart of ā ribozyme domain. *Nature Struct. Biol.* **4**: 553-558.

Cech T. R. (1986) RNA as an enzyme. *Sci. Am.* **255**: 64 – 65.

Chen J.H., Churchill M. E. A., Tullius T. D., Kallenbach N. R., Seeman N. C., (1988) Construction and analysis of monomobile DNA junctions. *Biochemistry* **85** (16): 6032-38.

Chen J.H., Kallenbach N. R., Seeman N. C., (1989) A specific quadrilateral synthesized from DNA branched junction. *J. Am. Chem. Soc.* **111**: 6402- 6407.

Chen L., Cai L., Zhang X., Rich A., (1994). Crystal structure of a four-stranded intercalated DNA: d(C4). *Biochemistry*.**33**: 13540-13546.

Chen S.M. and Chazin W.J. (1994) Two dimensional ^{1}H-NMR studies of immobile Holliday junctions: nonlabile proton assignment and identification of crossover isomers. *Biochemistry* **33** (38): 11453- 11459.

Cheng A. J. and Van Dyke M. W., (1993). Monovalent cation effects on intermolecular purine-purine-pyrymidine triple-helix formatio. *Nucleic Acids Res.* **21**: 5630- 5635.

Cheng Y. K. and Pettitt B. M. (1992a). Stabilities of double- and triple-stranded helical nucleic acids. *Prog. Biophys. Mol. Biol.* **58**: 225-257.

Churchill M. E. A., Tullius T. D., Kallenbach N. R., Seeman N.C. (1988). A Holliday recombination intermediate is two-fold symmetric. *Proc. Natl. Acad. Sci. USA.* **85** (13): 4653 – 4656.

Cooper J.P. and Hagerman P. J. (1987) Gel electrophoretic analysis of the geometry of DNA four-way junction. *J. Mol. Biol.* **198** (4): 711-719.

Cooper J.P. and Hagerman P. J. (1989) Geometry of a branched DNA structure in solution. *Proc. Natl. Acad., Sci. USA* **86** (19): 7336- 7340.

Delcourt S. G., and Blake R. D. (1991) Stacking energies in DNA.*J. Mol. Chem.* **266**: 15160–15169.

Duckett D. R., Murchie A. H., Diekmann S., von Kitzing E., Kemper B. and Lilley D.M. (1988) The structure of the Holliday junction, and its resolution. *Cell* **55** (1): 79-89.

Duckett D. R, Lilley D. M. J., (1991) Effects of base mismatches on the structure of the four-way DNA junction. *J. Mol. Biol.* **221** (1): 147-161.

Duckett D. R., Murchie A. H., Lilley D. M. J., (1990) The role of metal ions in the conformation of the four-way junction. *EMBO J.* **9** (2): 583-90.

Durand M., Peloille S., Thuong N.T., Maurizot J. C., (1992a) Triple-helix formation by an oligonucleotide containing one $(dA)_{12}$ and two $(dT)_{12}$ sequences bridged by two hexaethylene glycol chains. *Biochemistry* **31**: 9197 – 9204.

Felsenfeld G., Davies D. R., Rich A., (1957). Formation of three-stranded polynucleotide molecule. *J. Am. Chem. Soc.* **79**: 2023 – 2024.

Frank-Kamenetskii M. D., Malkov V. A., Voloshin O. N., Soyfer V. N., (1991). Stabilization of PyPuPu triplexes with bivalent cations. *Nucleic Acids Res. Symo. Ser.* **24**: 159 – 162.

Furlong J. C. and Lilley D. M. J. (1986) Highly selective chemical modification of cruciform loops by diethyl pyrocarbonate. *Nucleic Acids Res.* **14** (5): 3995 – 4007.

Gehring K., Leroy J., Guéron M., (1993). A tetrameric DNA structure with protonated cytosine-cytosine base pairs. *Nature* **363**: 561-565.

Gellert M., Mizuuchi K., O'dea M. H., Ohmori H., Tomizawa J., (1979). DNA gyrase and DNA supercoiling . *Cold Spring Harbor Symp. Quant. Biol.* **43**: 35-40.

Germann M. W., Kalisch B. W., Lundberg P., Vogel H. J., van de Sande J. H., (1990). Pertubation of DNA hairpins containing the EcoR-I recognition site by hairpin loops of varying size and composition: Physical (NMR and UV) and enzymatic (EcoR-I) studies. *Nucleic Acids Res.* **18**: 1489-1498.

Gotoh O. (1983). Prediction of melting profiles and local helix stability for sequenced DNA. *Adv. Biophys.* **16**: 1 – 52.

Gough G. W., Sullivan K. M., Lilley D. M. J., (1986). The structure of the cruciforms in the supercoiled DNA: probing the single-stranded character of nucleotide bases with bisulphite. *EMBO J.* **5**: 191-196.

Grainger R. J., Murchie A. H., Lilley D. M. J., (1998) Exchange between stacking conformers in a four-way DNA junction. *Biochemistry* **37** (1): 23-32.

Gralla J. and Crothers D.M., (1973) Free energy of imperfect nucleic acid helices. II Small hairpin loops. *J. Mol. Biol.* **73**:497-511.

Guschlbauer W., Chantot J., Thiele D. (1990) Four-stranded nucleic acid structures 25 years later: from guanosine gels to telomere DNA. *J. Biomolecular Structure & Dynamics.* **8**: 491 - 511

Hampel K. J., Burkholder G. D., Lee J. S., (1993). Plasmid dimerization mediated by triplex formation between polypyrimidine-polypurine repeats. *Biochemistry* **32**: 1072- 1077.

Harding C. C., Henderson E., Watson T., Prosser J. K., (1992). Monovalent cation induced structural transitions in telomeric DNAs: G-DNA folding intermediates. *Biochemistry* **30**(18): 4460 – 4472.

Harding C. C., Watson T., Corregan M., Bailey C., (1991). Cation dependent transition between quadruplex and Watson-Crick hairpin forms of d(CGCG$_3$GCG) *Biochemistry* **31**(3): 833 – 841.

Henderson E. R., Moore M., Malcolm B. A., (1990). Telomere G-strand structure and function analysed by chemical protection, base analogue substitution and utilization by telomerase in vitro. *Biochemistry* **29**: 732-737.

Hilbers C. W., Heus H. A., van Dongen M. J.P., Wijmenga S. S., (1994). The hairpin elements of nucleic acids structure: DNA and RNA folding. In Nucleic acids and molecular biology, vol. 8 p56 – 104/; Springer- Verlag, Berlin Heidelberg.

Hilbers C. W., Blommers M. J. J., van de Ven F. J. M., van Boom J. H., van der Marel G. A., (1991). High resolution NMR studies of DNA hairpins with four nucleotides in the loop region. *Nucleosides Nucleotides* **10**: 61-80.

Holliday R., (1964) A mechanism for gene conversion in fungi. *Genet. Res.*: **5**, 282 – 304.

Horne D. A. and Devarn P. B. (1991) Effects of an abasic site on the triple helix formation characterized by affinity cleaving. *Nucleic Acids. Res.* **19**: 4963 4965.

Hüsler P. L. and Klump H.H. (1994). Unfolding of a branched double-helical three-way junction with triple-helical ends. *Arch. Biochem.Biophys.* **313**: 29-38.

Hüsler P. L. and Klump H.H. (1995) Thermodynamic characterization of a triple helical three-way junction containing a Hoogsteen branch point. *Arch. Biochem.Biophys* **322** (1): 149-166.

Jetter M. C., and Hobbs F. W. (1993). 7,8-dihydro-8-oxoadenine as a replacement for cytosine in the third strand of triple helices. Triplex formation without hypochromicity. *Biochemistry* **32**: 3249- 3254.

Jin R., Gaffney B. L., Wang C., Jones R. A., Breslauer K. J., (1992). Thermodynamics and structure of a DNA tetraplex: a spectroscopic and calorimetric study of the tetramolecular complex of d(TG_3T) and d($TG_3T_2G_3T$). *Proc. Natl. Acad. Sci. USA* **89**: 8832-8836.

Kallenbach N. R., Ma R., Seeman N. C., (1983) An immobile nucleic acid junction constructed from oligonucleotides. *Nature* **305**: 829-831.

Kang H. and Tinoco I. Jr., (1997). A mutant RNA pseudoknot that promotes ribosomal frameshifting in mouse mammary tumor virus. *Nucleic acids Res.* **25**: 1943-1949.

Kimball A., Guo Q., Kallenbach N. R., Cunningham R. P., (1990). Conformational isomers of Holliday junctions. *J. Biol. Chem.* **265**: 6544 – 6547.

Klump H. H., Calorimetric studies of DNAs and RNAs. (1990) Landolt-Börnstein, Numerical data and functional relationships in Science and Technology, New Series, , group vii, Vol.1, 241-256.

Kolk M. H., Heus H. A., Hilbers C. W., (1997). The structure of isolated, central hairpin of the HDV genomic rybozome. *EMBO J.* **16**: 3685-3692.

Krakauer H., Sturtevant J. M., (1968). Heats of helix-coil transition of the poly A- poly U complexes. *Biopolymers* **6**: 491 – 512.

Lee J. S. Woodsworth M. L., Latimer L. J., Morgan A. R., (1984). Poly(pyrimidine).poly(purine) synthetic DNAs containing 5-methylcytosine form stable triplexes at neutral pH. *Nucleic Acids Res.* **12**: 6603 – 6614.

Leontis N. B., Hills M. T., Piotto M., Ouporov I. V., Malhotra A., Gorenstein D. G., (1995). Helical stacking in three-way junctions containing two unpaired pyrimidines: proton NMR studies. *Biophys. J.* **68** (1): 251 – 265.

Lu M., Guo Q., Marky L. A., Seeman N. C., Kallenbach N. R., (1992) Thermodynamics of DNA branching. *J. Mol. Biol.* **223** (2): 781 – 789.

Lu M., Guo Q., Mueller J. E., Kemper B., Studier F. W. (1990). Characterization of a bimobile DNA junction. *J. Biol. Chem.* **265** (28): 16778-85.

Lu M., Guo Q., Seeman N.C. and Kallenbach N. R., (1991) Parallel and antiparallel Holliday junctions differ in structure and stability. *J. Mol. Biol.* **221** (4): 1419-1432.

Lyamichev V. I., Voloshin O. N., Frank-Kamenetskii M. D., Soyfer V. N., (1991). Photofootprinting of DNA triplexes. *Nucleic Acids Res.* **19** (7): 1633 – 1638.

Lyamichev V. I., Frank-Kamenetskii M. D., Soyfer V. N., (1990). Protection against UV-induced pyrimidine dimerization in DNA by triplex formation. *Nature* **344** (: 568 – 570.

Makube N., Klump H. H., Pikkemaat J., Altona C. (1999) Thermodynamic properties of an intramolecular DNA four-way junction. *Arch. Biochem. Biophys.* **364** (1): 53-60.

Manor H., Rao B. S., Martin R. G., (1988). Abundance and degree of dispersion of genomic $d(GA)_n.d(CT)_n$ sequences. *J. Mol. Evol.* **27**: 96-101.

Manzini G., Xodo L. E., Gasparotto D., Quadrifoglio F., van der Marel G. A., van Boom J. H. (1990). Triple helix formation by oligopurine-olipyrimidine DNA fragments – electrophoretic and thermodynamic behavior. *J. Mol. Biol.* **213**: 833 - 843.

Marky L. A., Kallenbach N. R., Seeman N.C., A McDonough, Breslauer K.J., (1987), The melting behavior of a DNA junction structure: A calorimetric and spectroscopic study. *Biopolymers* **26**: 1601-1620.

Marky L. A. and Breslauer K.J. (1987) Calculating thermodynamic data for transitions of any molecularity from equilibrium melting curves. *Biopolymers* **26**: 1601-1620.

Mergny J., Lacroix L., Han X., Leroy J., Hélène C. (1995). Intramolecular folding of pyrimidine oligodeoxynucleotides into an I-DNA motif. *J. Am. Chem. Soc.* **117** (35); 8887 – 8898.

Mergny J., Sun J. S., Rougée M., Montenay-Garestier T., Barcelo F., Chomilier J., Hélène C. (1991b) Sequence specificity in triple helix formation: experimental and theoretical studies of the effect of mismatches on triple helix stability. *Biochemistry* **30**: 9791 9798.

Michel F.,and Westhof E. (1990). Modeling of the three dimensional architecture of group I catalytic introns based on comparative sequence analysis. *J. Mol. Biol.* **216**: 585 610.

Miick S. M., Fee R. S., Millar D. P., Chazin W. J. (1997). Crossover isomer bias is the primary sequence-dependent property of immobilized Holliday junctions. *Proc. Natl. Acad. Sci. USA* **94** (17): 9080-9084.

Milligan J. F., Krawczyk S. H., Wadwani S., Matteucci M. D., (1993). An antiparrallel triple helix motif with oligo-deoxynucleotide containing 2'deoxyguanosine and 7-deaza-2'deoxyxanthosine. *Nucleic. Acids. Res.* **21**: 327 – 333.

Mills M., Völker J., KlumpH.H., (1996) The triple helical structures involving inosine: There is a penalty for promiscuity. *Biochemistry*: **35**: 13338-133344

Møllegaard N. E., Murchie A.I.H., Lilley D.M.J., Nielsen P.E (1994) Uranyl photoprobing of a four-way DNA junction: evidence for specific metal ion binding. *EMBO J.* **13** (7): 1508-1513.

Moser H., and Dervan P. B., (1987). Sequence-specific cleavage of double-helical DNA by triplex helix formation. *Science* **238**: 648 – 650.

Mueller J. E., Seeman N. C., (1991). Design and synthesis of a knot from single stranded DNA. *J. Am. Chem Soc.* **113**: 6306 – 6308.

Murchie A. I. H., Clegg R. M., von Kitzing E., Duckett D. R., Diekmann S., Lilley D. M. J. (1989) Flourescence energy transfer shows that the four-way DNA junction is a right handed cross of antiparallel molecules. *Nature (London)* **341** (6244): 763 – 766.

Murchie A. I. H., Portugal J., and Lilley D. M. J., (1991) Cleavage of the four-way junction by a restriction enzyme spanning the point of strand exchange. *EMBO J.* **10**(3): 713-718

Murray N. L. and Morgan A. R., (1973). Enzymic and physical studies on the triplex dTn.dAn.rUn [(deoxyribosylthymine)$_n$.(deoxyadenosine)$_n$.(ribouridine)$_n$)]. *Can. J. Biochem.* **51**: 436 – 449.

Olivas W. M. and Maher L. J., III (1995a). Competitive triplex/quadruplex equilibria involving guanine-rich oligonucleotides. *Biochemistry* **34**: 278 – 284.

Ono A., Ts'o P. O. P., Kan L. S., (1991b). Triplex formation of oligonucleotides containing 2'-O-methyl-pseudoisocytidine in substitution for 2'-deoxycytidine. *J. Am. Chem. Soc.* **113**: 4032-4033.

Overmars F. J. J., Pikkemaat J. A., van den Elst H., van Boom J. H., Altona C., (1996). NMR studies of three-way junctions containing two unpaired thymidine bases: the influence of the bases at the junction on the stability of the stacking conformers. *J. Mol. Biol.* **255** (5): 702 – 703.

Overmars F. J. J and Altona C., (1997) NMR study of the exchange rate between two stacked conformers of a model Holliday junction. *J. Mol. Biol.*, **273** (3): 519-524.

Overmars F. J. J., Lanzotti V., Galeone A., Pepe A., Mayol L., Pikkemaat J. A., Altona C., (1997) Design and NMR study of an immobile DNA four-way junction containing 38 nucleotides. *Eur. J. Biochem.* **249** (2): 576-583.

Panayotatos N., and Wells R. D. (1981) Cruciform structures in supercoiled DNA. *Nature* **289**: 466–470.

Panyutin I. G., Kovalsky O. I., Budowsky E. I., Dickerson R. E., Rikhirev M. E., Lipanov A. A., (1990). G-DNA: a twice folded DNA structure adopted by single stranded oligo(dG) and its implication for telomeres. *Proc.Natl. Acad. Sci.* **87** (3): 867 – 870.

Pikkemaat J. A., van den Elst H., van Boom J. H., Altona C., (1994) NMR studies and conformationl analysis of a DNA junction formed in a linear synthetic oligonucleotide. *Biochemistry* **33** (49): 14896-14907

Pikkemaat J. A., Overmars F. J. J., Dreef-Tromp C. M., van den Elst H., van Boom J. H., Altona C., (1996) Conformational aspects of an uncharged phosphate analogon built at the branch point of a DNA four-way junction. *J. Mol. Biol.* **262**: 349-357.

Pilch D. S., Brousseau R., Shafer R. H., (1990a). Thermodynamics of triple helix formation: spectrocopic studies on the $d(A)_{10}{\cdot}2d(T)_{10}$ and $d(C^{+}{}_3T_4C^{+}{}_3){\cdot}d(G_3A_4G_3){\cdot}d(C_3T_4C_3)$ triple helices. *Nucleic Acids Res.* **18**(19): 5743 – 5740.

Pleij C. W., Rietvield K., Bosch L. (1985) A new principle of RNA folding based on pseudonotting. *Nucleic Acids Res.*, **13**: 1717 – 1731.

Pleij C. W., (1990) Pseudoknots: a new motif in the RNA game. *Trends Biochem Sci.* **15**: 143 – 147.

Plum G. E., Park Y. W., Singleton S. F., Dervan P. B., Breslauer K. J., (1990). Thermodynamic characterization of the stability and melting behavior of a DNA triplex: a spectroscopic and calorimetric study. *Proc. Natl. Acad. Sci. USA.* **87**: 9436 – 9440.

Plum G. E. and Breslauer K. J. (1995a). Thermodynamics of an intramolecular DNA triple helix: a calorimetric study and spectroscopic study of the pH and salt dependence on thermally induced structural transitions. *J. Mol. Biol.* **248**: 679 – 695.

Plum G. E., Pilch D. S., Singleton S. F., Breslauer K. J., (1995b). Nucleic acid hybridization: triplex stability and energetics. *Annu. Ref. Biophys. Biomol. Struct.* **24**: 319 – 350.

Pöhler J. R. G., Duckett D. R., Lilley D. M. J., (1994) Structure of four-way junction containing a nick in one strand. *J. Mol. Biol.* **238**: 62 – 74

Rietveld K., van Poelgeest R., Pleij C. W., van Boom J. H., Bosch L., (1982) The t-RNA-like structure at the 3' terminus of turnip yellow mosaic virus RNA. Differences and similarities with canonical tRNA. *Nucleic Acids Res.* **10**: 1929 – 1946.

Roberts R. W, and Crothers D. M. (1991). Specificity and stringency in DNA triplex formation. *Proc. Natl. Acad. Sci. USA.* **88**: 9397 – 9401.

Roberts R. W, and Crothers D. M. (1996). Kinetic discrimination in the folding of intramolecular triple helices. *J.Mol.Biol.* **260**: 135 – 146.

Rosen M. A., Pate D. J., (1993a). Conformational differences between bulged pyrimidines (C-C) and purines (A-A, I-I) at the branch point of three-stranded DNA junctions. *Biochemistry* **32**: 6563 - 6575.

Rougée M., Faucon B., Mergny J. L., Barcelo F., Giovannangéli C., Garestier T., Hélène C., (1992). Kinetics and thermodynamics of triple-helix formation: effects of ionic strength and mismatches. *Biochemistry* **31**: 9269 – 9278.

Ruskin B., and Green M. R. (1985). The role of the three splice site consensus sequence in mammalian pre-mRNA splicing. *Nature* **317**: 732 – 734.

Seeman N. C., (1982) Nucleic acids junctions and lattices. *J. Theor. Biol.* **99**: 237-247.

Seeman N. C., and Kallenbach N. R. (1983) Design of immobile nucleic acid junctions. *Biophys. J.* **44** (2): 201-209.

Seeman N.C., Chen J., Kallenbach N. R.(1989) Gel electrophoresis analysis of DNA branched junctions. *Electrophoresis* **10** (5-6): 345-354.

Seeman N.C. and Kallenbach N. R. (1994). DNA branched junctions. *Annu. Rev. Biomol. Struct.* **23**: 53-86.

Sen D. and Gilbert W., (1990). A sodium-potassium switch in the formation of four-stranded G4-DNA. *Nature* **344**: 410-414.

Sen D. and Gilbert W., (1988) Formation of parallel four-stranded complexes by guanine-rich motifs in DNA and its implications for meiosis. *Nature* **334**: 364 – 366.

Senior M. M., Jones R. A., Breslauer K. J., (1988). Influence of loop residues on the relative stabilities of DNA hairpin structures. *Proc. Natl. Acad. Sci. USA* 85: 6242-6246.

Senior M. M., Jones R. A., Breslauer K. J., (1988). Influence of dangling thymine residues on the stability and structure of two DNA duplexes. *Biochemistry.* **27**: 3879-3885.

Shen L. X., and Tinoco I. Jr., (1995). The structure of an RNA pseudoknot that causes efficient frameshifting in mouse mammary tumor virus. *J. Mol. Biol.* **247**: 963-978.

Shindo H., Torigoe H., Sarai A., (1993). Thermodynamic and kinetic studies of DNA triplex formation of an oligopyrimidine and a matched duplex by filter binding assay. *Biochemistry* **32**: 8963 – 8969.

Sigal N. and Alberts B. (1972) Genetic recombination: the nature of a crossed strand –exchange between two homologous DNA molecules. *J. Mol. Biol.* **71**: 789 – 793.

Simorre J. P, Legault P., Hangar A. B., Michiels P., Pardi A. (1997). A conformational change in the catalytic core of the hammerhead ribozyme upon cleavage of an RNA substrate. *Biochemistry* **36**: 518-525.

Sinden R. R. (1994) DNA structure and function. Chapter 6. Academic Press. San Diego, California. pp217- 258.

Sinden R. R., and Wells R.D., (1992). DNA structure mutations and human disease. *Curr. Opin. Biotechnol.* **3**: 612 – 622.

Soyfer V. N. and Poteman V. N. (1986). Triple-helical nucleic acids. Springer – Verlag New York.

Sundquist W. I., and Klug A., (1989). Telomeric DNA dimerizes by formation of guanine tetrads between hairpin loops. *Nature* **342**: 825-829.

Uhlenbeck O. C., Borer P. N., Dengler B., Tinoco JR I. (1973) Stability of RNA hairpin loops: A_6-C_m-U_6. *J. Mol. Biol.* **73**: 483 – 496.

van Belkum A., Abrahams J. P., Pleij C. W., Bosch L., (1985) Five pseudonots are present at the 204 nucleotides long 3' noncoding region of tobacco mosaic virus RNA. *Nucleic Acids Res.* **13**: 7673 – 7686.

Völker J., Lindsey G.G, Klump H. H. (1993) Energetics of a stable intramolecular DNA triple helix formation. *J. Mol. Biol.* **230**: 1278 – 1290.

Völker J., Klump H. H., (1994). Electrostatic effects in DNA triplex helices. *Biochemistry* **33**: 13502 – 13508.

Wang S., Booher M.A., Kool E. T. (1994). Stabilities of nucleotide loops bridging the pyrimidine strand in DNA pyrimidine-purine-pyrimidine triplexes: special stability of the CTTTG loop. *Biochemistry* **33**: 4639 – 4644.

Watson J. D. and Crick F. H. C. (1953b) Molecular structure of nucleic acids. *Nature (London)* **171**: 737 – 740.

Welch J. B., Walter F., Lilley D. M. J. (1995). Two inequivalent folding isomers of the three-way DNA junction with unpaired bases: sequence-dependence of the folded conformation. *J. Mol. Biol.* **251** (4): 507 – 509.

Wemmer D. E., Wand A. J., Seeman N. C., Kallenbach N. R. (1985). NMR analysis of DNA junctions: Imino proton NMR studies of individual arms and intact junction. *Biochemistry* **24**: 5745 – 5749.

Williamson J. R., Raghuraman M. K., Cech T. R., (1989) Monovalent cation-induced structure of telomeric DNA: The G-quartet model. *Cell* **69**: 871-880.

Wilson W.D., Hopkins H. P., Mizan S., Hamilton D. D., Zon G., (1994). Thermodynamics of DNA triplex formation in oligomers with or without cytosine bases: influence of buffer species, pH and sequence. *J. Am. Chem. Soc.* **116**: 3607 – 3608.

Xodo L. E., Alunni-Fabbroni M., Manzini G., Quadrifoglio F.,(1993) Sequence-specific DNA triplex formation at imperfect homopurine-homopyrimidine sequences within a DNA plasmid. *Eur.J. Biochem.* **212:** 395 – 401.

Xodo L. E., Manzini G., Quadrifoglio F.,(1990) Spectroscopic and calorimetric investigation on DNA triplex formed by d(CTCTTCTTTCTTTTCTTTCTTCTC) and d(GAGAAGAAAGA) at acidic pH. *Nucleic Acids Res.* **18**: 3557 – 3564.

Xodo L. E., Manzini G., Quadrifoglio F., van der Marel G., van Boom J., (1991). Effect of 5-methylcytosine on the stability of the triple-stranded DNA – a thermodynamic study. *Nucleic Acids Res.* **19**: 5625- 5631.

Zhang Y., Seeman N. C., (1992). A solid-support methodology for the construction of geometrical objects from DNA. *J. Am. Chem. Soc.* **114**: 2656 – 2663.